Title

Relative functions of feedforward, feedback, and horizontal connections in the central visual pathway

Author

Kim, Taekjun

Publication Date

2014

Peer reviewed|Thesis/dissertation

Relative functions of feedforward, feedback, and horizontal connections in the central visual pathway

By

Taekjun Kim

A dissertation submitted in partial satisfaction of the

requirements for the degree of

Doctor of Philosophy

in

Vision Science

in the

Graduate Division

of the

University of California, Berkeley

Committee in charge:

Professor Ralph D. Freeman, Chair
Professor Michael A. Silver
Professor Friedrich T. Sommer

Fall 2014

Relative functions of feedforward, feedback, and horizontal connections in the central visual pathway

Abstract

Relative functions of feedforward, feedback, and horizontal connections in the central visual pathway

By

Taekjun Kim

Doctor of Philosophy in Vision Science

University of California, Berkeley

Professor Ralph Freeman, Chair

Visual information processing in the central visual pathway is mediated by three main types of inter-cellular connections. These are feedforward, feedback, and horizontal connections. Most neurophysiological studies have been conducted in a perspective of feedforward connections assuming a hierarchical model. They revealed that convergent feedforward inputs determine size and structure of classical receptive fields (CRFs) of recipient cells in a higher level area. Non-feedforward connections are known to integrate visual information from outside the CRF and use this information to modulate the CRF activity. But relative roles of feedback and horizontal connections are not clear. My research interest is to figure out different functions for three major pathways in vision. In order to do this, I measure single unit activity in cat visual cortex while specific visual or magnetic stimulation is being applied to provide weighted activity from feedforward, feedback, and horizontal connections.

In Chapter 1, we introduce visual stimuli specially designed to maximize relative differential involvements of three main types of neural connections. The approach is based on well-established anatomical and physiological features of neural projections in the central visual pathway. We show clear segregation of fast and slow components of surround modulation. Then, we present supporting evidences that they are primarily mediated by feedback and horizontal connections, respectively.

Chapter 2 quantitatively describes transcranial magnetic stimulation (TMS) effects on neural activity. We focus specific stimulation parameters with limited visual stimuli and examine how TMS affects response selectivity (orientation, spatial frequency & contrast tuning) of visual neuron. Our findings suggest that TMS interrupts the existing balance between sub-cortical and intra-cortical inputs for a relatively extended time period.

According to anatomical studies, proportions of sub-cortical and intra-cortical inputs to a single cell in the visual cortex are clearly different depending on cortical layers. In Chapter 3, we examine how intra-cortical inputs are differently contributing to direction selectivity of visual neurons by comparing various features of direction selectivity among multiple layers. Consistent with the classical view, our results show that linear estimation of direction selectivity (only sub-cortical inputs are considered) is quite accurate in input layers but substantially smaller in non-input layers, suggesting a considerable non-linear contribution of intra-cortical connections in these layers.

Lastly, Chapter 4 describes issues related to trial-to-trial variability. Spiking response of a V1 single neuron to repeated presentations of the same visual stimulus is too variable to explain excellent behavioral performance in discrimination task. From the viewpoint of experimenter who controls the parameters of visual stimuli systematically, this trial-to-trial variability can be regarded as unpredictable noise which may reduce potential performance of neural computation. The source and advantage of trial-to-trial variability is not yet understood. Here, I introduce several response variability related issues that we already know and need to know.

Contents

List of Figures

Acknowledgements

I would never have been able to finish my dissertation without the guidance of my committee members, help from friends, and support from my family.

First of all, I would like to thank my great advisor Prof. Ralph Freeman. He patiently guided me to develop the ability to think logically and provided me with an excellence atmosphere for doing research. His financial support also helped me concentrate on the research without worries. I thank my committee members, Prof. Michael Silver and Prof. Fritz Sommer for their interest in my work. They taught me how to think about experiments and results from different aspects of view, and helped me write a better dissertation. Additionally, I am grateful to Prof. Cliff Schor, Prof. Bruno Olshausen, & Prof. David Whitney who helped me a lot during the qualifying exam with their encouragement, insightful comments, and advises. Prof. Marty Banks was a great Graduate advisor. He listened to my worries, encouraged me and enhanced my confidence to keep pursuing my Ph.D

Dr. Baowang Li and Dr. Bart Moore were not only wonderful labmates but also reliable advisors whenever I confronted difficulties in the lab. Catherina Min was a good friend who I could ask a favor when I had an English-related problem as a non-native speaker. Thanks for their generous help, I could get used to new environment and system very smoothly. I am also grateful to Dr. Brian Pasley, who is an alumnus of Freeman Lab, for initiating the line of TMS research and for teaching me how to use the device.

I would also like to thank my family, Seungho Kim, Pileun Lee, and Soojin Kim and many friends who I newly met in Berkeley. They were always supporting me and encouraging me with their wishes.

Chapter 1

Selective stimulation of neurons in visual cortex enables segregation of slow and fast connections

Preface: This chapter has been published in the journal, Neuroscience: Taekjun Kim and Ralph Freeman (2014), and is included with permission from all authors. The dissertation author was the primary author of this paper.

1.1 Abstract

Organization of the central visual pathway is generally studied from a perspective of feedforward processes. However, there are horizontal connections and also strong feedback from extrastriate to primary visual cortex. Here, we use visual stimuli designed to maximize relative differential involvements of these three main types of connections. The approach relies on differences between stimulation within the classical receptive field (CRF) and that of the surround region. Although previous studies have used similar approaches, they were limited primarily to spatial segregation of neural connections. Our experimental design provides clear segregation of fast and slow components of surround modulation. We propose that these are mediated by feedback and horizontal connections, respectively, but other factors may be involved. Our results imply that both horizontal and feedback connections contribute to integration of visual information outside the CRF and provide suppressive or facilitative modulation. For a given cell, modulation may change in strength and sign from suppression to facilitation or the reverse depending on surround parameters. Sub-threshold input from the CRF surround increases local field potential (LFP) power in distinct frequency ranges which differ for suppression and facilitation. Horizontal connections have delayed CRF-surround modulation and are sensitive to position changes in the surround. Therefore, surround information beyond the CRF is initially processed by fast connections which are putatively feedback, whereas spatially tuned mechanisms are relatively slow and presumably mediated by horizontal connections. Overall, our results suggest that convergent fast (feedforward) inputs determine size and structure of the CRFs of recipient cells in visual cortex and that fast connections from extrastriate regions (feedback) plus slow tuned connections (horizontal) within visual cortex contribute to spatial influences of CRF surround activation.

1.2 Introduction

The classical RF (CRF) of the visual system refers to spatial territory within which appropriate stimulation can generate spike activity from a single neuron. Stimulation outside the CRF cannot independently activate the neuron, but it can influence responses to CRF stimulation. CRF organization changes from early to central visual pathways. Most neurophysiological studies assume a hierarchical processing model such that information is encoded sequentially along the pathway (Hubel & Wiesel, 1962).

However, along with serial processing, parallel information flow occurs with a feedforward mechanism (M. Livingstone & Hubel, 1988; Nassi & Callaway, 2009). Anatomical studies demonstrate two additional major types of intercellular connections. One is feedback from extrastriate regions (Budd, 1998; Galuske, Schmidt, Goebel, Lomber, & Payne, 2002; Peters, Payne, & Budd, 1994; Sherman &

Guillery, 1996). The other is a horizontal pathway between adjacent cells in visual cortex (Bosking, Zhang, Schofield, & Fitzpatrick, 1997; Hirsch & Gilbert, 1991; Kisvárday, Tóth, Rausch, & Eysel, 1997; McGuire, Gilbert, Rivlin, & Wiesel, 1991; Rockland & Lund, 1983). Feedback and horizontal connections share some similar characteristics. They do not exhibit retinotopic alignment as in the feedforward system (Alonso, 2002; Angelucci & Bullier, 2003). They represent large visual areas. They have many synaptic connections which are relatively weak as shown by inactivation of feedback which has minimal effects on spiking activity of cortical cells (Bullier, Hupé, James, & Girard, 2001; Hupé et al., 1998). Feedback and horizontal input do not appear to affect spike generation unless there is simultaneous feedforward activation (Bringuier, Chavane, Glaeser, & Frégnac, 1999; Toth, Rao, Kim, Somers, & Sur, 1996).

Considered together, the three main neural connection types appear to have different functions. Feedforward processing consists of clear input to retinotopically aligned target cells. Non-feedforward connections may integrate visual information from outside the CRF which may modulate CRF activity (Angelucci & Bullier, 2003; Cavanaugh, Bair, & Movshon, 2002a, 2002b; Seriès, Lorenceau, & Frégnac, 2003; Walker, Ohzawa, & Freeman, 1999). The relative roles of feedback and horizontal connections are not clear but conduction velocities may provide clues. Onset times of surround suppression in V1 have been reported to be nearly constant over wide areas outside the CRF (Bair, Cavanaugh, & Movshon, 2003). However, the method used to reach this conclusion did not provide isolation of temporal parameters of horizontal transmission. Our current protocol is designed specifically to incorporate this important feature (see Experimental procedures and Results sections).

We use visual stimulation patterns intended to separate functional activity of the three major visual connection types. Two sets of stimuli are designed to differentially activate CRF and non-CRF regions in order to provide activity that emphasizes feedforward, feedback, or horizontal connections. Although we cannot confirm that we have exclusively isolated these three types of connections, our findings are consistent with their selective activation. Results show that activation outside the CRF can result in suppression or facilitation which can change depending on surround (non-CRF) parameters. The amount of response modulation of the CRF region varies with surround position. We find that excitatory and inhibitory inputs from surround areas are associated with different local field potential (LFP) frequency ranges. There are also temporal response modulation changes dependent on stimulus configurations. Overall, our results identify and imply some important functional differences in visual processing of feedforward, feedback, and horizontal connections.

1.3 Materials and Methods

Experiments were conducted using anesthetized and paralyzed cats (2.4~3.5kg, 12 female). All procedures followed the guidelines by NIH and by the Animal Care and Use Committee at the University of California, Berkeley.

1.3.1. Surgical preparation

Initial anesthesia was induced with isoflurane (3%). After venous catheters were inserted, anesthesia was continued with intravenous infusion of propofol (20mg/kg·hr) combined with fentanyl (10μg/kg·hr). A tracheotomy was performed, a tracheal cannula was inserted and the animal was artificially ventilated (25% O2 & 75% N2O). A craniotomy was then made in both hemispheres at 4mm posterior and 2mm lateral to Horsley-Clarke zero. The dura was incised carefully and reflected, then the cortical surface was covered with agar and wax. After the surgery, propofol and fentanyl infusion rates were reduced to an appropriate level for stabilized anesthesia (propofol: ~6-8mg/kg·hr, fentanyl: 4μg/kg·hr) which was determined individually for each animal. After stabilization, a continuous intravenous infusion of pancuronium (0.2mg/kg·hr) was initiated to block eye movements.

1.3.2. Recording procedures

Neural activity was recorded with two-channel tungsten microelectrodes. The signals from each electrode were amplified, bifurcated and then differentially filtered to extract single unit activity (500Hz~8MHz, digitized at 25kHz) and local field potentials (0.7~170Hz, digitized at 500Hz). Electrode penetrations were made down the medial bank of the postlateral gyrus to a depth of 5~6mm. Cells were encountered in multiple layers at RF eccentricities within the central 15° of the visual field (DeAngelis, Ohzawa, & Freeman, 1993a). RF eccentricity information for individual neurons was not recorded for this study. Once a unit was identified by spike waveform, optimal RF parameters were measured using drifting sinusoidal grating stimuli in the following sequence: orientation → spatial frequency → temporal frequency → binocular phase (for binocular cell) → size. RF dimension was determined as the peak of a size tuning curve for which response of a neuron ceases to increase. For cells that didn't show clear peaks in size tuning curves, we used the smallest inner diameter at which a cell stopped responding to an annulus grating stimulus as in a previous study (Cavanaugh et al., 2002a).

1.3.3. Design of visual stimuli

A crucial part of these experiments is the use of carefully selected visual stimuli that permit maximized separation of the three types of neural connections noted above. Anatomical findings show that feedforward connections cover a small visual space that is limited to the projection of the CRF region (Alonso, Usrey, & Reid, 2001; Angelucci & Bressloff, 2006). Therefore, the role of non-feedforward connections can be investigated by comparisons of visual responses to CRF activation versus those for which stimulation includes both CRF and adjacent non-CRF regions.

Since non-feedforward includes both feedback and horizontal connections, we require stimuli to separate them. For this, we note different characteristics for these two types of connections in spatial and temporal domains. Anatomical studies with use of retrograde tracers show that feedback connections can convey information to V1 from a much larger visual space than that for horizontal connections (Angelucci & Bressloff, 2006; Angelucci et al., 2002; Salin, Bullier, & Kennedy, 1989; Salin, Girard, Kennedy, & Bullier, 1992). In this case, the spatial extent of horizontal connections is approximately matched to the size of a low contrast summation field. This implies that beyond the low contrast summation field, feedback connections may dominate in surround suppression. In previous studies, surround suppression for spatial locations close to and far from the CRF was used to investigate horizontal connections (Hashemi-Nezhad & Lyon, 2012; Shushruth et al., 2013). However, the distribution of labeled neurons in V1 following injection of an anatomical tracer only covers monosynaptic connections, so the complete spatial extent of a horizontal pathway is not clear. Surround input is probably also transmitted via polysynaptic horizontal connections which will cause an enlargement of the spatial extent.

Besides a difference in spatial extent, another distinction between horizontal and feedback connections is conduction velocity. Axons of horizontal connections are thin and unmyelinated with slow conduction velocities (Grinvald, Lieke, Frostig, & Hildesheim, 1994; Salami, Itami, Tsumoto, & Kimura, 2003). Feedback and feedforward connections between macaque V1 and V2 have similar conduction velocities, which are about ten times faster than those of a horizontal type within V1 (Girard, Hupé, & Bullier, 2001). Hence, if visual information of a non-CRF stimulus is conveyed through horizontal connections with slow conduction velocities, its arrival time should be more delayed as the non-CRF stimulus is placed further away from the CRF (Bringuier et al., 1999). In contrast, if it is conveyed through feedback connections with fast conduction velocities, arrival time delay, independent of center-surround distance, will be negligible. However, data suggest that surround information is conveyed by both types of neural connections so that the initial part of surround modulation is mediated by feedback (Bair et al., 2003; Hupé et al., 2001) and the later part by horizontal connections (Liu, Hashemi-Nezhad, & Lyon, 2013).

Comparisons of surround modulation time courses between stimulation of near and far distance conditions from the border of the CRF allow us to separate horizontal and feedback components. We have devised two sets of stimulus patterns by which center-surround distance is systematically varied as depicted in Figure 1.1.

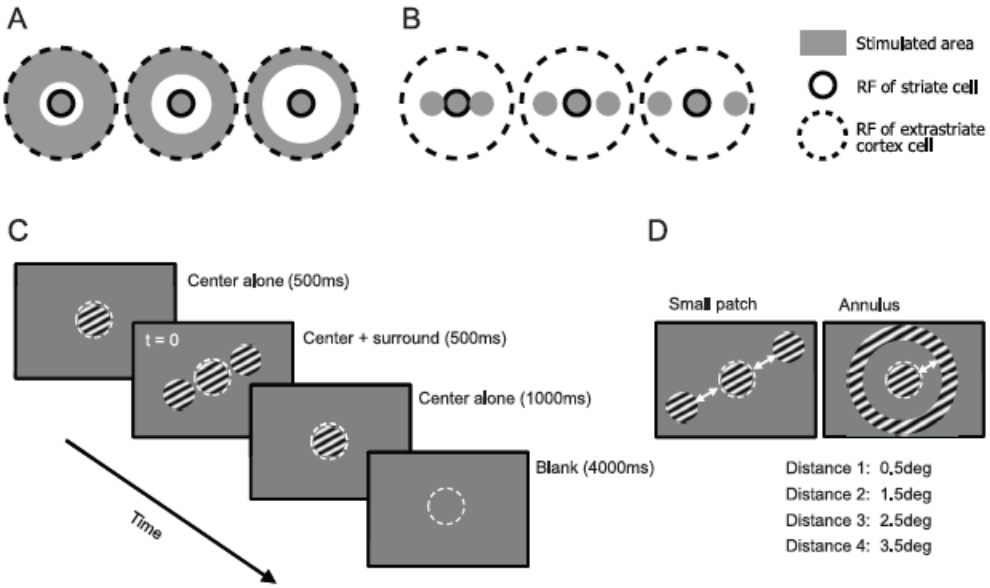

Figure 1.1. Two sets of center-surround (CRF-outside CRF) stimuli: annulus surround (left) and small patch surround (right). With both sets, distance between center and surround stimuli is systematically varied. In annulus surround pattern **(A)**, annuli of different widths are used so that increments of center-surround distances are accompanied by decreases of total stimulated area. In small patch surround pattern **(B)**, change of center-surround distance doesn't cause increase or decrease of total stimulated area. **(C)** Sequence of a trial. Optimal sinusoidal moving gratings are used to stimulate CRF and surround regions of a cell under study. The center (CRF) stimulus (2000ms duration, 50% contrast) is presented first, followed by surround stimuli (500ms duration, 100% contrast) after a 500ms temporal interval. **(D)** Small patch surround stimuli and annulus surround are tested in separate blocks. For small patch surround blocks, two patch surround stimuli are positioned symmetrically with respect to the center stimulus along the axis of preferred orientation. Inter-patch distances (white arrows) are chosen randomly as one out of four values (0.5~3.5deg, 1deg step) for each trial. For annulus surround blocks, the outer diameter of the annulus is fixed at 30deg. Therefore, four levels of center-surround distance are controlled by the inner diameter of the annulus. In addition to four "center + surround" and four "surround alone" conditions, a "center alone" presentation is tested as a control.

Distances are defined as visual angles between edges of center and surround stimuli. In the annulus surround pattern (Figure 1.1A), annuli of different widths are used outside the CRF. In the small patch surround pattern (Figure 1.1B), two patches of CRF size are presented symmetrically along the axis of preferred orientation with different inter-patch distances. For both stimuli sets, increments of center-surround distance are expected to cause analogous effects on the horizontal component of surround modulation. First, the modulation onset should be delayed because of slow conduction velocity. There should also be a decrease of surround modulation magnitude. Horizontal connections between neighboring neurons in V1 are denser than those among distant cells (Bosking et al., 1997; Kisvárday et al., 1997). Therefore, as center-surround distance increases, surround modulation caused by horizontal connections should get weaker and slower.

We next consider the feedback component of surround modulation for variation of the center-surround distance. For the annulus surround pattern, an increase of center-surround distance should be accompanied by a decrease in activation of feedback connections since the amount of visual input to extrastriate cortex is reduced. So a difference between near and far surround conditions should affect both feedback and horizontal connections. Because of this, a previous study in which annulus surround stimuli were used to compare near vs. far surround conditions (Bair et al., 2003), did not isolate horizontal connections. In contrast, the small patch surround pattern we have used here permits selective control of horizontal connections without substantial change in activation of feedback. This follows from the observation that the visual space covered by feedback connections is much larger than the CRF size of a V1 cell (Angelucci & Bressloff, 2006; Angelucci & Bullier, 2003; G. H. Henry, Salin, & Bullier, 1991; Salin et al., 1989, 1992). Therefore, spatial resolution of feedback connections is worse than that for the horizontal type. Based on these factors, the stimulus patterns we use here are expected to provide data for center-surround distance effects on surround modulation and to differentiate horizontal and feedback contributions. Details of our stimulus procedures with temporal and spatial parameters are depicted in Figure 1.1 C,D.

1.3.4. Data analysis

1.3.4.1. Spike density function

To observe the time course of surround modulation, spike density functions for "center alone" and "center+surround" conditions are compared. Spike trains were digitized at 25kHz and resampled at 1kHz. They were convoluted with a kernel which resembles a post-synaptic potential (Thompson, Hanes, Bichot, & Schall, 1996). The kernel is expressed by the following equation.

$$R(t) = [1 - \exp(-t/\tau_g)] \times [\exp(-t/\tau_d)] \quad (1)$$

where $R(t)$ is rate as a function of time. $R(t)$ is computed with two time constants for the growth phase (τ_g =1ms) and the decay phase (τ_d =20ms).

2.4.2. Z-scored LFP spectrogram

The spectrograms of the local field potential (LFP) signals (digitized at 500Hz) were computed using the Chronux toolbox in Matlab (500ms sliding window with 10ms step size, frequency range 10~100Hz). The resultant time-frequency LFP power matrix follows a 1/f2 relationship. Since we are interested in relative rather than absolute power change for each frequency band depending on an event (e.g., onset of surround stimulus), the raw LFP power matrix is transformed to a z-score based on mean and standard deviation values during a baseline period (>250ms before stimulus onset & >750ms after stimulus offset) for each frequency band.

$$P_{zscore}(f,t) = \frac{P(f,t) - \mu(P(f,t_{baseline}))}{\sigma(P(f,t_{baseline}))} \quad (2)$$

where $P_{zscore}(f,t)$ and $P(f,t)$ are z-scored and raw LFP power at a frequency f and time t, $\mu(P(f,t_{baseline}))$ and $\sigma(P(f,t_{baseline}))$ are the mean and standard deviation of raw LFP power computed during baseline period at a given frequency f.

1.4 Results

We studied 89 cells from 12 animals. There were 127 recording sessions of which 92 employed both annulus and small patch surround stimuli for given cells yielding direct comparisons. For 24 cells, we tested different spatial phases of the center stimulus.

Drifting sinusoidal gratings were used to stimulate the CRF and non-CRF surround regions of recorded cortical cells. To prevent saturation of neural response and to maximize inputs from surround regions, contrast values for CRF and non-CRF stimuli were differently set at 50% and 100%, respectively. Optimal parameters of grating stimuli are used as determined by CRF mapping procedures. Optimal sizes of RF centers may vary depending on mapping methods or stimulus contrast (M P Sceniak, Ringach, Hawken, & Shapley, 1999; Seriès et al., 2003). Here, we use a summation RF method with 50% stimulus contrast (Cavanaugh et al., 2002a). Size of the RF center is defined as the peak or asymptote of the size tuning curve for which response of a neuron ceases to increase. The CRF measured with a high contrast stimulus (high contrast summation RF: hsRF) is generally smaller than that measured with low contrast (low contrast summation RF: lsRF). However, hsRF is not simply an underestimation of CRF center. Feedforward connections from LGN integrate signals within the hsRF of visual cortical neurons. The size of lsRF is approximately matched to the spatial extent of horizontal connections (Angelucci & Bressloff, 2006). The goal of the current study is to understand the different functions of horizontal and feedback connections in visual information processing. In order to manipulate both horizontal and feedback components of surround modulation, we have defined the CRF based on the predominantly feedforward driven hsRF.

Each trial begins with onset of a center stimulus (duration = 2000ms). Surround stimuli, which have a shorter duration (500ms), follow the center stimulus with 500ms onset delay (i.e., the center stimulus is presented earlier and lasts longer than that for the surround). This is important because it enables the observation of both the beginning and end points of surround modulation. For each trial, a distance between center and surround stimuli is randomly chosen from four predetermined values. For the nearest distance condition, edges of center and surround stimuli are separated by 0.5 degree visual angle. For the other three conditions, center and surround stimuli are separated further by progressive 1 degree steps. A “center alone” and four “surround alone” conditions are also included in the test sequence as control conditions. For most cells, nine separate stimulus conditions are tested

and repeated 20~70 times.

1.4.1. Magnitude of center-surround modulation varies linearly with distance between center and surround stimuli.

Figure 1.2 shows neural responses of a representative cell for which small patch surround stimuli induced suppressive modulation. This simple cell has an f1/f0 > 1, and its spike density function has periodic peaks as determined by temporal frequency (7 cycles/second) (Figure 1.2A). Dashed and solid curves indicate spike density functions computed for "center alone" and "center + the nearest (dist1) surround" conditions, respectively. Both curves are aligned at onset time of the surround (0 on time axis). Two downward arrows at the top of the curves indicate onset and offset times of the surround. Note that suppressive modulation (lower amplitude of solid curve) is apparent only during the 0~500ms time period during which surround regions of the CRF are co-stimulated with that of the center.

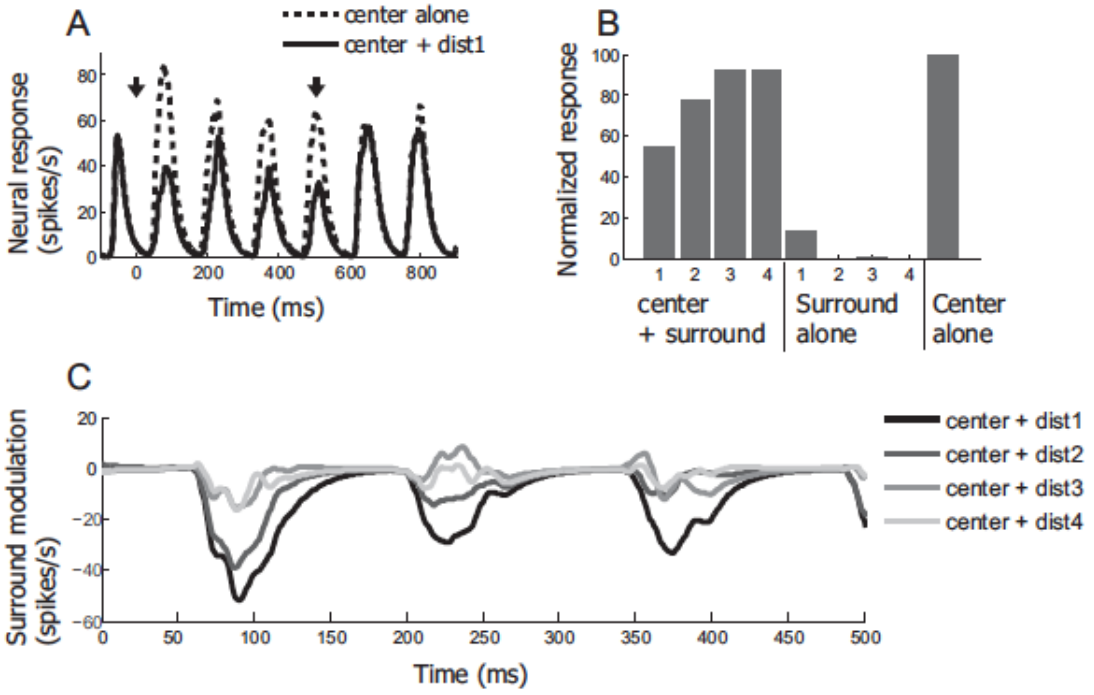

Figure 1.2. A representative cell showing suppressive center-surround modulation. **(A)** Dashed and solid curves are spike density functions computed for "center alone" and "center + surround (dist1)" conditions, respectively. Time 0 indicates onset of surround stimulus whose duration is 500ms. Onset and offset of surround stimulus are indicated by two downward arrows. Note that the magnitude of the solid curve is lower than that of the dashed only from the 0 to 500ms interval, demonstrating that the neural response to the center stimulus is suppressed by the surround. **(B)** For each of 9 stimulus conditions, mean spike count during the 0~500ms period is computed and then normalized with the value computed for "center alone" condition. The smaller numbers for the x-axis represent the nearer center-surround distances. In this case, strength of surround suppression

gets weaker as center-surround distance increases. **(C)** Each curve is created by subtracting the spike density function for "center alone" condition from that of each "center + surround" condition. Nearer center-surround distances are depicted in darker shades. For efficient comparisons between the four distances, curves are truncated to the interval from 0 to 500ms.

We quantified the magnitude of surround modulation by counting the number of spikes generated during the 0~500ms time period noted above. The values computed for 9 stimulus conditions (four "center + surround", four "surround alone" & one "center alone") are normalized to the value of the "center alone" condition. A value smaller (or larger) than 100 means suppressive (or facilitative) surround modulation. These data are shown in the histogram of Figure 2B. For the "center + dist1" condition, the neural response is suppressed by 50%. As expected, the suppressive modulation magnitude is gradually decreased as center-surround distance increases. This linearly decreasing pattern of suppressive modulation is shown in Figure 2C which gives the time course of surround modulation. Each curve here is created by subtraction of the spike density function of "center alone" from that of each of the four "center + surround" conditions. In the "center+dist1" condition, surround suppression begins to arise at around 60ms after surround onset time, and it is very slightly delayed or unchanged in subsequent distance conditions. Note that the latency of surround modulation may be less than 60ms, and that there is no spike between 0 and 60ms.

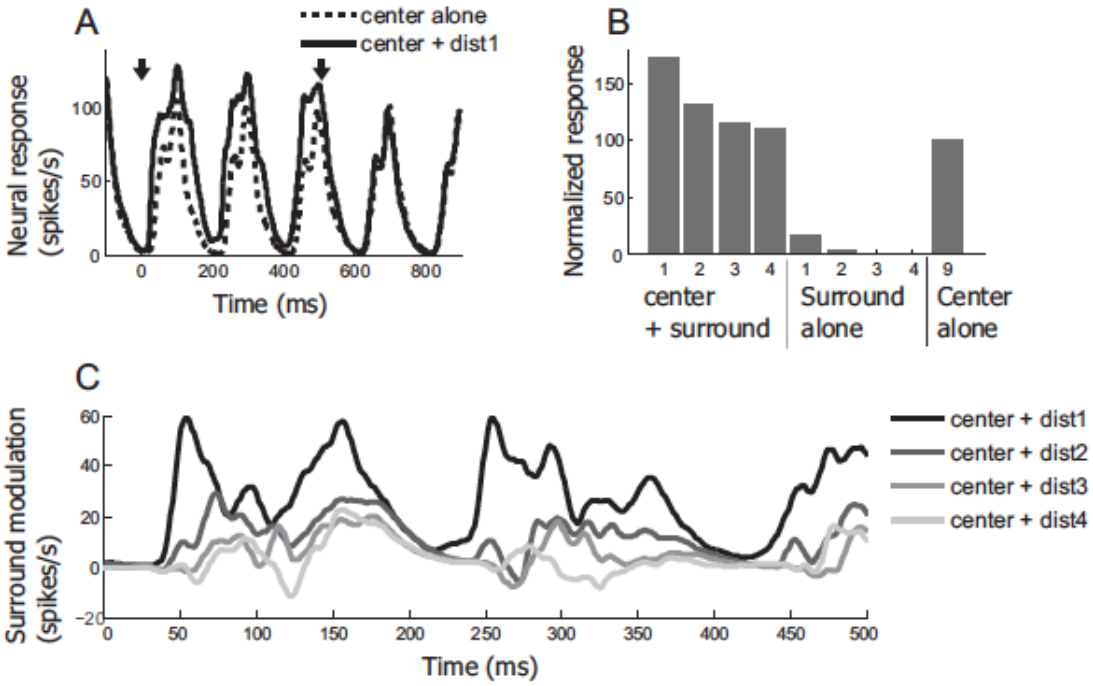

Figure 1.3. An example cell which exhibits facilitative center-surround modulation. The same conventions are used as in Figure 1.2. **(A)** Spike density functions computed for "center alone (dashed)" and "center + dist1 (solid)" conditions. Arrows indicate times at which the surround is presented (first arrow) and when it is turned off (second arrow). **(B)** Normalized responses for 9 stimulus conditions. Strength of surround facilitation becomes weaker as center-surround distance is increased. **(C)** Time course of surround modulation. Surround facilitation tends to be diminished and delayed as surround distance from the center (CRF) is increased.

Results from another cell are presented in Figure 1.3 for which the same conditions are considered as in the previous figure. Unlike the cell shown in Figure 1.2, this cell exhibits facilitative instead of suppressive modulation. In the "center + dist1" condition, neural response is about 1.6 times stronger than that for the "center alone" condition. And the strength of facilitative modulation exhibits a linearly decreasing pattern with increments of center-surround distance. Surround alone elicits weak spiking activity (5th and 6th bars in Figure 1.3B), indicating possible minimal overlap with the CRF. However, low spiking activity for the surround alone condition is not likely to be a direct cause of the relatively strong facilitative effect. The magnitude of the facilitative effect is much stronger than the value expected from linear summation of spiking activity of "center alone" and "surround alone" conditions, indicating that additional sub-threshold facilitative inputs from the surround must be involved. In addition, the observation of spiking activity for the surround alone condition is not limited to the facilitation case. As shown in Figure 1.2B, spiking activity in the surround alone condition (the 5th bar) is often associated with strong suppressive modulation (the 1st bar).

An interesting feature of this example is that surround modulation latency varies systematically depending on center-surround distance. In the "center + dist1" condition, facilitative modulation begins around 40ms after surround onset. It is delayed gradually as center-surround distance increases. This time-distance relationship of center-surround modulation may be explained as follows. Surround signals are transmitted through horizontal connections with slow conduction velocities. The initial portion of surround modulation may be mediated by fast feedback connections. But feedback connections from extra striate areas may require relatively strong visual input along with large CRFs. Also, surround modulation may require an integration process for activation. This idea is supported by a previous finding that the latency of surround suppression is negatively correlated with its strength (Bair et al., 2003). In this case, strong surround input can trigger immediate modulation, but if it is weak, time is required for it to be effective.

The above two representative results illustrate that our small patch surround stimuli can induce either suppressive or facilitative modulation of the response. In both cases, effective strength of surround modulation decreases as center-surround distance increases.

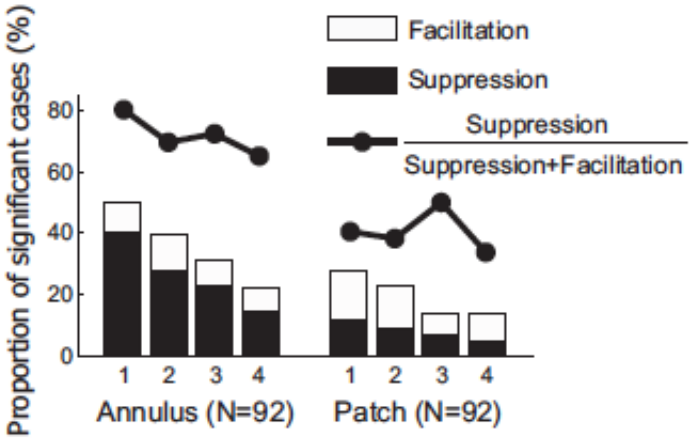

Figure 1.4. Proportions of significant modulation for annulus and small patch surround conditions (Two-sided Mann-Whitney U-test ($p<0.05$)). Although, for both conditions, proportions of significant modulation cases (filled and unfilled bar areas) decreases as center-surround distance increases, bar heights for annulus conditions are nearly twice as tall as those for small patch application at corresponding center-surround distances. This demonstrates that the annulus surround is more effective for the induction of significant surround modulation. In addition, the dominant sign of surround modulation is suppression for the annulus pattern, but it is facilitation for the small patch. Furthermore, for the annulus pattern, relative ratios of suppression (filled circles) diminish with increasing center-surround distance. This suggests that suppression requires stronger surround input than facilitation.

Next, we consider the annulus surround stimulus. For 92 recordings, both annulus and small patch surround stimuli were tested with the same cell. For these cases, Figure 1.4 shows proportions of significant (Two-sided Mann-Whitney U-test ($p<0.05$)) modulation cases as a function of center-surround distance for both sets of surround stimuli, (left: annulus surround, right: small patch surround). Filled and unfilled bars represent suppressive and facilitative modulation, respectively. For the "center + dist1" condition of annulus surround, about 50% of the population data show significant suppressive or facilitative modulation. The proportions of significant modulation cases decrease as center-surround distance increases. In the "center + dist4" condition, less than 30% of the data show significant modulation. This decreasing pattern is also clearly seen for small patch surrounds, but with much smaller proportions. To summarize, at a given distance, the annulus surround is a more effective way to modulate neural response. It seems clear that the stronger effect of an annulus surround is due to a larger amount of visual input compared with that for the small patch condition.

Another interesting result is that the dominant sign of surround modulation is changed from suppression to facilitation when the annulus stimulus is replaced by a small patch. Neurons with inhibitory or facilitatory regions beyond the CRFs tend to

be grouped in clusters of facilitation or inhibition (Yao & Li, 2002). If annulus and small patch surround stimuli are tested for different neural populations, there may be biased sampling. But in the current study, we can rule out this factor, because the two different types of surround stimuli are tested using the same population of cells.

We should also consider the possibility that the annulus stimulus may cover several zones of facilitation and suppression. There is a report of a spatial arrangement of opposing contextual interactions with collinear (end-zone) facilitation and lateral (side) inhibition (Kapadia, Westheimer, & Gilbert, 2000). Our small patch surround stimuli are always presented at both end-zones of a preferred orientation axis. Thus, if a cell receives facilitative input from the end-zones, and the magnitude of this facilitation is weaker than suppressive areas from other regions in the annulus, it could cause a result like that of Figure 1.4. In this context, note that surround suppression can originate from a localized region and that suppressive areas are sometimes spatially asymmetric (Walker et al., 1999). However, the most effective suppressive surround regions are end-zones (Walker et al., 1999). Therefore, it is likely that most of our results may be attributed to end-zone effects.

To examine this question more closely, consider the data curves above the histograms in Figure 4. Each point indicates a relative ratio (RR) of bar height data in black (RR_{filled}) as follows.

$$RR_{filled}(Stim, Dist) = \frac{H_{filled}(Stim, Dist)}{H_{filled}(Stim, Dist) + H_{unfilled}(Stim, Dist)} \times 100 \qquad (3)$$

where $H_{filled}(Stim, Dist)$ and $H_{unfilled}(Stim, Dist)$ are heights of filled and unfilled bars respectively for a given stimulus pattern (*Stim:* annulus or patch) and center-surround distance (*Dist:* dist1~dist4). For the annulus surround, suppression is dominant compared to that for facilitation for the "center + dist1" condition. This dominance is gradually lost as center-surround distance is increased along with the decreasing amount of visual input (80% in dist1 → 65% in dist4). This suggests that suppressive modulation requires stronger input from the surround compared to that for facilitation, and we consider this in more detail in the following section.

1.4.2. Suppressive modulation requires stronger input from surround region than that for facilitation

The finding that suppressive modulation requires stronger surround input than that for facilitation implies that inhibitory interneurons have higher activation thresholds than those for excitation. This idea has been postulated in computational models for integration of surround inputs (Schwabe, Obermayer, Angelucci, & Bressloff, 2006; Somers, Todorov, & Siapas, 1998). If this is correct and both excitatory and inhibitory interneurons are involved in center-surround modulation of neural activity, then the process of increased surround strength should be as follows.

1) No modulation → 2) Weak facilitation → 3) Strong facilitation → 4) Weak facilitation → 5) Weak suppression → 6) Strong suppression

Excitatory interneurons with low activation thresholds are relatively easily activated even by weak surround input, and this gives rise to facilitation (i.e., 1) No modulation → 2) Weak facilitation). The magnitude of facilitation increases as surround input gets stronger (i.e., 2) Weak facilitation → 3) Strong facilitation). But once surround input exceeds the activation threshold of inhibitory interneurons, facilitation begins to decrease and change to strong suppression (i.e., 3) Strong facilitation → 4) Weak facilitation → 5) Weak suppression → 6) Strong suppression). A decrease of surround input will cause changes in the opposite direction. If neural response is suppressed by an annulus surround, suppression may be maintained (but weakened) or changed to facilitation with a small patch surround. Alternatively, if the neural response of a cell is facilitated by an annulus surround, the magnitude of facilitation might vary, but the same effect should occur for a small patch surround. Either stronger or weaker facilitation for a small patch can occur as in the changes from points 4) to 3), or from points 3) to 2).

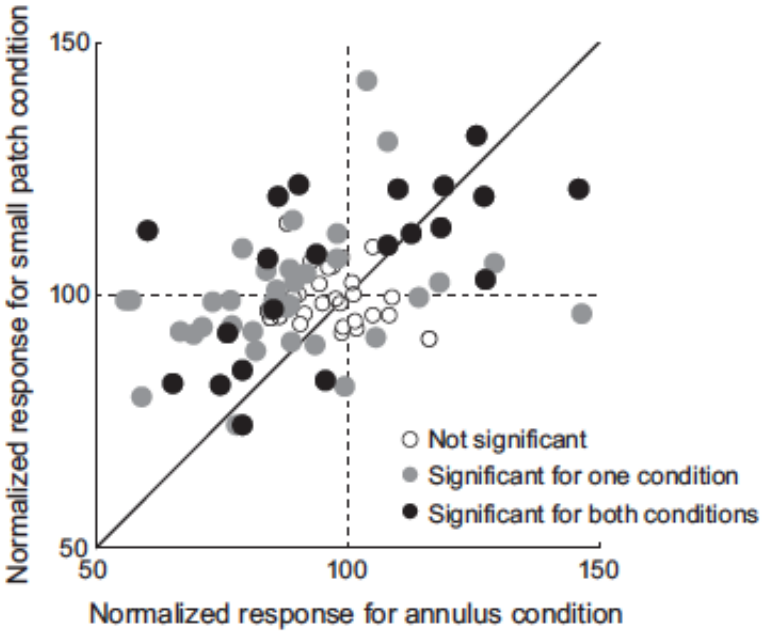

Figure 1.5. Modulation strength comparison: annulus vs. small patch pattern. Each circular symbol (N = 92) represents the mean value of normalized responses for four "center + surround" conditions (e.g., 1~4th bar in Figure3B). Abscissa values are for annulus conditions and ordinate levels are for small patch trials. Shading of circles convey statistical significance (two-sided Mann-Whitney U-test ($p<0.05$)) of center-surround modulation (open circles: not significant for either condition, gray filled: significant for only one condition. black filled: significant for both conditions). Symbols in left half of the graph mean that suppressive modulation is induced by annulus surround pattern. Almost all symbols in left half of the graph are positioned above the diagonal line (55 vs. 9). This means that

neural responses to small patch surround patterns are stronger than those for the annulus. This follows because of surround facilitation (in 2nd quadrant, top left) or weakened surround suppression (in 3rd quadrant, bottom left). Symbols in the right half (facilitation cases for the annulus pattern) are positioned mainly in the 1st quadrant (top right), and rarely in the 4th quadrant (bottom right). Within the 1st quadrant, symbols are evenly distributed with respect to the diagonal line (9 vs. 9). This means that surround facilitation induced by the small patch surround can be either weaker or stronger than that caused by the annulus. These results support the idea that suppressive modulation requires stronger surround input than that for facilitation (see details in text).

To test these predictions, we compare response magnitude for the annulus surround pattern with that for small patches. In Figure 1.5, each data point represents an individual cell. For each cell, neural responses of the four "center + surround" conditions are normalized (as in Figure 1.2B) and then averaged (annulus surround: abscissa, small patch surround: ordinate). Therefore, a value smaller (or larger) than 100 on each axis means suppressive (or facilitative) surround modulation. Statistical significance (two-sided Mann-Whitney U-test ($p<0.05$)) of surround modulation for each data point is expressed as different shading levels within circular data points (open circles: not significant for either condition, gray filled: significant for only one condition. black filled: significant for both conditions). The vertical dashed line divides suppressive modulation (left) from that for facilitation (right) for the annulus surround pattern. Similarly, the horizontal dashed line separates suppressive (below) from facilitative modulation (above) for the small patch surround stimuli.

The normalized response for the annulus condition is positively correlated with that for the small patch. ($r=0.47$, $p<0.0001$), indicating that there is a general trend of suppressive (facilitative) modulation from the annulus and the small patch. However, data points on the left half of Figure 1.5 are more numerous than those on the right (64 vs. 28, one-sample t-test, $p<0.01$), showing that the dominant sign of surround modulation for the annulus is suppression. Furthermore, most data in the left half fall above the diagonal line (55 vs. 9, paired-sample t-test, $p<0.01$). This means that the neural responses to small patch surrounds are stronger than those for the annulus condition (small patch facilitation in the 2nd quadrant (top left) or suppression in the 3rd (bottom left)). For data points in the right half, nearly all are in the 1st quadrant (top right). The data points in the 4th quadrant (bottom right) do not exhibit significant (Two-sided Mann-Whitney U-test ($p<0.05$)) suppression for the small patch. Within the 1st quadrant, data points are evenly distributed with respect to the diagonal line (9 vs. 9, paired-sample t-test, $p=0.74$). This means that surround facilitation induced by small patch stimuli can be weaker or stronger than that induced by an annulus. These results are consistent with our predictions as outlined above.

1.4.3. Annulus surround stimulus increases LFP power spectra in the range of high gamma frequency

We establish here that center-surround modulation caused by an annulus differs

from that for a small patch in magnitude and in sign. When an annulus or a small patch is presented without a center stimulus (i.e., "surround alone" condition), by definition, neither can evoke spiking activity. To make a difference in center-surround modulation, outside CRF stimuli must have different effects at sub-threshold levels.

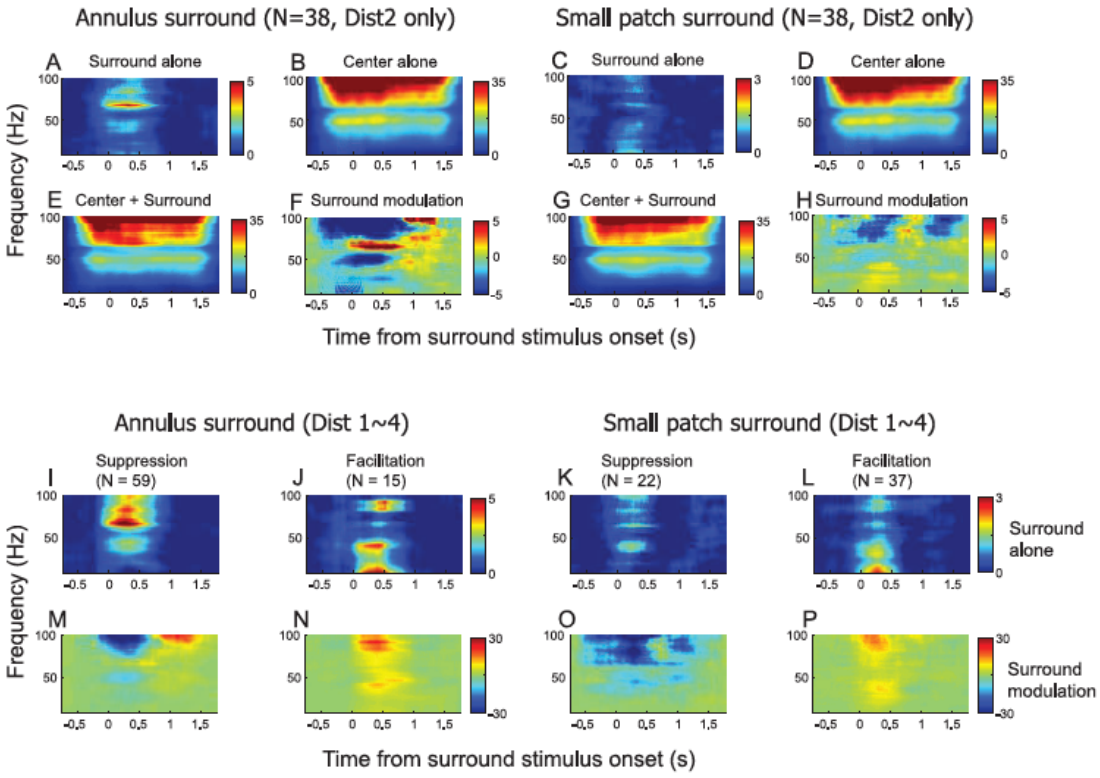

Figure 1.6. Population average z-scored LFP spectrograms. For a 10~100Hz frequency range, LFP power change from the baseline is plotted as a function of time. (Left two columns) Annulus surround pattern, (Right two columns) Small patch surround pattern. **(A~H)** To exclude effects of spiking activity on LFP spectrograms, 38 tests are used for which the "surround alone (dist2)" condition, for both surround patterns, does not evoke spiking activity. For the "surround alone" condition, the annulus causes a larger change in LFP power than that for the small patch (A vs. C), and the main change is focused on the high gamma frequency range (approximately 60~80Hz). This 60~80Hz frequency specific change in annulus surround alone result is also revealed in F, reflecting center-surround modulation of the LFP spectrogram. **(I~P)** Z-scored LFP spectrogram comparisons: surround suppression vs. surround facilitation. For each surround pattern, population data are divided into two groups: suppression vs. facilitation. Again, the tests included in this analysis do not evoke spiking responses for the "surround alone" condition so they are distinguishable only at subthreshold levels (I, J, K, & L). Note for the annulus surround, that increased LFP power in the 60~80Hz range (as shown in panel A) is clear for suppression (I), but not for facilitation (J). Regardless of surround type, facilitation cases of the "surround alone" conditions (J & L) are similar in that LFP power change for the low frequency range is bigger than that for high frequencies. Depending on the sign of modulation, center-surround effects in LFP spectrograms show the largest differences in the 80~100Hz frequency range (M vs. N or O vs. P). LFP power in this range decreases for suppression cases, but increases for facilitation.

Local field potentials (LFPs) are believed to reflect mainly dendritic activity, i.e., neuronal input, including sub-threshold components (Logothetis, 2003; Mitzdorf, 1985). We computed z-scored LFP power spectrograms (see Experimental procedures section) for "surround alone" conditions and compared effects for annulus and small patch surround stimuli. For the nearest (dist1) "surround alone" condition, surround stimuli often partially invade the CRF and generate weak but significant spiking activity (see Figures 1.2 and 1.3). In order to exclude an effect of spiking activity on LFP signals in the "surround alone" condition, 38 recordings are used for which spiking activity in the "surround alone (dist2)" condition is zero.

For both surround stimulus patterns, the "surround alone" condition yields LFP power spectra as shown in Figure 1.6A & C. Responses were clearly much larger for the annulus surround compared to that for the small patch. In addition, for the annulus pattern, increased LFP power spectra is focused mainly in a high gamma frequency range (around 60~80Hz). In contrast, the small patch surround pattern yields LFP power increases in a lower frequency range (less than 40Hz).

We next created a center-surround modulation matrix of LFP spectrograms by subtraction of the "center alone" LFP spectrogram (Figure 1.6B & D) from that of the "center + surround" (Figure 1.6E & G). The resultant matrix (Figure 1.6F & H) is then compared with the "surround alone" LFP spectrogram (Figure 1.6A & C). During the 0~500ms interval, the data in Figure 1.6A & F share the property that LFP power is maximally increased in the 60~80Hz frequency range. Also, during the same interval, data in Figure 1.6C & H both have maximum LFP power increases in the <40Hz frequency range. The center-surround modulation of the LFP spectrogram also has features that are not consistent with linear summation. In Figure 1.6F & H, the blue coded component indicates that LFP power is lower for the "center + surround" condition compared to that for "center alone". This is different from the data in Figure 1.6A & C, since the LFP spectrograms of "surround alone" conditions have only positive values.

1.4.4. In "surround alone" condition, increased LFP power spectra (high gamma range) is associated with suppressive modulation.

We show above that a sub-threshold level difference between "surround alone" conditions for the two types of surround is reflected in the LFP signal. Although the LFP signal evoked only by an annulus surround shows stronger amplitude than that for a small patch over the entire frequency range (10~100Hz), the difference is most salient at high gamma levels (around 60~80Hz). Previous studies show that large gratings tend to produce stronger power in the gamma frequency range (Berens, Keliris, Ecker, Logothetis, & Tolias, 2008a; Gieselmann & Thiele, 2008; Jia, Smith, & Kohn, 2011). However, our findings show that suppression is more prominent than facilitation for the annulus surround conditions (Figures 1.4 & 1.5). To pursue this in the local field potential domain, we examine increased LFP power

in the 60~80 Hz frequency range to determine if it is associated with suppressive modulation and stimulus size. For each surround pattern, population data are divided into two groups based on differences of spike response between "center only" and "center + surround" conditions: one for suppressive and the other for facilitative modulation. For each annulus and small patch surround type, facilitation and suppression groups are taken from different neural populations. In this way, we do not have a center-surround distance limit for the creation of Figure 1.6I~J (Dist1~4 conditions are all considered). Cases that show spiking activity for "surround alone" conditions are not included in the analysis.

For the annulus surround pattern, LFP spectrograms in "surround alone" condition clearly differ with the sign of surround modulation. For the suppression group (Figure 1.6I), the largest increase of LFP power is observed in a >60Hz frequency range as shown above in Figure 1.6A. For the facilitation group (Figure 1.6J), an increase of LFP power is apparent in a <40Hz frequency range. These results show that coherent gamma rhythms for the annulus (Figure 1.6A vs. C) are not entirely due to different stimulus size. Furthermore, although differences between the two groups for the small patch surround are less clear than those for the annulus, a prominent dissimilarity is clear. An increase of LFP power in the <40Hz frequency range is much bigger for facilitation than for suppression (Figure 1.6K & L). The differences in center-surround modulation of LFP spectrograms between suppression and facilitation are reflected in the highest frequency range (>80Hz). Regardless of stimulus pattern, suppression (Figure 1.6M & O) and facilitation (Figure 1.6N & P) groups are characterized by decreased and increased LFP power, respectively. These results are consistent with a previous study that showed positive correlation between high gamma LFP and spiking activity (Belitski et al., 2008).

1.4.5. Time course of surround modulation

Surround modulation latency is the time when the spike density function of a "center + surround" condition begins to be differentiated from that of "center alone". Since conduction velocities of feedback connections are on average 10 times faster than those of the horizontal type (Girard et al., 2001), observation of variation of surround modulation latency, depending on center-surround distance, is necessary in order to demonstrate that horizontal and feedback connections are separated in our experimental design.

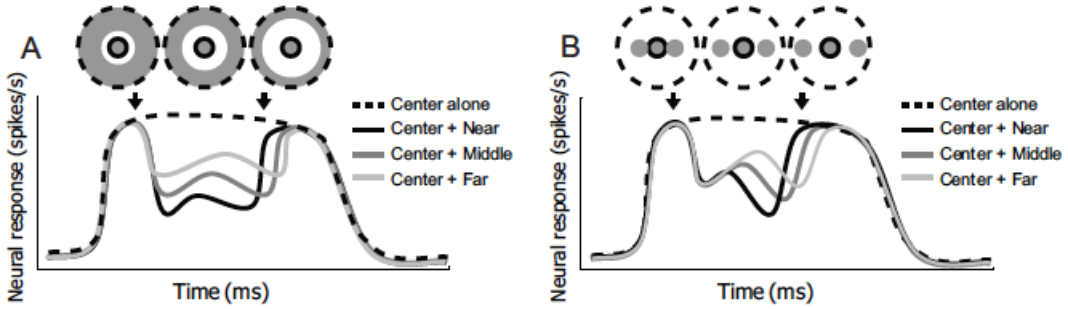

Figure 1.7. Predictions for time course of surround modulation. The first and second downward arrows represent onset and offset of surround stimuli, respectively. Therefore, the center stimulus is presented earlier and lasts longer than that for the surround. Time courses depicted in darker shades indicate nearer center-surround distances. The predictions are based on the following assumptions. 1) Surround modulation is mediated by both feedback and horizontal connections. 2) There is limited interaction between the two types of neural connections. 3) Given that conduction velocities of feedback connections are much faster than those for the horizontal type, the earliest part of surround modulation is mediated by feedback connections. 4) The onset of the feedback component of surround modulation is minimally affected by center-surround distance. 5) The onset of the horizontal component of surround modulation is increasingly delayed as center-surround distance increases. **(A)** Annulus surround pattern: Increasing center-surround distance causes decrease in both feedback and horizontal components of surround modulation. So, differences between middle and far conditions occur at the same time as those between near and far. **(B)** Small patch surround pattern: Increasing center-surround distance causes selective decrease of horizontal component of surround modulation. So, differences between middle and far conditions are delayed more than those between near and far.

We note above (Experimental procedures section) that the annulus surround pattern is not appropriate for selective control of the horizontal connection component of surround modulation, because both horizontal and feedback types are weakened as center-surround distance increases. Based on this, we make a simple prediction about surround modulation latency in Figure 1.7A. The prediction is that surround modulation consists of feedback and horizontal components. Interaction between the two components and the possible contribution of feedforward connections (Ozeki et al., 2004; Webb, Dhruv, Solomon, Tailby, & Lennie, 2005) may be involved but are not considered. The dashed curve represents neural response for the center alone condition and the other three solid curves in grayscale indicate those for center + near, middle, and far surround conditions in order of darkness. Onset and offset times of surround stimuli are marked as two downward arrows at the top of the curves. Fast feedback connections are responsible for the initial part of surround modulation. Depending on center-surround distance, this feedback component varies in magnitude but not in latency. A slow horizontal component occurs in a later part of surround modulation. It varies in latency as well as magnitude for subsequent surround stimuli. Figure 1.7B shows a different prediction for a small patch surround. The same conventions are used as in Figure 1.7A. Since small patch surrounds are designed to maintain activation levels of feedback connections, regardless of center-surround distance, initial parts of

surround modulation are constant both in magnitude and latency. The differences between near and far surround conditions are expected to be only revealed in a subsequent horizontal component participation.

As noted below, it is difficult to define surround modulation latency for most cells in our population (see Discussion). As an alternative, we use a population surround modulation function so that curves of individual neurons (e.g., Figure 1.2C or Figure 1.3C) are normalized and then averaged. The analysis is as follows. First, we choose 41 of 97 annulus surround tests for which neural activity is significantly suppressed (two-sided Mann-Whitney U-test, $p<0.05$) for the nearest (dist1) "center + surround" condition. Second, for each of these 41 tests, surround modulation curves of four "center + surround (dist 1-4)" conditions are transformed to z-scores using a baseline (from -500ms to 0ms before surround stimulus onset) mean and standard deviation. Third, the resulting baseline adjusted z-score surround modulation curves are averaged across the 41 tests. The same procedure is used for 16 small patch surround tests that show significant (two-sided Mann-Whitney U-test, $p<0.05$) surround suppression. The results are depicted in Figure 1.8A (annulus) and Figure 1.8C (small patch). Again, two downward arrows indicate onset and offset of surround stimuli. Different levels of center-surround distance are expressed as the degree of darkness of solid curves (The darker is the nearer). The main predictions for the four annulus and small patch conditions are as follows. In the annulus condition, differences depending on center-surround distances are reflected in both feedback and horizontal components. Therefore, stronger modulation for a closer surround location will be observable even from the earliest part of the surround modulation time course. Modulation onset delay for a far surround, which is supposed to appear in a later portion of the time course (horizontal component), is problematic because feedback and horizontal components are not entirely separated. For the small patch condition, however, only the horizontal component is affected by center-surround distance, so this can be segregated from the feedback role by subtracting the modulation time course of "center + dist4" from each of the "center + dist1,2,3" time courses. Compared with the difference between "center + dist1" and "center + dist4", those between "center + dist2 or 3" and "center + dist4" are not only smaller in magnitude but also temporally delayed. And these systematic variations are reflected in later rather than earlier parts of the modulation time course.

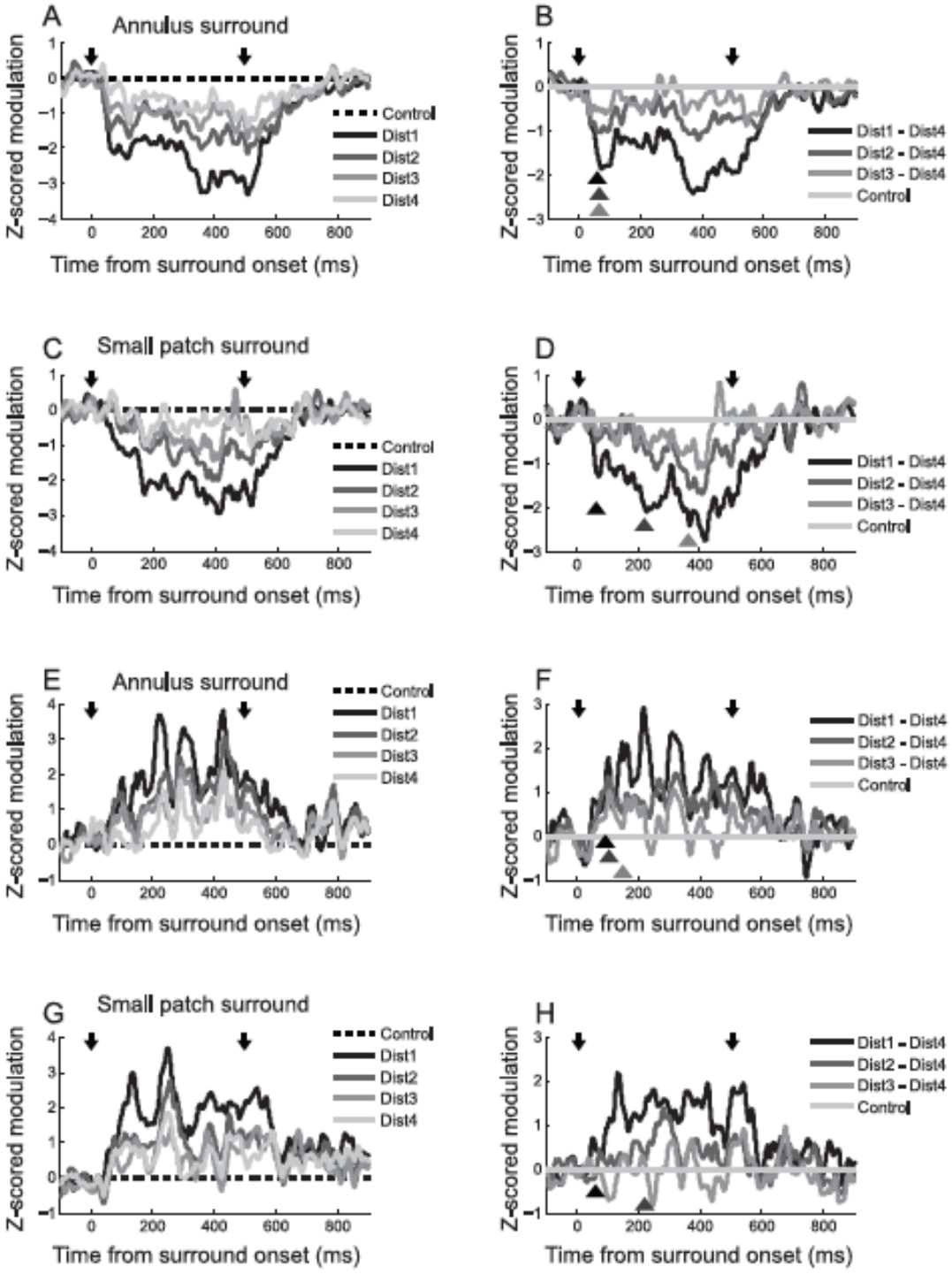

Figure 1.8. Time course of surround modulation: Suppression (A, B: Annulus surround / C, D: Small patch surround), Facilitation (E, F: Annulus surround / G, H: Small patch surround). Two downward arrows indicate onset and offset of surround stimuli, respectively. Nearer center-surround distances are depicted in darker shades. **(A, C, E, G)**: Differences between "center alone" control and each of four "center + surround" conditions are z-score normalized using mean and standard deviation of differences during baseline periods (from -500ms to 0ms before surround stimulus onset). The dashed line serves as a reference for comparison among conditions. **(B, D, F, H)**: Dist4 curve is

subtracted from each of four gray curves. The positions of three triangles indicate onset times of significant difference (two-sided Wilcoxon signed rank test in the 100ms sliding window, $p<0.05$) between each of Dist1~3 curves and control (Dist4). In (H), difference between Dist3 and Dist4 is not statistically significant, so only two triangles are drawn. For annulus surround pattern (B, F), differences between the resultant three curves appear from the initial part of the modulation without substantial difference in onset delay depending on center-surround distance. However, for the small patch surround pattern (D, H), difference between Dist2 or 3 and Dist4 appear later than those between Dist1 and Dist4.

The time course for surround modulation is illustrated In Figure 1.8. In Figure 1.8A, suppression begins around 50ms after annulus onset and is maintained while center and surround regions of the CRF are stimulated together (0~500ms). At the end of the surround period, suppression is diminished and disappears about 300ms later than surround offset. As predicted in Figure 1.7A, surround modulation curves are similar in shape and have varying effects depending on center-surround distance. In Figure 1.8B, modulation curve of "center + dist4" condition is subtracted from those of the other nearer conditions. Onset times of significant difference (two-sided Wilcoxon signed rank test in the 100ms sliding window, $p<0.05$) are marked as triangles below the curves. Differences between "center + middle (dist2 or 3)" and "center + far (dist4)" conditions are seen from the earliest part of the surround modulation time course. A similar pattern is seen for the difference between "center + near (dist1)" and "center + far (dist4)" conditions (Figure 1.8B).

On the other hand, when surround modulation is induced by small patch stimuli, overall shapes differ depending on center-surround distances (Figure 1.8C). For the "center + dist1" condition, suppression begins at around 50ms as it does for the annulus surround. But for the other three conditions ("center + dist2,3,4), it occurs tens of milliseconds later. We do not predict an earlier onset for the "center + dist1" condition. Feedforward connections may be involved in the earlier suppression onset. Previous studies suggest that feedforward connections participate in the initial part of surround suppression by withdrawal of excitation (Ozeki et al., 2004; Webb et al., 2005). However, feedforward connections to early surround suppression are spatially limited to very close surround areas (Angelucci & Bressloff, 2006) . Therefore, if feedforward contributions occur in the "center + dist 1" condition but not in the other (further distance) configurations, a result like that illustrated in Figure 1.8C is likely.

Except for the "center + dist1" condition, the other three curves ("center + dist 2,3,4" conditions) of Figure 1.8C resemble those of Figure 1.7B in that relative differences among the three curves occur in a later part of the modulation time course (>200ms). Moreover, consistent with the prediction outlined above, the onset of differences between "center + middle (dist2 or 3)" and "center + far (dist4)" conditions is relatively delayed compared to those between "center + near (dist1)" and "center + far (dist4)" conditions (triangles in Figure 1.8D). Similar results occur for the time course of facilitative surround modulation (15 annulus surround tests & 26 small patch surround tests, Figure 1.8E~H). Considered together, these results

suggest that differences depending on center-surround distances for small patch stimuli are mediated mainly by slow horizontal connections (but see Discussion 4.5 for limitations).

In the cat's visual cortex, the average cortical magnification factor for 1 degree in the central visual field is assumed to be 1 (1 mm2/deg2) and conduction velocities of horizontal connections range from 0.1 to 0.4m/s (Albus, 1975; Angelucci & Bullier, 2003; Bringuier et al., 1999; Girard et al., 2001; Grinvald et al., 1994). Previous studies have shown that sub-threshold input from visual stimuli presented outside the CRF is transmitted with a velocity which is well matched to conduction times in the horizontal connection system (Bringuier et al., 1999; Grinvald et al., 1994). When these values are considered in the current study, modulation onset delay between near and far surround conditions (temporal interval between adjacent triangles in Figure 1.8D) is expected to be as short as tens of milliseconds. However, we observe much longer modulation onset delay times (about 150ms) in our data. This suggests that unlike sub-threshold input, supra-threshold suppression or facilitation may require additional integration processes.

1.5 Discussion

We have designed visual stimuli to differentially activate three major routes of visual processing: feedforward, feedback, and horizontal connections in order to determine relative functional differences. To achieve this, stimuli are presented within and beyond the CRF. Two different surround stimulus patterns (annulus and small patch) are used and distances are varied between CRF stimuli and those in the surround. Both patterns cause response modulation that decreases as center-surround distance is increased. Annulus stimuli have mainly suppressive effects while small patch patterns more frequently cause facilitation. This difference is also expressed for different frequency bands of LFPs. As CRF-surround distance is varied, modulation time course changes as follows. For the annulus, differences between near, middle, and far surround positions occur from the initial phase of modulation. For the small patch, center-surround distance dependent changes occur at later phases of the modulation time course. Moreover, temporal delay between middle and far surround conditions is increased compared to that between near and far positions. This implies that center-surround distance dependent changes of response modulation are due mainly to activation levels of slow horizontal connections.

1.5.1. A comparison of annulus and small patch stimuli

In previous studies with these types of stimuli, center-surround distance was varied by either an annulus whose outer diameter was fixed and inner diameter systematically varied (Bair et al., 2003; Ichida, Schwabe, Bressloff, & Angelucci,

2007; Levitt & Lund, 1997) or by small patches whose position was progressively moved away from the CRF (Bringuier et al., 1999; Kim, Kim, Kim, & Lee, 2012; Mizobe & Polat, 2001). With both types of surround stimuli, the magnitude of modulation is gradually decreased with increasing distance between center and surround. While our current results are consistent with this, our stimulus design additionally provides detailed comparisons for each neuron between annulus and small patch stimuli. This provides new insights about relative pathway functions.

One obvious difference between the two types of surround stimuli we have used here is that surround areas occupied by an annulus are much larger than those for small patches. For this reason, at a given center-surround distance, an annulus can induce modulation more effectively than that for a small patch. A larger stimulated area (i.e., a stronger surround input) also seems to be related to higher occurrence rates of suppressive (rather than facilitative) modulation for annulus compared to small patch conditions (Figure 1.4 & 1.5) as considered below.

Note that the small patch surround is different from the annulus type in that the former is independent of stimulus size variation. This is advantageous, because it allows activation levels of feedforward connections to be relatively stable. Therefore, in the small patch surround condition, differences in modulation that depend on center-surround distance are probably mediated by horizontal connections. In summary, we show here that time courses of surround modulation for small patch conditions are clearly distinguished from those for the annulus (Figure 1.8).

1.5.2. Surround modulation: suppression vs. facilitation

Previous investigations show that modulation is strong when center and surround stimuli share similar stimulus parameters (Blakemore & Tobin, 1972; Cavanaugh et al., 2002b; DeAngelis, Freeman, & Ohzawa, 1994). In addition, surround regions separated by identical distances from the center do not necessarily produce the same modulation effects (Cavanaugh et al., 2002b; Kapadia et al., 2000; Walker et al., 1999). Effective positions of surround stimuli are often asymmetric and an influential location is frequently one or both end-zones on the axis of preferred orientation. These characteristics may be mediated by long-range horizontal connections in cortical layer 2/3 (Chisum, Mooser, & Fitzpatrick, 2003; Hirsch & Gilbert, 1991; Malach, Amir, Harel, & Grinvald, 1993; McGuire et al., 1991; Rockland & Lund, 1983). Anatomically, they extend several millimeters parallel to the cortical surface (Bosking et al., 1997; Kisvárday et al., 1997).

Reports vary regarding frequencies of suppressive and facilitative modulation. Some find mainly suppressive modulation (Cavanaugh et al., 2002b; DeAngelis et al., 1994; Grinvald et al., 1994; Walker et al., 1999) while others report prevalent facilitation (Kapadia, Ito, Gilbert, & Westheimer, 1995; Nelson & Frost, 1985; Toth et al., 1996). Cortical neurons with similar extra-CRF properties (inhibitory or excitatory) may be clustered (Yao & Li, 2002). This finding is consistent with our current data in that

surround modulation induced by a given stimulus pattern may cause either suppression or facilitation. However, we also find that for a given cell, the sign of modulation can change from suppression to facilitation as center-surround distance increases or size of the surround stimuli decreases. This finding is in accord with a previous result showing that facilitative surround modulation can be changed into suppression by increasing surround size or center contrast (Ichida et al., 2007). Considered together, suppressive modulation may require stronger input from the surround than that for facilitation.

Surround modulation has also been studied with visual stimuli of varying contrast levels (Levitt & Lund, 1997; Polat, Mizobe, Pettet, Kasamatsu, & Norcia, 1998; Toth et al., 1996). We have not varied contrast in the current work but consider here how it may be relevant to our scheme. To encompass surround facilitation or suppression, both excitatory and inhibitory interneurons must be involved. Specific interneurons must receive input from the CRF and surrounding region. Inhibitory interneurons should have higher activation thresholds than excitatory types. When input to interneurons is not strong because of low stimulus contrast or long center-surround distances or small sized visual stimuli, excitatory interneurons (but not inhibitory) are activated so that surround facilitation can occur. If input is strong enough to activate inhibitory interneurons, surround facilitation will be canceled out and replaced by surround suppression. Our current data (see Figure 1.5) are consistent with this process.

1.5.3. Gamma frequency range of local field potential

The annulus surround is more effective for inducing modulation than the small patch. The dominant sign of modulation is also different for the two stimulus patterns. For the annulus, suppression dominates facilitation. For the small patch, facilitation occurs slightly more often (Figure 1.4). The CRF stimulus for the current experiments is always defined as the optimal grating that evokes maximum neural response. By definition, the annulus and small patch surround stimuli cannot evoke any spike activity in the “surround alone” condition. However, with power spectral analysis of the LFP, we observe that surround stimuli are distinguishable at sub-threshold levels (Figure 1.6). In the “surround alone” condition, the annulus causes more change in LFP power than the small patch, and the main change is focused in the high gamma frequency range. The magnitude of gamma frequency LFP monotonically increases with size of the visual stimulus (Berens, Keliris, Ecker, Logothetis, & Tolias, 2008b; Gieselmann & Thiele, 2008; Jia et al., 2011), and the maximum increase occurs when a stimulus overlaps the CRF surround (Gieselmann & Thiele, 2008). Another variable that can affect gamma frequency LFPs is stimulus contrast. High stimulus contrast apparently causes considerable LFP gamma oscillation, and the maximum increase of gamma frequency power occurs when single unit activity is saturated (Henrie & Shapley, 2005). The results above suggest that gamma frequency oscillations in LFPs may reflect activation of inhibitory interneurons in addition to the responses to stimulus size or contrast levels. Our current data are consistent with this idea. Increased gamma frequency LFP power

for the “annulus surround alone” condition appears only with the suppression group (Figure 1.6I) and not for facilitation (Figure 1.6J).

1.5.4. Surround modulation latency

Comparisons of surround modulation time courses between different center-surround conditions are required to determine if horizontal and feedback components are effectively separated in our experimental design. If differences depending on center-surround distance arise only from the horizontal component, they should be apparent in relatively delayed phases of the modulation time course. Furthermore, differences between dist2 or 3 and dist4 conditions should appear at delayed times with weaker magnitudes compared with those between dist1 and dist4 conditions.

Ideally, surround modulation latency should be defined and compared for individual cells using each of the four center-surround distance conditions. Population data could be summarized in distributions. However, this is problematic because of response variability, occasional weak modulation, and the confounding of suppressive and facilitative patterns within single time courses. Furthermore, responses from simple cells, whose neural activity oscillates at the temporal frequency of the moving grating, often obscures measurement of onset time of surround modulation. If we analyze only complex cells with strong modulation, this can result in a biased outcome. Instead, we use population surround modulation functions for latency comparisons. For this analysis, cells that exhibit significant modulation (two-sided Mann-Whitney U-test ($p<0.05$)) for the dist1 condition are included. Surround modulation functions for individual cells are normalized before being averaged. These procedures minimize the possibility of a biased outcome.

1.5.5. Fast feedback and slow horizontal connections

Previous studies of different functions of feedback and horizontal connections in center-surround modulation rely largely on spatial domain analysis (Angelucci & Bressloff, 2006; Hashemi-Nezhad & Lyon, 2012; Shushruth et al., 2013). This assumes that a surround which is distant from the CRF is out of range of cortical horizontal connections. The assumption is that comparisons between near and far surround conditions will elucidate the role of cortical horizontal connections in surround suppression. The finding that orientation tuning of surround suppression is apparent in near (but not far) surround conditions (Hashemi-Nezhad & Lyon, 2012; Shushruth et al., 2013), suggests that feedback circuits are less orientation biased than horizontal types.

Attempts to segregate feedback and horizontal connections based on differences in the temporal domain are clearly limited. The conduction velocity of horizontal connections is 10 times slower than that of feedback types (Girard et al., 2001). Therefore, surround modulation that is mediated by horizontal connections must be delayed and more sensitive to position change in the surround compared with those

of a feedback type. Orientation-tuned surround suppression is reported to be temporally delayed compared with orientation-unturned surround suppression (C. A. Henry, Joshi, Xing, Shapley, & Hawken, 2013; Liu et al., 2013; Xing, Shapley, Hawken, & Ringach, 2005). However, there appears to be no evidence that the onset of surround modulation is systematically delayed as distance between center and surround stimuli increases. In a previous study of the time-distance relationship for surround suppression in the visual cortex, onset time was reported to be relatively constant as distance between center and surround stimuli was varied (Bair et al., 2003). If surround suppression is mediated by thin unmyelinated horizontal connections from adjacent cortical neurons, the latency of suppression for a distant surround stimulus should be substantially delayed compared to that for a nearby surround. So the finding noted above of non-delayed rapid suppression is probably caused by fast feedback connections from higher visual areas (Bair et al., 2003; Hupé et al., 2001).

In the current study, we use two sets of surround stimulus patterns which demonstrate that the annulus type used in a previous study (Bair et al., 2003) does not permit isolation of temporal parameters of horizontal connection transmission. With our annulus, center-surround distance is controlled by annuli of different widths whose outer diameter is fixed. Increments of center-surround distance are accompanied by decreases of stimulated surround areas (see Figure 1.1A). This causes decreased activation of feedback connections from extra striate cortex and horizontal branches from nearby cortical cells. Therefore, differences of modulation depending on center-surround distance occur from the beginning of the modulation time course which is mediated by fast feedback connections. Differences due to slow horizontal connections are reflected in a later part of the modulation time course. However, differences at later times are also mediated by feedback connections. Hence, we cannot separate contributions of feedback and horizontal connections with the annulus surround. In contrast, the small patch surround allows relatively stable activation levels of feedback connections regardless of center-surround distance. Differences depending on center-surround distance are initially very small but become more obvious at later times in the modulation time course. Also, differences between middle and far surround positions are delayed relatively more than those of near and far, suggesting involvement of slow horizontal connections.

We have shown that the Bair et al. (2003) finding obtained in monkey V1, that surround modulation onset is fast and rarely affected by the inner diameter of an annulus surround, can be replicated in the cat's visual cortex. Additionally, using small patch surround stimuli, we have isolated a slow component of surround modulation which exhibits a systematic delay that depends on center-surround distance. However, our findings have limitations. First, our stimulus design and hypothesis are based on a parsimonious model that surround modulation is explained by linear summation of feedback and horizontal components. Interactions between two components and possible contribution of feedforward connections have not been fully examined. Therefore, we do not have direct evidence that only horizontal connections mediate the slow component of surround modulation.

Second, we do not have precise receptive field (RF) eccentricity information for individual neurons. Visual angles on the retina are mapped in visual cortex with different cortical distances depending on eccentricity. With detailed eccentricity information about individual neurons, it is possible to provide relatively precise estimations of conduction velocity using cortical coordinates of center and surround stimuli. Third, for the slow component of surround modulation which we segregated here, the difference of onset between near and far surround conditions is longer than the temporal delay predicted from well-known conduction velocity estimates. Previous studies suggest that sub-threshold input from the CRF surround is transmitted with conduction velocities which are matched with those of horizontal connections (Bringuier et al., 1999; Grinvald et al., 1994). Our results are different in that we observe supra-threshold modulation, so an additional input integration process may be involved which results in longer temporal delays. These issues may be best approached by use of intracellular recordings.

1.6 Conclusions

Identical CRF stimuli are processed differently depending on overall context. Although previous studies have utilized CRF-surround modulation to elucidate distinctive features of horizontal and feedback connections, the current work provides the following novel findings. First, our results show clearly that activation of inhibitory interneurons requires stronger input from the CRF surround compared with that of excitatory types. Second, sub-threshold inputs from the CRF surround are reflected in different frequency bands of LFP power spectra depending on whether they are suppressive or facilitative. And our current protocol provides a critical isolation of fast and slow components of surround modulation. Furthermore, we show that unlike fast components, slow types are delayed as distance between CRF and surround stimuli increases. Surround information that is not spatially tuned may be processed earlier by fast feedback connections. Spatially tuned surround stimuli presented at specific positions may be processed later by slow horizontal connections. This type of mechanism may apply, e.g., to spatial coarse-to-fine processing found for single neurons in the visual pathway (Allen & Freeman, 2006; Bredfeldt & Ringach, 2002; Frazor, Albrecht, Geisler, & Crane, 2004; Malone, Kumar, & Ringach, 2007; Mazer, Vinje, McDermott, Schiller, & Gallant, 2002; Menz & Freeman, 2003). The results presented here have an important application because they concern areas outside the CRF which by definition cannot initiate spike activity on their own. Manipulations of timing and spatial arrangements of CRF and surround stimuli may enable determinations of the participation of fast feedback and slow horizontal connections for processing global and local visual information.

Chapter 2

Transcranial magnetic stimulation changes response selectivity of neurons in the visual cortex

Preface: This chapter contains material from a manuscript submitted for publication: Kim, T., Allen, E.A., Pasley, B.N., & Freeman, R.D. Transcranial magnetic stimulation changes response selectivity of neurosn in the visual cortex (under review).

2.1 Abstract

Transcranial magnetic stimulation (TMS) is used to selectively alter neuronal activity of specific regions in the cerebral cortex. TMS is reported to induce either transient disruption or enhancement of different neural functions. However, its effects on tuning properties of sensory neurons have not been studied quantitatively. Here, we use specific TMS application parameters to determine how they may alter tuning characteristics (orientation, spatial frequency, and contrast sensitivity) of single neurons in the cat's visual cortex.

Single unit spikes were recorded with tungsten microelectrodes from the visual cortex of anesthetized and paralyzed cats (12 males). Repetitive TMS (4Hz, 4sec) was delivered with a 70mm figure-8 coil. We quantified basic tuning parameters of individual neurons for each pre- and post-TMS condition. The statistical significance of changes for each tuning parameter between the two conditions was evaluated with a Wilcoxon signed-rank test. We generally find long-lasting suppression of responses to visual stimulation which persists well beyond the TMS period. Pre- and post-TMS orientation tuning curves show similar peak values for a given neuron. However, strong suppression at non-preferred orientations following TMS tends to narrow the widths of tuning curves. Spatial frequency tuning exhibits an asymmetric change in overall shape, which results in an emphasis on higher frequencies. Contrast tuning curves show nonlinear changes that are consistent with a gain control mechanism. These findings suggest that TMS causes extended interruption of the balance between sub-cortical and intra-cortical inputs.

2.2 Introduction

Historically, numerous attempts have been made to alter brain activity in both normal and abnormal physiological conditions. A prominent approach has been used to modify function by use of the external application of electrical fields (Goddard, McIntyre, & Leech, 1969; Merton & Morton, 1980; Racine, 1972). In addition to attempts to alter normal function, approaches have been used to treat clinical disorders by use of electrical stimulation. A relatively noninvasive technique, transcranial magnetic stimulation (TMS), has been shown to modify motor function in the human brain (Barker, Jalinous, & Freeston, 1985; Pascual-Leone et al., 1995). This has led to numerous studies (M Hallett, 2000; Rossi, Hallett, Rossini, & Pascual-Leone, 2009; Wassermann & Lisanby, 2001).

Although consequences of specific parameters of TMS have been studied, numerous factors complicate interpretation. Variables include: different brain regions and cell types, various synaptic mechanisms, input and output patterns to local areas of the brain, and stimulation parameters. Reported TMS neural findings include: facilitation or suppression or both in specific brain areas (R. Chen, Classen, & Gerloff,

1997; Nakamura, Kitagawa, Kawaguchi, & Tsuji, 1997; Pascual-Leone, Valls-Solé, Wassermann, & Hallett, 1994; Peinemann et al., 2004). Variability of TMS effects is substantial within both normal and abnormal subject populations (Maeda, Keenan, Tormos, Topka, & Pascual-Leone, 2000; Valls-Sole et al., 1994). In addition, TMS effects may rely on initial cortical activation state or excitability levels of specific neural populations (Pasley, Allen, & Freeman, 2009; Siebner et al., 2004; Silvanto, Muggleton, Cowey, & Walsh, 2007)

This background suggests the need for a focused procedure with limited parameters. The physiological parameters of individual visual cortical neurons are well established. In addition, we have previously studied these responses in relation to hemodynamic signals and state dependent characteristics following TMS application (Allen, Pasley, Duong, & Freeman, 2007; Pasley et al., 2009). Here, we investigate how basic tuning properties of cortical cells are affected by repetitive TMS (rTMS).

Although TMS effects on neural selectivity have been addressed previously (Cattaneo, Rota, Walsh, Vecchi, & Silvanto, 2009; Hotson, Braun, Herzberg, & Boman, 1994; Silvanto, Muggleton, & Walsh, 2008), former work concerned neural selectivity at the population levels. They involved causal relations between targeted brain area and behavioral tasks. Our current study involves TMS effects on cortical response selectivity, quantified at a cellular level. Based on well-established knowledge of the central visual pathway, our findings provide clues for understanding neural mechanism of TMS effects.

2.3 Materials and Methods

2.3.1. Animal preparation

Single unit spikes and LFP data were collected from the visual cortex of anesthetized and paralyzed cats (12 males). All procedures were conducted in accordance with guidelines by NIH and by the Animal Care and Use Committee at the University of California, Berkeley. We induced initial anesthesia with 3% isoflurane and then inserted venous catheters for continuous infusion of drugs during surgery and recording. While a tracheotomy and a craniotomy (Horsley-Clarke coordinates P4L2) were performed, anesthesia was maintained with continuous propofol (20mg/kg·hr) and fentanyl (10μg/kg·hr). After the surgery, infusion rates of continuous propofol (6-8mg/kg·hr) and fentanyl (4μg/kg·hr) were adjusted individually for each animal to be at an adequate level of anesthesia. Then, to prevent eye movements, the animal was paralyzed with continuous pancuronium (0.2mg/kg·hr).

2.3.2. Transcranial magnetic stimulation (TMS)

TMS was delivered with a 70mm figure-8 coil connected to a Magstim Rapid stimulator (Magstim Company, Whitland, UK). Electrode penetration was made at an angle of A45, M0 (Figure 2.1A). This allows the figure-8 coil to be positioned obliquely near the transverse plane superior to the visual cortex (Allen et al., 2007; Pasley et al., 2009). The midpoint of the coil was centered on the left visual cortex craniotomy, 1.5-2cm from the skull. TMS pulse trains (4Hz, 4sec) were delivered by a TTL digital pulse at 80-100% stimulation intensity. At this intensity and range of distances, the induced electric field strength is estimated to be 100-160 V/m (Salinas, Lancaster, & Fox, 2007).

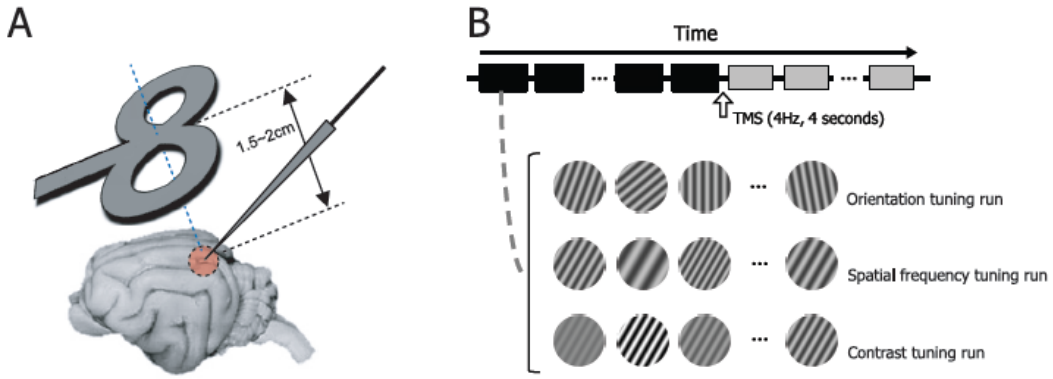

Figure 2.1. Experimental paradigm. **A.** Figure-8 coil is positioned obliquely near the transverse plane superior to the visual cortex (1.5-2cm apart from the cortical surface). Its midpoint is aligned to the left visual cortex craniotomy (Horsley-Clarke coordinates P4 L2). Tungsten electrode penetration is made at an angle of A45, M0. **B.** We examine how rTMS alters selectivity of cells in the visual cortex. To do this, we measure orientation, spatial frequency, and contrast tuning properties of cells and compare the properties between pre- and post-TMS conditions. For each orientation tuning run, 7-10 differently oriented circular grating patches (stimulus duration: 2 seconds, inter-stimulus interval: 2 seconds) are presented in a cell's classical receptive field in each trial (depicted as squares below the time arrow). 4Hz TMS pulse train is delivered for 4 seconds in the inter-trial interval (10 seconds) between 15th and 16th trials. Black and gray colors are used to represent pre- and post-TMS conditions, respectively.

2.3.3. Recording procedure

Neural activity was recorded with two-channel tungsten microelectrodes. Amplified raw signals from each electrode were bifurcated and fed into a band-pass filter to extract spike (500Hz - 8MHz) and LFP (0.7-170Hz) activity. Single units were identified based on spike waveform. Time stamps of single unit spikes and digitized LFPs were saved at resolution of 25kHz and 500Hz, respectively. Analysis methods and results from LFP data are available in Supplementary Materials.

Once a single unit was well isolated, several procedures were run to find the optimal drifting sinusoidal grating stimulus (50% contrast) that evokes the maximum

response of the unit (orientation → spatial frequency → temporal frequency → binocular phase (for binocular cell) → size). The resulting parameters were used to obtain detailed quantitative tuning properties for the main measurements.

To get detailed orientation tuning, we used 10 orientation values for each trial spanning 90° with the pre-determined optimal orientation as the center (e.g., 0-90° at intervals of 10°). The other parameters of drifting sinusoidal grating stimuli were fixed at optimal values. Both stimulus duration and inter-stimulus interval were set at 2 seconds, so a total of 40 seconds was required for all 10 tested orientations to be presented per trial. Short TMS pulse trains (4Hz, 4sec) were delivered just before the beginning of the 16th trial (Figure 2.1B). Fifteen trials before (1st-15th trials) and after (16th-30th trials) the TMS delivery were used to create two orientation tuning curves for the comparison between pre- and post-TMS conditions. Pre- and post-TMS trials corresponded to times of around -12.5 to 0 minutes and 0 to 12.5 minutes, respectively. Procedures to obtain spatial frequency and contrast tuning curves were identical to those for orientation, but the range of 10 tested values was fixed regardless of a cell's preference (Spatial frequency: 0.1-2 c/deg; Contrast: 5~100%; values were evenly distributed on a logarithmic scale). For some cells, fewer values (7 or 8) were tested to save time.

2.3.4. Data analysis

2.3.4.1. Fitting of basic tuning curves

To quantify the effects of TMS on orientation tuning properties, individual tuning curves were fitted with a Gaussian function as follows.

$$R(x) = K \times \exp\left(\frac{-(x-\mu)^2}{2\times\sigma^2}\right) + R_0 \qquad (1)$$

where K is the maximum neural response, x is the orientation, μ is the preferred orientation, σ is the standard deviation of the Gaussian, and R_0 represents the baseline neural response when visual stimulation is not provided. The spatial frequency tuning curves were also fitted with the same function as above, but note that they are not Gaussian shaped when the x-axis is transformed to a logarithmic scale.

The contrast tuning curves were fitted using the Naka-Rushton function (Albrecht &

Hamilton, 1982).

$$R(c) = \frac{R_{\max} c^n}{c^n + c_{50}^n} + R_0 \qquad (2)$$

where $R_{\max}$ is the asymptotic maximum neural response, c is the contrast, c_{50} is the

contrast at which the fitted curve reaches half of the maximum, n is the power function exponent, and R_0 represents the baseline neural response when visual stimulation is not employed.

For individual neurons, tuning parameters were computed for each pre- and post-TMS condition. In order to understand the overall effects of TMS on functional tuning, the statistical significance of changes for each tuning parameter between two conditions was evaluated with a Wilcoxon signed-rank test.

2.4 Results

We studied 133 neurons from the visual cortices of 12 animals. We examined in detail effects of TMS on tuning properties of orientation, spatial frequency, and contrast sensitivity for 35, 32, and 25 cells, respectively (a total of 92 neurons). The excluded cells were either not affected by TMS due to poor positioning of the magnetic coil, lost during recording, or exhibited erratic behavior such as sudden neuronal silence or spike bursts independent of TMS application that prevented quantitative analysis.

2.4.1. TMS effects on orientation tuning: representative neurons

In previous initial studies, we used short TMS pulse trains and found, in most cases, that single unit neural responses in visual cortex were substantially suppressed for long periods (Allen et al., 2007; Pasley et al., 2009). Our current experiments yield similar findings. For this result in Figure 2.2A, the orientation of a grating has been varied between 40° and 130° in 10° steps presented in random order. Orientation is represented along the ordinate and response strength is color-coded according to the scale on the right. Neural activity is strongest in the red region and weakest in the blue. The abscissa shows trial number and time relative to application of TMS. At the top, a scale shows black filled circles followed by gray and then open which represent, respectively, pre-TMS, post-TMS, and recovery conditions. The downward open arrow indicates when TMS has been applied. A relatively wide range of orientations, centered at the peak value of 80°, is active prior to application of TMS. During the first 15 trials prior to delivery of TMS, which corresponds to -12.5 to 0 minutes, neural activity for all orientations tested is relatively stable. After TMS is delivered between the 15th and 16th trial (time = 0), there is a clearly diminished response over the range of tested orientations. Note for this case and in general, TMS induced suppression is sustained for several minutes or more after completion of a 4 second TMS application (see time axis at the bottom of Figure 2.2A).

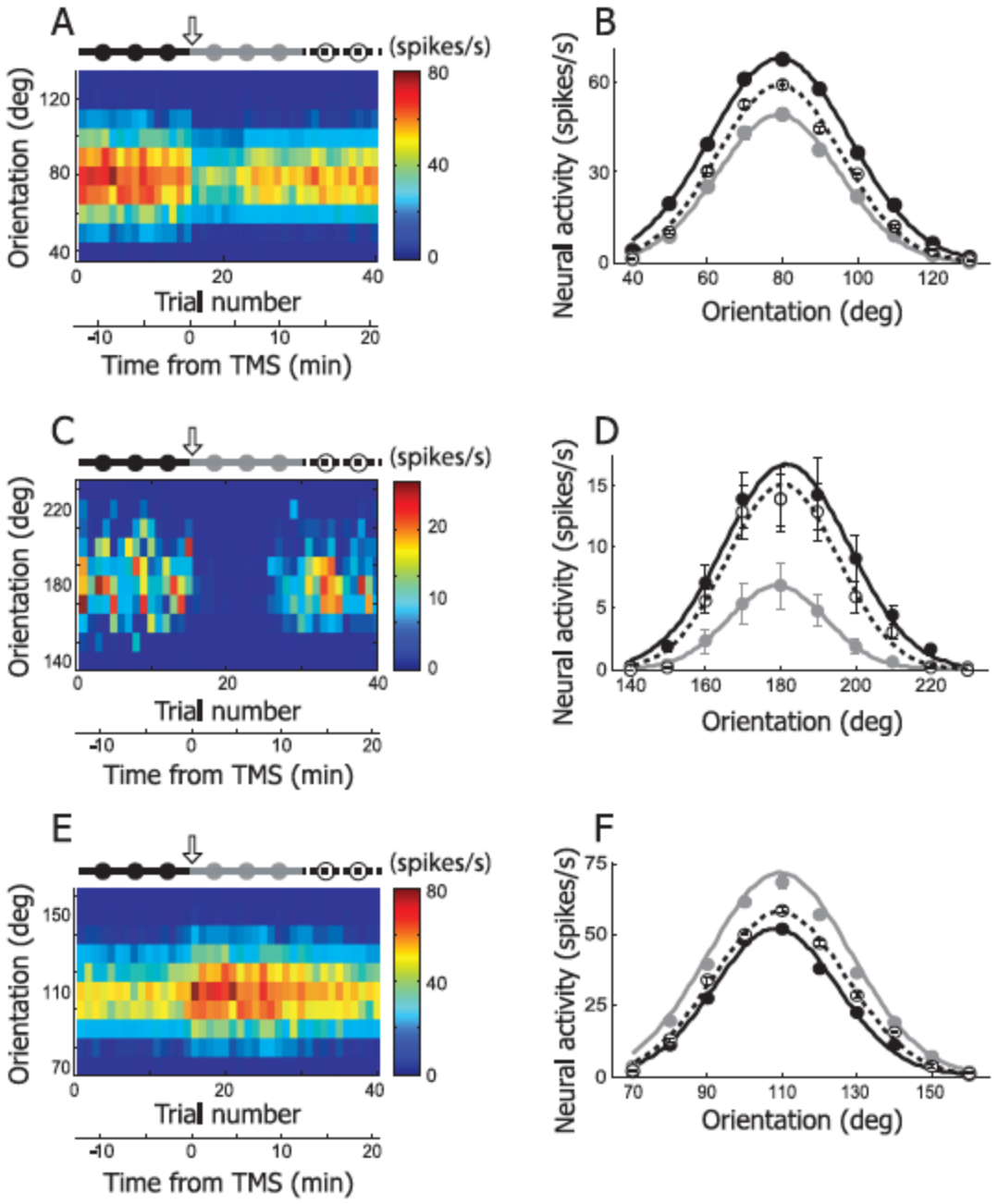

Figure 2.2. Three examples showing TMS effects on orientation selectivity. **A.** Neural response of an example cell is depicted as a form of matrix. X- and Y-axis indicate trial number and orientation, respectively. In each trial (column), 10 different orientations (40-130°, 10° step) were tested. Response magnitude is coded with colors on a blue-red scale. 4Hz rTMS (downward arrow) was delivered for 4 seconds just before the 16th trial. The set of 40 trials was divided into three groups based on elapsed time from TMS delivery: pre-TMS (1-15th trials, black filled circles and line), post-TMS (16-30th trials, gray filled circles and line), and recovery (31-40th trials, open circles and dotted line) conditions. Trial number was translated into time from TMS delivery. Neural response was abruptly changed as soon as TMS was applied. The TMS effect was reversible and it lasted for approximately 10 minutes. **B.** Three orientation tuning curves were created from the cell depicted in (A). Black, gray, and open circles are mean neural responses for 10 different orientations computed in pre-TMS, post-TMS, and recovery conditions, respectively. Error bar indicates standard error of

mean. When not visible, error bars are smaller than circles. In these three conditions, the preferred orientation is not changed but response magnitude is clearly diminished in post-TMS condition compared with the other two conditions. More detailed analysis of TMS-effects on orientation selectivity will be dealt in Figure 2.5A~D. **C, D.** Another example cell showing TMS effects on orientation selectivity. The same conventions are used as in (A), (B). The black circle at 180° is hidden by the open one. **E, F.** Our rTMS (4Hz, 4sec) mainly caused prolonged suppression of neural responses in cat's visual cortex (80 out of 92 units). But, in small number of cases, TMS-induced facilitation was also observable. One example is presented here.

These results are shown graphically in Figure 2.2B. Maximum suppression occurs at 80° and responses are reduced on both sides of the peak over the entire responsive part of the tuning curve. Note that the change in neural activity is similar in shape but not in magnitude (black vs. gray line curve), for the preferred orientation (80°) and non-preferred (e.g., 100°). Also, recovery is not complete as the dashed line curve remains lower than that of the pre-TMS condition even at a recovery period of 12.5-22.5 minutes after TMS application.

Another example, presented in Figure 2.2C & D, shows an effect of TMS that is more pronounced than in the previous case. Substantial suppression occurs immediately following TMS delivery (downward open arrow). Note in Figure 2.2C and D, the very low response level during the period indicated by gray dots. The suppression lasted for 12.5 minutes. It is also clear in this case and many others that the lower response after TMS results in a narrowing of the tuning width. Although, again, the recovery brings the response level back to nearly that of pre-TMS delivery, the overall tuning curve response is still slightly lower (dashed line curve) at times of 12.5 to 22.5 minutes after TMS application. The final example of Figure 2 (E and F) is an exception to the general finding that our 4Hz rTMS nearly always results in prolonged suppression of neural responses (80 out of 92 units). For a small number of cases, as in this example, TMS caused facilitation instead of suppression. Note that the pre-TMS filled circles section of the response is considerably lower than that following application of TMS as illustrated by the gray line graph. Again, maximum facilitation occurs at the preferred orientation (110°) and effects tapering off on either side of optimal. Recovery data for this example (dashed line) shows that restoration remains relatively limited and clearly below that of the facilitation level even after periods of 12.5 to 22.5 minutes following TMS.

2.4.2. TMS effects on spatial frequency tuning: representative neurons

As for orientation, spatial frequency is a fundamental parameter of sinusoidal grating stimuli. Similar data to those for orientation are shown using the same format as in Figure 2.2 for TMS effects on spatial frequency selectivity (Figure 2.3). In Figure 2.3A, results are shown for a cell from which responses were obtained for seven spatial frequencies (0.13-1.2 c/deg, evenly distributed on a logarithmic scale) for a total of 40 trials. A short TMS pulse train was applied just before the 16th trial (downward arrow), corresponding to time zero. Graphical results are shown in Figure 3B for spatial frequency tuning curves during pre- and post-TMS conditions,

along with a recovery period. Data have been fit with the same equation as that used for orientation tuning. However, since the spatial frequency axis (X-axis) is transformed to a logarithmic scale, the fitted curve is not Gaussian shaped but has a longer tail on the left side. In the case of TMS-induced suppression, as in this example, the area under the gray curve (post-TMS condition), is smaller than those under the other two curves. The fitting asymmetry causes TMS suppression to be more prominent at low compared to high spatial frequency ranges. In the recovery phase (dashed lines), the original tuning curve is nearly reproduced with slightly diminished response levels. Another example is shown in Figure 2.3C, D. Although the effect of TMS is similar to that of the previous example, the difference between low and high spatial frequencies is more accentuated. In this case, following TMS, high spatial frequencies yield slightly greater neural responses. The recovery curve is again similar to that prior to TMS, but the peak is slightly shifted to the right. A third example (Figure 2.3E, F) shows again the very unusual case of TMS induced facilitation in spatial frequency tuning. Note that the strongest effects are exhibited at low spatial frequencies. Once again, the recovery data (dashed line) show a nearly identical, but slightly reduced, tuning curve as that prior to TMS.

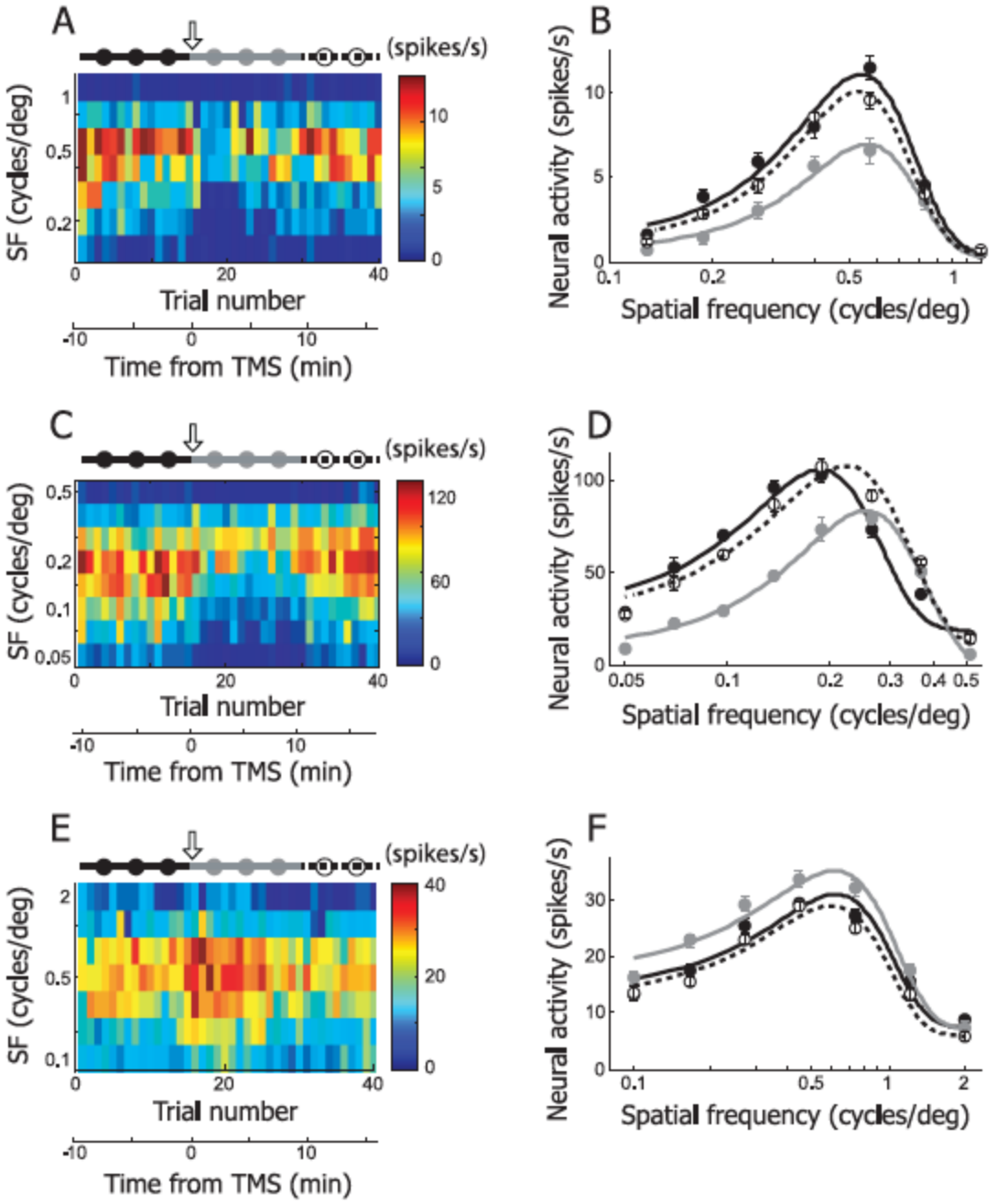

Figure 2.3. Three examples showing TMS effects on spatial frequency selectivity. **A.** In this example cell, neural responses for 7 different spatial frequencies (0.13-1.2 c/deg, evenly distributed along a logarithmic scale) were recorded in 40 trials. The plotting conventions are the same as in Figure 2A. 4Hz rTMS (downward arrow) was applied just before the 16th trial. The set of 40 trials was divided into three groups to create tuning functions in pre-TMS (1-15th trials, black filled circles and line), post-TMS (16-30th trials, gray filled circles and line), and recovery (31-40th trials, open circles and dotted line) conditions. **B.** Spatial frequency tuning curves of pre-TMS, post-TMS and recovery conditions were created from the cell depicted in (A). Equation used for curve fitting is the same as the one used for orientation tuning, but the spatial frequency tuning curve plotted here is not Gaussian shaped, because the x-axis has been transformed to logarithmic scale. The area under the gray curve (post-TMS condition) is smaller than those under the other two curves. Note that TMS-induced suppression is more apparent in low spatial frequency range than high spatial frequency

range. More detailed analysis of TMS-effects on spatial frequency selectivity are shown in Figure 2.5E-H. **C, D.** Another example cell showing TMS effects on spatial frequency selectivity. **E, F.** This example shows TMS-induced facilitation in spatial frequency tuning run.

2.4.3. TMS effects on contrast-response function: representative neurons

The third basic property of cortical tuning that we examined for TMS effects is contrast sensitivity. This is a fundamental tuning parameter and has been investigated in numerous studies of visual function (Albrecht & Hamilton, 1982; Ohzawa, Sclar, & Freeman, 1982; M P Sceniak et al., 1999). Figure 2.4 contains three examples showing effects of TMS on contrast sensitivity. Display format is the same as in the previous figures. In the first example (Figure 2.4A), neural responses are plotted for 10 different contrast values ranging from 5 to 100%, evenly distributed on a logarithmic scale, and recorded in 40 trials. There is a steady gradual increase in response strength as contrast is increased. The sigmoid shaped response function, typical in contrast sensitivity measurements both behaviorally and neurophysiologically, is shown in Figure 2.4B. The curves here are fitted with a Naka-Rushton function (see Materials and Methods). The result of TMS application is a substantial suppression across the entire contrast range with an emphasis in the mid values (gray filled circles). Note that the suppression after TMS varies with contrast levels such that at low and high contrasts, effects are minimal and they are most extensive in the middle range. The subsequent recovery data (open circles with dashed line) is close to but still beneath the original control runs (black filled circles). Another example, Figure 2.4C & D, is similar to the previous cell. But TMS effects are more evenly distributed across a broad contrast range with minimal at the lowest levels. Note also that in this example, recovery data (dashed lines) are superimposed on original control responses with the exception of the highest contrast values tested. The third example, Figure 2.4E & F, shows a more linear contrast response function than in the previous cases. However, there is a striking difference in this case, because TMS has a facilitation effect rather than one of suppression and this is shown clearly throughout the range of contrasts tested except at 100%. For this example, the matrix in Figure 2.4E is missing a component from post-TMS time 12.5 to 22.5 minutes, because neural responses were not recorded during a recovery condition.

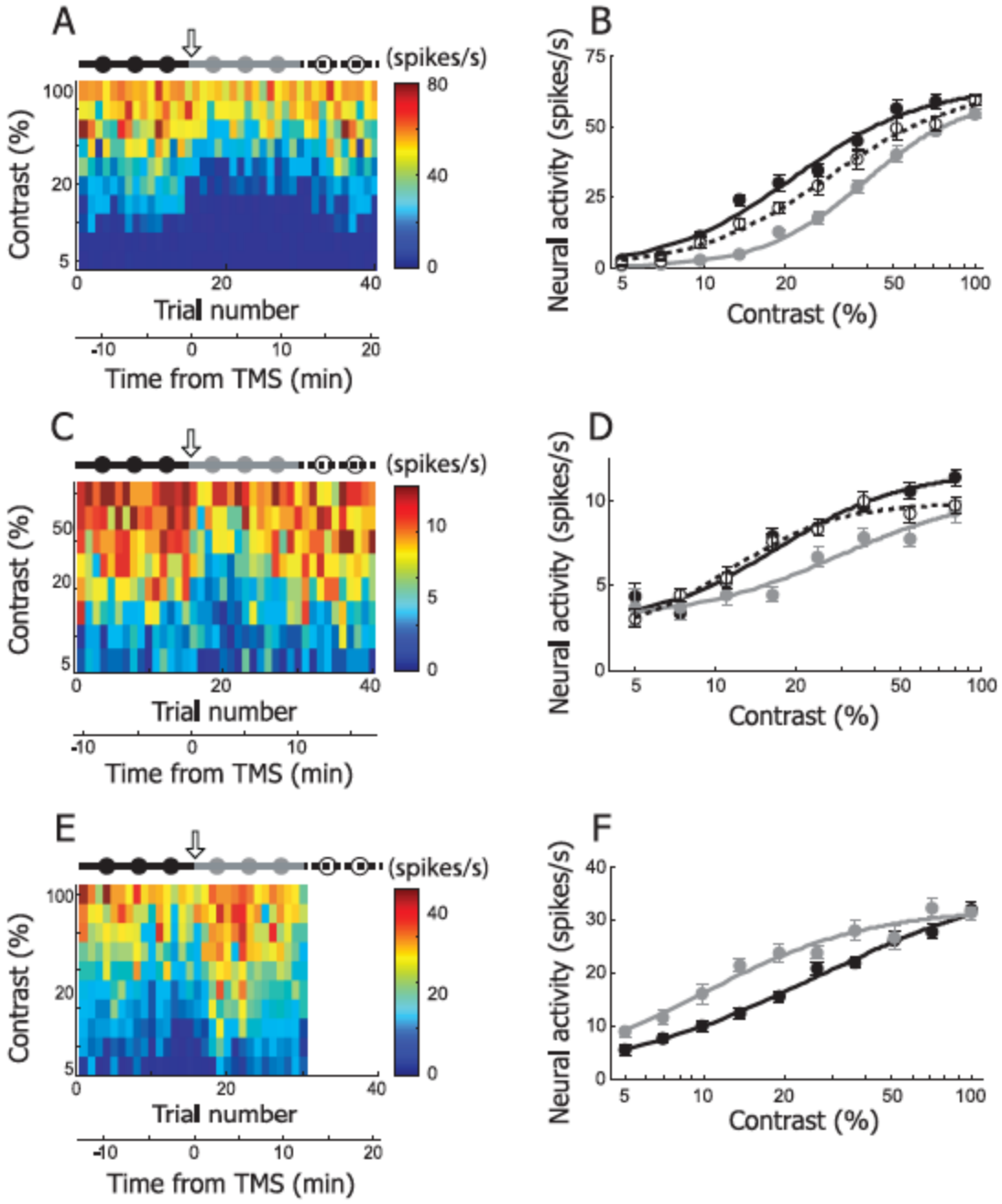

Figure 2.4. Three examples showing TMS effects on contrast selectivity. **A.** In this example cell, neural responses for 10 different contrast values (5-100%, evenly distributed in logarithmic scale) were recorded in 40 trials. The plotting conventions are the same as in Figure 2A. 4Hz rTMS (downward arrow) was applied just before the 16th trial. The set of 40 trials was divided into three groups to create tuning functions in pre-TMS (1-15th trials, black filled circles and line), post-TMS (16-30th trials, gray filled circles and line), and recovery (31-40th trials, open circles and dotted line) conditions. **B.** Contrast tuning curves of pre-TMS, post-TMS and recovery conditions were created from the cell depicted in (A). The curves are fitted with the Naka-Rushton function, $R(c) = \frac{R_{\max} c^n}{c^n + c_{50}^n} + R_0$. The area under gray curve (post-TMS condition) is smaller than those of the other two curves. Note that despite of TMS-induced suppression for middle contrast levels, response

magnitude at the lowest (5%) and highest (100%) contrast is comparable in pre- and post-TMS condition. More detailed analysis of TMS-effects on contrast selectivity are shown in Figure 2.5I-L. **C, D.** Another example cell showing TMS effects on contrast selectivity. **E. F.** This example shows TMS-induced facilitation in contrast tuning run. Neural response for the recovery condition was not recorded, so the matrix in (A) is blank between 31st and 40th trials.

2.4.4. TMS effects on response selectivity based on spike activity: population data

Our next step is to determine if TMS effects on response selectivity, which we have shown here for representative cells, are general in our data population. To quantify TMS-induced changes in orientation selectivity, we compare Gaussian fitting function parameters used for pre- and post-TMS conditions (Figure 2.5A). The main results derived from spike activities of 35 cells are as follows. First, a decrease of response magnitude is reflected in parameter K, which determines the height of the tuning curve (i.e., the maximum response). For most cells, parameter K in the pre-TMS condition is bigger than that for the post-TMS condition (Figure 2.5B) and the difference is statistically significant (Wilcoxon signed-rank test, $p<0.001$), confirming that the our 4Hz rTMS is much more likely to cause suppression (filled triangles) than facilitation (open squares) of neural activity. This TMS-induced suppression does not cause a horizontal shift (i.e., change of preferred orientation) of the tuning curve (Wilcoxon signed-rank test, $p=0.41$, Figure 2.5C). However, TMS effects on orientation selectivity are not entirely explained by vertical scaling of the tuning curve of the pre-TMS condition. Strong suppression by TMS at non-preferred orientations often results in near-zero firing rates which are not different from spontaneous spike activity, so that the width of the orientation tuning curve becomes narrower (Wilcoxon signed-rank test, $p<0.01$, Figure 2.5D). A smaller width of the tuning curve means that a cell responds to a more limited range of visual stimuli (i.e., sharper orientation tuning). Previous studies have suggested that intracortical inhibition contributes to neural response suppression and sharp orientation tuning (G. Chen, Dan, & Li, 2005; Okamoto, Naito, Sadakane, Osaki, & Sato, 2009; Shapley, Hawken, & Xing, 2007; Sillito, 1975). We discuss below the role that intracortical inhibition may play in the observed effects of TMS on orientation selectivity.

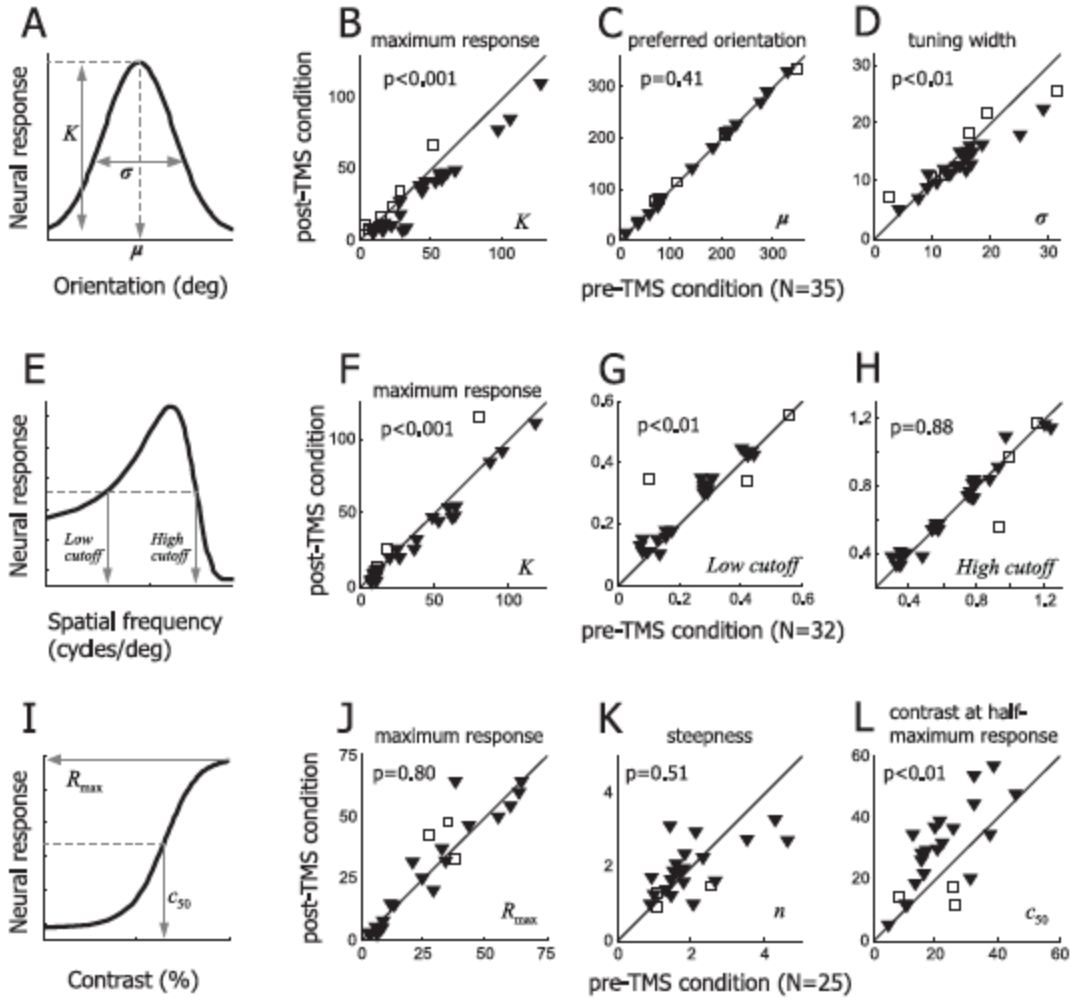

Figure 2.5. Summary of TMS effects on response selectivity. **A, B, C, D.** TMS effects on orientation selectivity were tested in 35 cells. (A) Three parameters (K, μ, σ) representing the maximum neural response, preferred orientation, and tuning width are derived from the Gaussian fitting function. (B) Parameter K is compared between pre- and post-TMS conditions. Difference between the two conditions is significant (Wilcoxon signed-rank test, p<0.001). TMS-induced suppression and facilitation cases are indicated by filled triangles and open squares, respectively. (C) Parameter μ is compared between pre- and post-TMS conditions. Regardless of suppression or facilitation, the preferred orientation is not affected by TMS. (D) Parameter σ is compared between pre- and post-TMS conditions. TMS-induced suppression often makes orientation tuning sharper, and this change (reduced tuning width) is statistically significant (Wilcoxon signed-rank test, p<0.01). **E, F, G, H.** TMS effects on spatial frequency selectivity were tested in 32 single units. (E) Parameter K represents the maximum neural response. Low and high cutoff spatial frequencies were defined as the lower and higher spatial frequencies evoking the half-maximum neural response, respectively. (F) Parameter K is significantly decreased in post-TMS condition (Wilcoxon signed-rank test, p<0.001). (G) Low cutoff spatial frequency is significantly higher in post-TMS than pre-TMS conditions (Wilcoxon signed-rank test, p<0.01). (H) High cutoff spatial frequency is not significantly changed between pre- and post-TMS conditions. **I, J, K, L.** TMS effects on contrast selectivity were tested in 25 single units. (I) Three parameters (R_{max}, n, c_{50}), taken from Naka-Rushton function, represent the saturated neural response, steepness of curve, stimulus contrast producing the half-maximum neural

response, respectively. (J) Parameter $R_{\max}$ is not significantly changed by TMS (Wilcoxon signed-rank test, p=0.80). (K) Parameter n is compared between pre- and post-TMS conditions and was not affected by TMS. (L) Parameter c_{50} is significantly increased in post-TMS condition (Wilcoxon signed-rank test, p<0.01). Considering (J) and (L) together, results suggest that TMS effects on neural response are better explained by contrast gain rather than response gain control.

TMS-induced changes in spatial frequency tuning are similar to those observed for orientation tuning. First, 4Hz rTMS causes suppression of neural responses. Thus, parameter K, representing the maximum neural response, is significantly smaller in post-TMS condition than in pre-TMS (Wilcoxon signed-rank test, p<0.001, Figure 2.5F). Again, TMS-induced suppression and facilitation cases are expressed as filled triangles and open squares, respectively. Second, like preferred orientation, the preferred spatial frequency associated with the strongest neural response is rarely changed by TMS (Wilcoxon signed-rank test, p=0.5, data not shown). Furthermore, spatial frequency tuning width in a post-TMS condition tends to be smaller than that for a pre-TMS. However, unlike orientation tuning, decreases of tuning width do not reach statistical significance (Wilcoxon signed-rank test, p=0.12, data not shown).

An unexpected finding is that TMS-induced suppression is concentrated in the low frequency range. When spatial frequencies are higher than a cell's preferred value, neural response is minimally suppressed or even increased in some cases (Figure 2.3). To quantify this asymmetric effect of TMS on spatial frequency, we define the low and high spatial frequency cutoffs as lowest and highest spatial frequencies that yield neural activity stronger than half-maximum values of Gaussian-fitted spatial frequency tuning curves (Figure 2.5E). Our population data (32 cells) show that the low spatial frequency cutoffs in post-TMS conditions are significantly higher than those in pre-TMS (Wilcoxon signed-rank test, p<0.01, Figure 2.5G). However, the high spatial frequency cutoffs don't show systematic increases or decreases after TMS (Wilcoxon signed-rank test, p=0.88, Figure 2.5H). These asymmetric changes in overall shape result in an emphasis on higher spatial frequencies.

As stimulus contrast varies from low to high, neural responses to the contrast varying stimulus are gradually increased until they are saturated at given contrast values. Therefore, if a neural response is suppressed by TMS, the neuron requires a higher stimulus contrast to produce a response as strong as for the pre-TMS condition. We note that two different types of gain control can be involved in the suppression related change of the contrast-response function. If maximum neural responses (i.e., saturated neural responses) for pre- and post-TMS conditions are comparable, even they are produced at different contrast values, contrast-response functions in post-TMS conditions may be overlapped with rightward shifts of pre-TMS conditions. This phenomenon exemplifies contrast gain control (Ohzawa et al., 1982; Ohzawa, Sclar, & Freeman, 1985). On the other hand, if the maximum response in a post-TMS condition is lower than that for pre-TMS (even if response saturation for the two conditions occurs at similar contrast values), contrast tuning

in post-TMS will be better explained by a vertical scaling rather than a horizontal shift of the pre-TMS condition. This case represents response gain control (Reynolds, Pasternak, & Desimone, 2000; Sengpiel, Baddeley, Freeman, Harrad, & Blakemore, 1998).

Among contrast tuning curve fitting parameters, R_{max} and C_{50} are good indicators to judge which type of gain control is more relevant to TMS-induced suppression. R_{max} and C_{50} represent the maximum (i.e., saturated) neural response and the stimulus contrast producing a half-maximum response, respectively. If response gain control is involved, R_{max} is decreased but C_{50} is rarely affected. In the case of contrast gain control, on the other hand, C_{50} but not R_{max} is changed.

Results from our population data (25 cells) confirms that TMS-induced suppression is likely to be mediated by contrast gain control. First, we don't find any significant difference between R_{max} values of pre- and post-TMS conditions (Wilcoxon signed-rank test, $p=0.8$, Figure 2.5J). Data points above the diagonal line in Figure 2.5J could be interpreted as TMS-induced facilitation, but this is true for only a minority of cases. If the neural response following TMS is not fully saturated, even at the highest stimulus contrast, R_{max} at that stage (even if it is suppressed (filled downward triangles)) can be larger than that for the pre-TMS condition. Second, C_{50} is significantly larger in the post-TMS compared to the pre-TMS condition (Wilcoxon signed-rank test, $p<0.01$, Figure 2.5L). However, the steepness (i.e., shape) is not systematically affected by TMS delivery (Wilcoxon signed-rank test, $p=0.51$, Figure 2.5K).

2.5 Discussion

In this study, we have investigated effects of TMS on tuning properties of visual cortical neurons. To limit variables and obtain clear results, we have used a fixed delivery of TMS (4Hz, 4sec). We show that a short TMS pulse train generally induces prolonged but reversible suppression of neural activity. Our main finding is that response selectivity of individual neurons is significantly altered following delivery of TMS. Specifically, although the peaks of individual orientation tuning curves are rarely changed, there is strong suppression at non-preferred orientations which generally narrows the widths of the tuning curves. Suppression also occurs for spatial frequency tuning but these effects are not symmetric regarding optimal spatial frequencies. Specifically, spatial frequency tuning curves tend to be altered primarily in low frequency ranges. Changes in contrast tuning curves are also found. They are explained by rightward horizontal shifts in response functions, suggesting that the effects of TMS on contrast tuning are mediated by contrast gain control. Finally, TMS-induced changes in spike responses are also observable in LFP signals, especially at high frequencies (70-100 Hz, see Supplementary Materials).

2.5.1. TMS effects: Suppression vs. Facilitation

Although the dominant effect of our 4Hz rTMS is suppression, facilitative effects are also occasionally observed (12 out of 92 cells). TMS-induced facilitation shows a similar time course of neural activity change as with suppression but in an opposite direction. In general, TMS modulates cortical activity in a frequency-dependent manner (Aydin-Abidin, Moliadze, Eysel, & Funke, 2006; Eldaief, Halko, Buckner, & Pascual-Leone, 2011; Mark Hallett, 2007; Valero-Cabre, Payne, & Pascual-Leone, 2007). Findings include reduced cortical activity following low frequency (1Hz) TMS and increased levels after high frequency stimulation (>10Hz). The stimulation frequency we used is at a mid-level (4Hz), which may be near the border of overlap between suppression and facilitation. In addition, magnetic coil position may affect findings of suppression and facilitation. In the visual cortex, TMS-induced suppression may require stimulation of stronger intensity than that for facilitation (Garry & Thomson, 2009; Kammer, Puls, Erb, & Grodd, 2005; Moliadze, Zhao, Eysel, & Funke, 2003; Schwarzkopf, Silvanto, & Rees, 2011), although we need to keep in mind that effects of stimulus intensity may be different for single pulse TMS and rTMS conditions. Since the intensity of the magnetic field induced by TMS decreases exponentially with distance from the coil (George, Lisanby, & Sackeim, 1999), when a coil is positioned further away from the skull, a high stimulus intensity may cause facilitation instead of suppression. Additionally, neurons in deeper cortical layers may be more facilitated than those in superficial regions.

Although we do not have histological identifications of specific cortical lamina, we can use recording depths to infer layers as done in previous work (D. L. Ringach, Shapley, & Hawken, 2002). Studies have shown that the major recipient of input from LGN is layer 4 which consists mainly of simple type cells (LeVay & Gilbert, 1976; McGuire, Hornung, Gilbert, & Wiesel, 1984). Complex cells reside mainly in upper and deeper layers (Alonso & Martinez, 1998; Gilbert, 1977; Martinez et al., 2005). We have used our cortical depth information along with standard physiological observations to infer populations of simple and complex cells. Our results show that effects of TMS are not significantly different for simple and complex cells.

In a simulation study, magnetic stimulation (MS) induces the largest depolarization at the soma. Increasing the diameter of the soma reduces the magnetic threshold for action potential generation (Pashut et al., 2011). In addition to the diameter of soma, number (or size) of axons may be an important feature which determines different TMS effects. Extracellular electrical stimulation in cortical gray matter directly activates axons but not cell bodies (Nowak & Bullier, 1998). And the soma is much more difficult to excite than the axon (McIntyre & Grill, 1999; Rattay, 1999). These results suggest differences of activation of cortical neurons that depend on TMS parameters. However, a detailed relationship of these factors to TMS-induced suppression or facilitation is not currently available.

In our study, facilitation cases are relatively rare, so there is not sufficient data to draw a meaningful relationship with cell types. Other work could be undertaken in which different stimulation frequencies and intensities can be used independently to determine details of occurrence of TMS-induced facilitation.

2.5.2. Long lasting effects of repetitive TMS

TMS can be applied with single stimulation (single-pulse TMS), or as pairs of stimuli with one or more coils (paired-pulse TMS), or as multiple stimuli in trains (repetitive TMS or rTMS) (Rossi et al., 2009). Depending on parameters (e.g., intensity, duration, inter-stimulus interval, etc.), cortical excitability can be increased or decreased (Aydin-Abidin et al., 2006; Eldaief et al., 2011; Fierro et al., 2005; Funke & Benali, 2011; Mark Hallett, 2007). Compared with other protocols, a main characteristic of rTMS is that it can induce long-term changes of cortical excitability (Rossi et al., 2009). This has led to use of rTMS as a noninvasive treatment in psychiatry. rTMS has been reported to be effective for depression, bipolar disorder, schizophrenia, aphasia, and chronic pain (Rossi et al., 2009; Wassermann & Lisanby, 2001). However, clinical applications rely on empirical findings that are not based on underlying neural mechanisms.

One can differentiate rTMS into two different protocols, 'conventional' and 'patterned' rTMS (Rossi et al., 2009). Conventional rTMS refers to the application of regularly repeated single TMS pulse. In a patterned protocol, the repetitive application of short rTMS bursts with a high inner frequency is interleaved by short pauses of no stimulation. The latter method is relatively new and may have some advantages over the conventional type in that it can induce similar changes in cortical excitability with shorter stimulus trains and lower stimulus intensities (Platz & Rothwell, 2010). However, this method also has a higher risk of seizure than other rTMS protocols (Oberman, Edwards, Eldaief, & Pascual-Leone, 2011), so it should be applied with caution.

Using the combined approach of electrophysiology and rTMS, we previously have shown that short TMS pulse trains (conventional rTMS; 4Hz, 4sec) could cause neural response suppression for sustained period. As a next step, we report here that basic response selectivities of neurons in visual cortex are altered during this time. Since response selectivity involves feedforward and intracortical connections (Bredfeldt & Ringach, 2002; G. Chen et al., 2005; Okamoto et al., 2009; Shapley et al., 2007; Sillito, 1975), TMS must affect these pathways as considered below.

2.5.3. Neural mechanisms involved in orientation tuning

Feedforward convergence from multiple LGN cells to a V1 neuron determines preferred orientation. Thalamocortical synapses are thought to be purely excitatory (Freund, Martin, Soltesz, Somogyi, & Whitteridge, 1989; Kharazia & Weinberg, 1994). Therefore, for a given spike threshold, orientation tuning for high contrasts should be broader than that for low. However, a feedforward-only mechanism

cannot produce sharp orientation tuning, nor can it explain contrast-invariant orientation tuning (Sclar & Freeman, 1982; Troyer, Krukowski, Priebe, & Miller, 1998). Previous studies of orientation tuning at different response latencies show that tuning width is decreased during the response (G. Chen et al., 2005; D. Ringach, Hawken, & Shapley, 1997). This is due to inhibitory inputs from neighboring cortical neurons that are delayed compared to feedforward inputs from LGN.

TMS effects on orientation selectivity (diminished neural responses & narrowed tuning width) are similar to the changes expected when intracortical inhibitions is enhanced. In addition, TMS effects are somewhat analogous to those of visual adaptation in that both effects are reversible. However, unlike adaptation-induced plasticity of orientation tuning which follows exposure to a given value and results in a peak orientation shift (Dragoi, Sharma, & Sur, 2000; Ghisovan, Nemri, Shumikhina, & Molotchnikoff, 2009), TMS application does not target a single orientation, so it does not alter preferred orientations of single cells.

We used 10 different orientation values covering a 90deg range to quantify orientation selectivity of an individual neuron. This method excludes a vector summation analysis which could also provide a measurement of orientation selectivity. We note that in our analysis, a lack of shift of preferred orientation is a solid finding and not due to an artifact. In our data population, mean value of orientation tuning width (parameter σ) is about 15 deg (see Figure 2.5). This means that for most cells, visual responses are reduced to zero at both ends of tested orientation range (see Figure 2.2). The vector summation method would not provide meaningful additional information for preferred direction of motion. We should also note that we did not test orientation selectivity in non-preferred direction since responses for this variable are generally very low.

2.5.4. Stronger suppression in low spatial frequency range

The main TMS effect for spatial frequency tuning is an asymmetric change in overall shape. Low but not high spatial frequency cutoff is significantly increased. These results suggest distinct neural circuits responsible for low and high spatial frequency processing.

A large proportion of LGN neurons show low-pass spatial frequency tuning, whereas most neurons in visual cortex have band-pass characteristics (Bredfeldt & Ringach, 2002; K. K. De Valois & Tootell, 1983; Maffei & Fiorentini, 1973). The transition from low- to band-pass spatial frequency tuning, like that from broad to sharp orientation tuning, may require intracortical inhibitory interneurons (Bauman & Bonds, 1991). Moreover, visual cortical neurons show temporal dynamics in spatial frequency tuning. The preferred spatial frequency shifts from low to high values (Allen & Freeman, 2006; Frazor et al., 2004; Mazer et al., 2002). Our finding of stronger TMS-induced suppression in the low spatial frequency range may be related to these previous results. The short TMS pulse train applied to visual cortex may disrupt the balance between feedforward excitatory inputs from LGN and inputs from

intracortical connections. Increased contribution of intracortical connections may result in diminished neural activity in the low spatial frequency range.

2.5.5. Contrast gain control

Cortical cells maintain sensitivity over a wide range of contrast by centering response range to specific local levels (Ohzawa et al., 1982, 1985). This contrast gain control process manifests as a horizontal shift of the contrast-response function.

TMS effects on the contrast-response function (increased C_{50} and unaffected R_{max}) are better explained by a rightward horizontal shift rather than a vertical scaling of the original function. This suggests that TMS-induced suppression may be mediated by a contrast gain control mechanism.

Contrast gain control is thought to be generated at an input stage (Matteo Carandini, 2000; Katzner, Busse, & Carandini, 2011). Within this framework, post-TMS neural response may be similar to that for a low contrast stimulus. However, this is at odds with previous findings and our current results. First, cortical orientation selectivity is contrast-invariant (Sclar & Freeman, 1982; Troyer et al., 1998), but TMS-induced suppression narrows the width of orientation tuning curves. Second, spatial frequency tuning for low contrast accentuates low spatial frequencies (Michael P Sceniak, Hawken, & Shapley, 2002), but TMS-induced suppression is stronger at low frequencies and neural responses to high frequencies are minimally altered. Contrast adaptation typically results in horizontal shifts of the contrast-response function (Bonds, 1991; M Carandini & Ferster, 1997; Gardner et al., 2005; Ohzawa et al., 1982, 1985). Therefore, short TMS pulse trains cause an effect similar to what is expected if a population of cortical cells, covering all orientations and a broad range of spatial & temporal frequencies, is adapted to a high contrast stimulus.

2.5.6. Limitations of current study

We have used a single parameter set for the current work to reduce possible variables. We should note that effects may be different for various cell types. If various cell types can be selectively affected by TMS with different parameters (intensity, frequency, duration, and so on), this would provide useful information.

It is also worth examining TMS effects on temporal dynamics of functional tuning. This analysis requires a reverse correlation method, which is more time consuming than what we have used in the current study. However, even under the assumption that TMS may induce larger contributions of intra-cortical processing, it does not necessarily follow that TMS effects on response selectivity are only observable at delayed response latency. Without TMS application, intra-cortical inhibition is forced to be later than feedforward input. However, if TMS causes a different neuronal state (e.g., elevated intra-cortical inhibition even before visual stimulation), TMS effects on response selectivity may occur from the earliest response latency.

Exact recovery times can be studied by detailed examination of relatively late trials (31st-40th trials in our protocol) following the post-TMS condition. We showed here that TMS effects are not permanent and that their influence on response selectivity gets weaker at delayed phases.

It is also desirable to determine if our results obtained in anesthetized animals can be translated into human TMS studies. Our stimulation parameters are somewhat different from those generally used for human rTMS. Most human studies tend to involve weaker stimulation intensities, but longer durations than what we have used here (Rossi et al., 2009). Effects of TMS in humans have been reported to last up to several hours (Huang, Edwards, Rounis, Bhatia, & Rothwell, 2005; Pascual-Leone et al., 1998; Ziemann et al., 2008). TMS – fMRI combined studies may provide correlations between TMS-induced behavioral changes and hemodynamic alterations in functionally related brain regions.

2.6 Conclusions

We have found that short rTMS pulses (4Hz, 4sec) applied over the cat's visual cortex cause long-lasting and reversible changes in neural activity. Neural responses to visual stimuli generally are clearly suppressed after TMS application and they gradually recover to levels close to pre-TMS conditions over a subsequent 10~15 minute periods. Facilitative effects are observed in a small number of cases (12 out of 92). The TMS-induced changes in neural responses are reflected at both input (LFPs) and output (spike activity) stages of cortical processing. These effects are accompanied by substantial changes in response selectivity, including sharper orientation tuning, selective suppression at low spatial frequencies, and response saturation at higher contrast values. These findings suggest that TMS interrupts the existing balance between sub-cortical and intra-cortical inputs for relatively extended time periods.

2.7 Supplementary Materials

2.7.1. Methods: Z-scored LFP spectrogram

For spectral analysis, the raw LFP spectrogram was calculated with Chronux software (http://chronux.org) and then transformed to z-scored LFP spectrogram. The equation used for z-score transformation is as follows.

$$P_{zscore}(x,f) = \sum_{t=0}^{200} \frac{P(x,f,t) - \mu(P(x,f,t_{baseline}))}{\sigma(P(x,f,t_{baseline}))} \Big/ 201 \qquad (1)$$

where $P_{zscore}(x,f)$ and $P(x,f,t)$ are z-scored and raw LFP power at a stimulus orientation (or spatial frequency or contrast) x, frequency f, and time t. Time t has 201 data points from 0 to 2000ms (stimulus duration, step size 10ms). $\mu(P(x,f,t_{baseline}))$ and $\sigma(P(x,f,t_{baseline}))$ are the mean and standard deviation of raw LFP power computed during the baseline period (>250ms before stimulus onset in pre-TMS condition) at a given stimulus x and a frequency f. Since the z-score computation is executed independently for each frequency, the z-scored LFP spectrogram does not follow a $1/f^2$ relationship. Instead, it reflects relative change of LFP power caused by visual stimulation, and thus enables us to see which frequency range is the most affected.

2.7.2. Results: TMS effects are reflected in LFPs: representative neurons

In the current study, the raw signals from which spike activity is extracted, also yields data for local field potentials (LFPs) via low-pass filtering. Since neural spike activity is thought to represent cell output and LFP is considered to primarily reflect synaptic inputs (Kreiman et al., 2006; Mitzdorf, 1987), it is of obvious interest to analyze both aspects of neural activity. Specifically, it is relevant to determine if TMS effects are analogous, in direction of effect and magnitude, for both types of neural analysis. In the case of LFPs, it is also possible to determine effects as a function of frequency range. This last parameter is examined for LFP effects of TMS application in Figure 2.6 which shows examples for orientation (A, B, C), spatial frequency (D, E, F), and contrast (G, H, I) from three representative cells. To analyze the data here, we have created a z-scored LFP spectrogram (see Materials and Methods) as a function of stimulus parameter. In the example for orientation (Figure 2.6A), there is a clear and relatively uniform suppression of neural spike activity for all orientations tested. Correspondingly, in the LFP domain (Figure 2.6B & C), there is also pronounced suppression following delivery of TMS. The X- and Y-axes indicate orientation and frequency, respectively. Colors close to red represent stronger z-scored LFP power for a given orientation and frequency. The z-scored LFP power is peaked for a 20-30° orientation, and gets weaker as orientation deviates from the optimal value. Note that this is quite similar to the orientation tuning curve based on spike activity (Figure 2.6A). This orientation tuning property is observable for a wide-range of frequencies above 40Hz. As for the pre-TMS condition, LFP power in the post-TMS condition (Figure 2.6C) also shows orientation tuning for a comparable range of frequencies but with weaker LFP power.

A similar result is shown for spatial frequency (Figure 2.6D, E & F). Note that for both orientation and spatial frequency, clear TMS effects are shown in the LFP domain primarily at high gamma frequencies (70~100 Hz) although there are some effects as low as 40 Hz. The data for contrast show relatively modest but clear spike reductions (Figure 2.6G) following TMS. However, there are only minimal effects in the LFP domain (Figure 2.6H & I). Considered together, these examples show that

TMS-induced spike activity suppression is associated with decreases in LFP power that are most pronounced in the high gamma frequency range (70-100Hz).

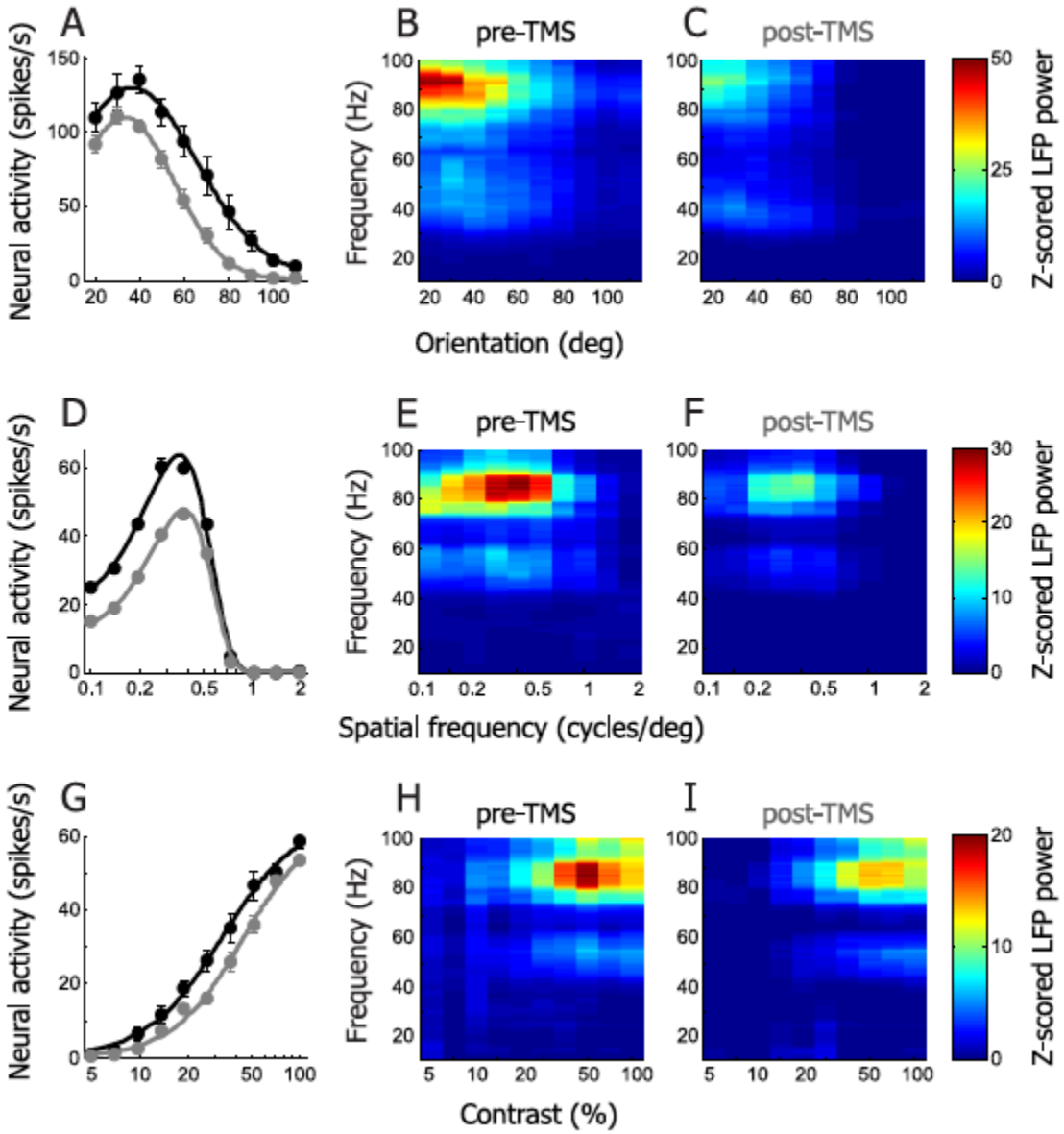

Figure 2.6. Effects of TMS on spike response are reflected in high-gamma LFPs. **A.** Orientation tuning curves for an example cell. Black and gray curves are pre- and post-TMS conditions, respectively. **B, C.** Z-scored LFP power spectrograms of the example cell for pre- (B) and post-TMS conditions (C). Colors closer to red indicate that the stronger LFP power increase is induced by visual stimulation at a given spatial frequency (c/deg) and a frequency (Hz) band. **D, E, F.** Spatial frequency tuning curves and LFP power spectrograms of an example cell. **G, H, I.** Contrast tuning curves and LFP power spectrograms of an example cell.

2.7.3. Results: TMS effects on response selectivity based on LFPs: population data

Although, for our three representative recording sites (Figure 2.6), LFP power differences between pre- and post-TMS conditions seem prominent in the 70~100Hz frequency, the correlation between LFP and spike activity is not restricted to this range. To examine LFP-spike correlation in detail, we divide total frequency range into nine groups (10~20, 20~30, ⋯, 90~100Hz) and compute correlations between orientation (or spatial frequency or contrast) tuning of spike activity and that of LFP power for each frequency group. This analysis has been carried out for 72 cells, and the mean spike-LFP power correlations are averaged and displayed in Figure 2.7A.

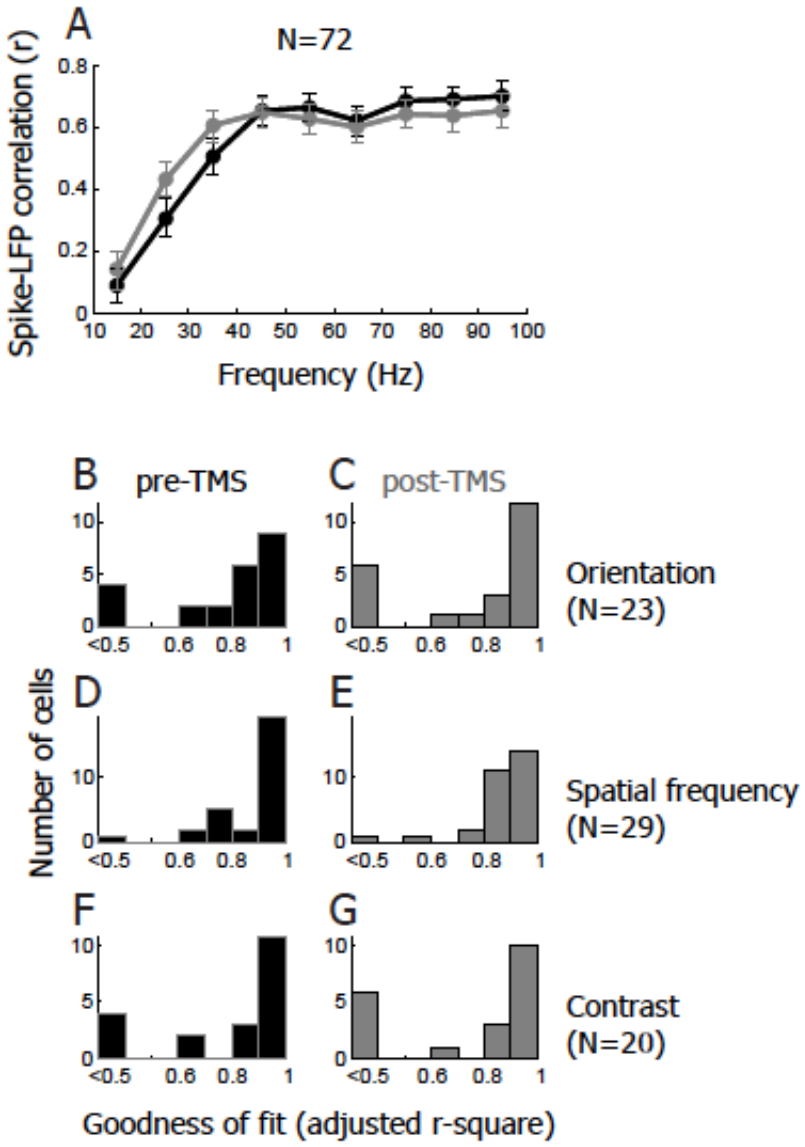

Figure 2.7. Spike-LFP correlation and goodness of fit of tuning curve based on high-gamma LFPs. **A.** We divide 10-100Hz LFP frequency range into 9 frequency bands and compute correlation coefficient between stimulus tuning based on spike activity and that based on LFP power in each frequency band. Black and gray lines indicate mean correlations of population data for pre- and post-

TMS conditions, respectively. Error bars indicate ±1 standard error of mean. **B.** In 23 cells, orientation tuning curves are calculated based on LFP power in 70-100Hz frequency range. The histogram shows the distribution of goodness of fit in pre-TMS condition. **C.** Distribution of goodness of fit for orientation tuning curves in post-TMS condition. **D, E.** Distributions of goodness of fit for spatial frequency tuning curves (N=29) in pre- (D) and post-TMS conditions (E). **F, G.** Distributions of goodness of fit for contrast tuning curves (N=20) in pre- (F) and post-TMS conditions (G).

In the range of 10-20Hz, LFPs are rarely tuned to stimulus parameters. Consequently, the spike-LFP correlation is less than 0.2. But for higher frequencies, as LFPs begin to have better response selectivity, the spike-LFP correlation is monotonically increased until saturation at around 0.7. To examine TMS-induced changes in LFP selectivity, it is possible to create various tuning curves based on LFP power in the range of 70-100Hz, where the strongest spike-LFP correlation is observed. From these curves, we find for most cells, that LFP power variations as a function of orientation (or spatial frequency or contrast) are well fit with a Gaussian (or Naka-Rushton for contrast) function. Note that we exclude bad fits prior to the examination of TMS-induced changes in LFP selectivity. We take advantage of adjusted r-square values as a standard of goodness of fit (Figure 2.7B-G). Only cells whose adjusted r-square values exceed 0.6 for both pre- and post-TMS conditions are included in the following analysis (orientation: 73.91%, 17/23. Spatial frequency: 96.55%, 28/29. Contrast: 80.00%, 16/20).

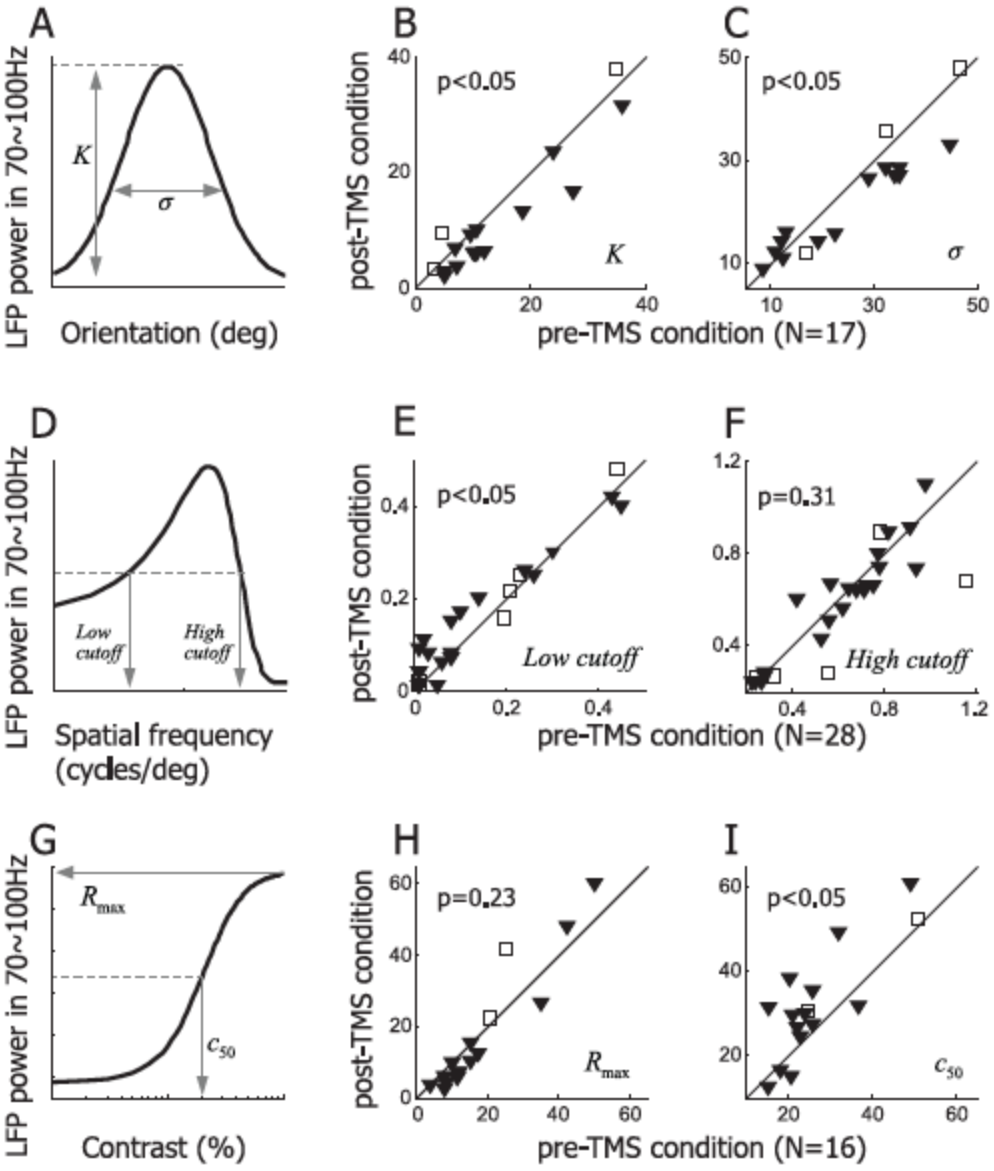

Figure 2.8. TMS effects on response selectivity of high-gamma LFPs. Cell whose goodness of fit is larger than 0.6 for both pre- and post-TMS conditions (Figure 2.7) are included in the analysis. Again, filled downward triangles and open squares represent TMS-induced suppression and facilitation cases, respectively. **A, B, C.** In 17 cells, orientation tuning curves are calculated based on LFP power in 70-100Hz frequency range. Parameter K (B) and σ (C) are significantly smaller in post-TMS than pre-TMS condition (Wilcoxon signed-rank test, $p<0.05$), indicating that TMS reduced response amplitude and narrowed orientation tuning of gamma-range LFP responses. **D, E, F.** In 28 cells, low spatial frequency cutoff (E) extracted from 70~100Hz LFP power is significantly higher in post-TMS condition (Wilcoxon signed-rank test, $p<0.05$), but high spatial frequency cutoff (F) doesn't show significant difference between pre- and post-TMS conditions. **G, H, I.** In 16 cells, contrast tuning curves based on 70~100Hz LFP power are compared. Parameter c_{50} but not R_{max} shows significant change caused by TMS, consistent with contrast gain modulation by TMS. These results above are consistent with those based on spike activity (Figure 2.5)

In the analysis using spike activity, we find two main effects of TMS on orientation selectivity: suppression of neural response and sharpening of the tuning curve. Here, we examine whether the same effects are present for LFP-based orientation selectivity. Parameter K, which determines the height of the tuning curve, and parameter σ, the width of the tuning curve, are compared between pre- and post-TMS conditions (Figure 2.8A). Figure 8B shows that parameter K values in the post-TMS condition are significantly smaller than those for pre-TMS (Wilcoxon signed-rank test, $p<0.05$). Filled triangles and open squares indicate suppression and facilitation cases, respectively. Differences of parameter σ are also significant (Wilcoxon signed-rank test, $p<0.05$). In Figure 2.8C, most dots are positioned below the diagonal line, indicating that the widths of orientation tuning curves in the post-TMS condition become narrower compared with those for pre-TMS.

In the case of LFP-based spatial frequency selectivity, asymmetric characteristics of response suppression may be explored. As for spike activity, TMS-induced suppression (filled triangles) is accompanied by significant increases of low spatial frequency cutoffs for LFP signals (Wilcoxon signed-rank test, $p<0.05$, Figure 2.8E). However, high spatial frequency cutoffs don't show systematic increases or decreases following TMS delivery (Wilcoxon signed-rank test, $p=0.31$, Figure 2.8F). These results indicate that TMS-induced suppression of LFP power is largely concentrated in the low spatial frequency range and is less evident for high spatial frequencies.

Finally, Figure 2.8G-I shows how R_{max} and $C_{50,}$ extracted from LFP-based contrast tuning curves, are affected by TMS delivery. Parameter R_{max}, the maximum response at saturation level, tends to decrease following TMS, but this change does not reach statistical significance (Wilcoxon signed-rank test, $p=0.23$, Supplementary Figure 3H). On the other hand, parameter C_{50}, the contrast level at a half-maximum response, is significantly increased in the post-TMS condition (Wilcoxon signed-rank test, $p<0.05$, Figure 2.8I). These results are again consistent with those based on spike activity (Figure 2.5), and therefore suggest that contrast gain control may be involved in TMS-induced prolonged suppression.

2.7.4. Discussion: Local field potentials

TMS application affects a large volume of cerebral cortex. Simultaneous activation of pre-synaptic terminals, post-synaptic membranes, and axons results in a massive synaptic bombardment of cortical networks which is quite different from natural synaptic transmission (Funke & Benali, 2011). Consequently, TMS disrupts the pre-existing synchronized temporal structure of ongoing spontaneous activity and this results in prolonged reduction of LFP power (Allen et al., 2007).

LFP is believed to primarily reflect dendritic currents caused by synaptic inputs from populations of neurons (Mitzdorf, 1987), as opposed to spike activity which represents neuronal output information. Here, we have determined that TMS effects

are reflected at both input and output stages of cortical processing. Short TMS pulse trains cause prolonged suppression of spike activity. And during the suppression, LFP signals are also decreased over a wide-range of frequencies.

Neuronal firing rate and LFP power are positively correlated, and this correlation is stronger as frequency is increased (Belitski et al., 2008; Ray & Maunsell, 2011). In the 70~100Hz range, LFP power has a response selectivity profile similar to that of spike activity, but it is not as sharp (e.g., compare Figure 2.3E with Figure 2.8C). This suggests that high-gamma LFP signals are a result of pooling of inputs from a large neural population including multiple orientation columns (Berens et al., 2008a). In order to extract tuning parameters from the LFP signal, we choose a 70-100Hz range and limit our analysis to sites which show a considerable goodness of fit (adjusted r-square >0.6). The sites selected may unavoidably show high spike-LFP correlation. Therefore, the similarity between TMS-induced changes in spike activity and those in the LFP signal is partially expected. In the future, signals from intracortical recordings may provide a more independent measure of the input stage of cortical processing than the LFP signals we use here. In addition, TMS effects may vary with cortical layer or cell types.

Chapter 3

Non-linearity of direction selectivity of neurons in the cat's visual cortex

Preface: This chapter is the dissertation author's original unpublished work.

3.1 Introduction

Most cells in the cat's visual cortex respond selectively to the direction of movement of an optimally oriented visual stimulus (Emerson, Bergen, & Adelson, 1992; Jagadeesh, Wheat, & Ferster, 1993). This property, called direction selectivity (DS), is first exhibited in the visual cortex (but, see Vaney & Taylor, 2002). Various linear models have been suggested to explain how direction selectivity can be derived from inputs from non-direction selective cells, such as LGN cells or non-DS simple cells (Adelson & Bergen, 1985; R. L. De Valois, Cottaris, Mahon, Elfar, & Wilson, 2000; Peterson, Li, & Freeman, 2004). However, the degree of DS predicted by a linear model is generally weaker than that measured with a drifting grating stimulus, indicating that there must be non-linear contributions to DS (DeAngelis, Ohzawa, & Freeman, 1993b; Peterson et al., 2004).

One approach to estimate the non-linear contribution to DS derivation, which we employed in this study, is to use the spatiotemporal profile of linear RF created by a reverse correlation technique (DeAngelis et al., 1993b). 2 dimensional Fourier analysis of the spatiotemporal (X-T) RF profile enables prediction of DS to a grating stimulus with a given spatial & temporal frequencies. With an assumption that the input to simple cells is quite linear (Jagadeesh, Wheat, Kontsevich, Tyler, & Ferster, 1997), we can consider the difference between tested- and predicted DS values as the non-linear contribution to DS derivation.

From a large database of cells and standardized anatomical reconstructions, we investigated how the non-linear component of direction selectivity of neurons varies depending on cortical layers. Our results show that simple cells, in which DS estimation from linear RF is applicable, are mainly distributed in the granular layer (layer 4, the primary recipient of LGN input). In supra-(layer 2/3) and infra-granular (layer 5 & 6) layers, proportions of simple cells were much smaller than that in the granular layer.

The distribution of direction selectivity index values (DSI, 0: non DS, 1: highly DS) is also clearly different depending on cortical layer. In layer 4, simple cells show a substantial diversity in DSI distribution from very low to high values. In layer 2/3, DSIs of complex cells, which account for a large majority of cells in these layers, are almost uniformly distributed, but those of simple cells are clearly biased to higher values. In layer 6, DSI distributions of simple and complex cells are comparable with both cell types showing clear peaks at the highest DSIs.

Our findings suggest that different characteristics of DSI distribution between the LGN input layer and the other non-input layers are due to non-linear component of direction selectivity. In layer 4, DSI values measured with grating stimuli were generally well predicted by DSI values that were estimated from spatiotemporal linear RF. However, in supra- and infra-granular layers, measured DSIs were significantly larger than estimated DSIs (indicating a larger non-linear contribution).

Finally, the correlation between measured and estimated DSIs was much lower in supra- and infra-granular layers compared to layer 4.

3.2 Materials and Methods

3.2.1. Cell recording

Extracellular recordings from well-isolated single units were made from cells in the striate cortex of anesthetized and paralyzed cats. Electrode penetration made along the medial bank of the post-lateral gyrus (P4L2, Horsley-Clarke coordinates) allowed us to measure spiking activity of neurons whose receptive field eccentricities are within the central 15deg of the visual field through multiple layers and orientation columns (DeAngelis et al., 1993b). Once a single unit is identified by the spike waveform, the optimal orientation, spatial frequency, and size are quantitatively measured with sinusoidal gratings drifting at 2Hz.

3.2.2. Histology

The historical reconstructions for previous experiments were reviewed and reliable data from 41 cats were recruited for analysis in the current study. Neurons were stained for Nissl substance with cresyl violet stain. The amount and distribution of Nissl substance varies with different types of neurons (and different layers). Individual neurons could be assigned to one of four layer groups based on the following criteria.

- Layer 2/3 (Supra-granular layer): Layer 2 and 3 are virtually indistinguishable. These layers are composed of approximately equal amounts of granular and small pyramidal cells.
- Layer 4 (Granular layer): Layer 4 is wide relative to layer 2/3, and consists of small granular cells interspersed among large stellar cells
- Layer 5 (Infra-granular layer): Layer 5 is the smallest layer in area 17, consisting of pyramidal cells with no clear columnar organization.
- Layer 6 (Infra-granular layer): Layer 6 is a relatively large layer consisting of multiform and fusiform cells organized into columns.

Formaldehyde fixation and subsequent steps (e.g., dehydration, embedding, etc) in the brain tissue processing produce about 20% decrease in linear dimension of the tissues (C. H. Fox, Johnson, Whiting, & Roller, 1985). Reconstructions were first evaluated to determine if lesion depths matched visually identified lesions with no more than a 25% margin of error. In order to minimize the error, all reconstructions that did not meet this criterion or did not contain at least 2 clearly identifiable lesions were excluded from the analysis.

3.2.3. Cell classification and direction selectivity index

We classified cells in the visual cortex as simple or complex by comparing the 1st harmonic (F1) to the DC (F0) of the peri-stimulus time histogram obtained with an optimal (spatial frequency & orientation) grating stimulus drifting at 2Hz. Simple cells have F1/F0 ratios greater than 1 (Skottun et al., 1991).

A direction selectivity index (DSI) was calculated for responses to preferred (p) and non-preferred (np) directions. Depending on cell types, F1 (for simple) or F0 (for complex) amplitude was used for the calculation.

$$DSI = 1 - \frac{np}{p} \qquad (1)$$

3.2.4. Predicted direction selectivity index

For simple cells, spatiotemporal linear RFs were measured with a reverse correlation procedure (Jones & Palmer, 1987). Detailed description of the procedure is available in elsewhere (DeAngelis et al., 1993b). Briefly, individual bar stimuli of either bright (32 cd/m^2) or dark (2 cd/m^2) luminance are displayed against gray background (17 cd/m^2), one at a time on 2 dimensional random grid locations for 40 msec. The cross-correlation between the stimulus sequence and the cells' spike response produce a linear spatiotemporal RF.

Given a linear spatiotemporal RF, a linear estimation of direction selectivity can be further determined by calculating the spatiotemporal amplitude spectrum by Fourier analysis. The amplitude spectrum is fitted with the following function to extract estimates of the cell's spatial and temporal frequency tuning curves.

$$A(sf, tf) = A_0 e^{-(sf - sf_0)/a)^2} \times \frac{1}{\Gamma(k)\theta^k} tf^{k-1} e^{-\frac{tf}{\theta}} \qquad (2)$$

where A_0, sf_0, a, k, θ are free parameters.

This function is slightly modified from that used in a previous study (DeAngelis et al., 1993b), and expressed as the product of a Gaussian (for spatial frequency) and a Gamma (for temporal frequency) distributions. The amplitude values at a given spatial frequency and 2Hz temporal frequencies are chosen as the predicted responses to a grating drifting in the preferred and non-preferred directions. A DSI value is computed from the predicted responses using Equation 1.

3.3 Results

3.3.1. Laminar distribution of simple and complex cells

For 899 cells in our database, we quantified the ratio between the amplitude of the 1st harmonic of the response and the mean spike rate at the preferred orientation.

437 cells in which this ratio was greater than 1 were classified as simple cells, and the other 462 cells were classified as complex.

A linear model successfully describes the receptive field of a simple cell as a result of combined inputs from multiple LGN cells whose receptive fields are positioned along the preferred orientation (Alonso et al., 2001; Hubel & Wiesel, 1962). Therefore, it is of interest to test whether simple cells are mainly found in cortical layers, which receive the majority of feedfoward projections from LGN cells.

Figure 3.1 compares the distribution of F1/F0 ratio in four layer groups. Consistent with classical descriptions, layer 4 is nearly entirely composed of simple cells (79.29%, 220 out of 281 cells). In contrast, complex cells are dominant in layer 2/3 & 5. Distribution of F1/F0 ratio in these layers resembles a mirror image of that of layer 4, reflecting a much higher proportion of complex cells (layer 2/3: 71.2%, 136 out of 191 cells; layer 5: 86.72%, 111 out of 128 cells) than simple types. In layer 6, however, F1/F0 distribution is not strongly biased towards one direction but showed a balance between simple cells (48.83%, 146 out of 299 cells) and complex cells (51.17%, 153 out of 299 cells).

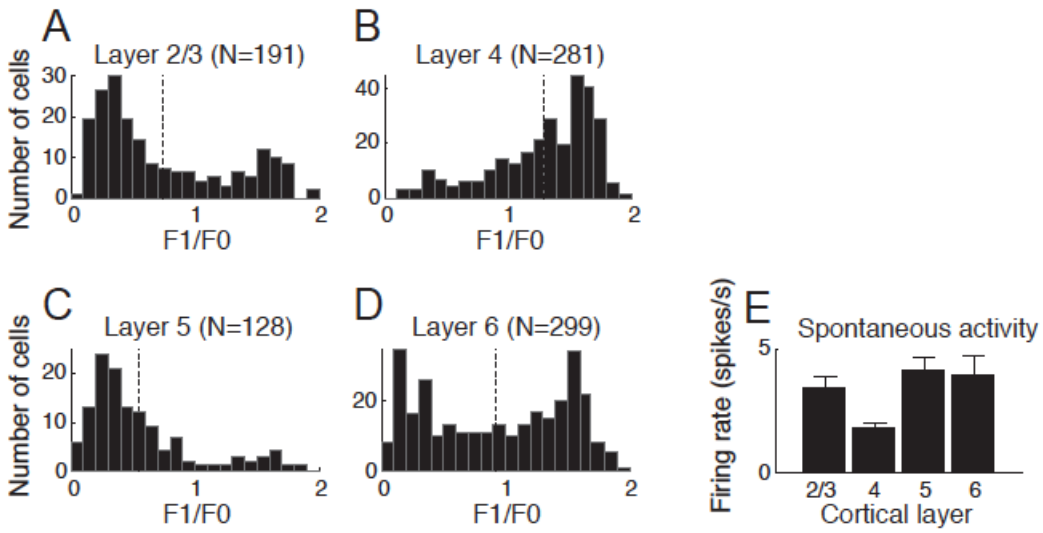

Figure 3.1. Comparison of F1/F0 distribution & spontaneous activity among four layer groups. **A** total of 899 cells in our database were assigned to one of four layer categories based on historical reconstruction. We classified simple and complex cells based on F1/F0 ratio and quantified spontaneous activity from each neuron. We then examined how these values differ depending on cortical layer. **A.** F1/F0 distribution in layer 2/3. 55 out of 196 cells were classified as simple cells (F1/F0 ratio greater than 1). **B.** F1/F0 distribution in layer 4. 220 out of 281 cells were classified as simple cells. **C.** F1/F0 distribution in layer 5. 11 out of 128 cells were classified as simple cells. **D.** F1/F0 distribution in layer 6. 146 out of 299 cells were classified as simple cells. **E.** Mean spontaneous activity of cells in layer 2/3, 4, 5, and 6. Error bar indicates standard error of mean.

Gilbert (1977) reported high spontaneous rates in layers 2/3 and 5, and low spontaneous rates in layers 4 and 6, reflecting stronger spontaneous activity in the special complex cells (those that do not show length summation within the CRF) than that in the normal complex and simple cells (Gilbert, 1977). Accordingly, we found that spontaneous activity in granular layer is significantly weaker than that of supra- and infra-granular layers.

3.3.2. Direction selectivity of simple and complex cells and their laminar relationships

Our data shows that there are substantial differences in direction selectivity depending on cell types and layers. Distributions of direction selectivity index (DSI) across layers, separated into populations of simple and complex cells are illustrated in Figure 3.2. In layer 4 (i.e., main LGN input), there tends to be more cells with higher DSI values (Figure 3.2B). This seems to be primarily due to the DSI distribution of simple cells, which occupy about 80% of total cells in this layer. DSI values of complex cells are more uniformly distributed, but the relatively small number of complex cells in layer 4 limit any definitive conclusions regarding the DSI distribution.

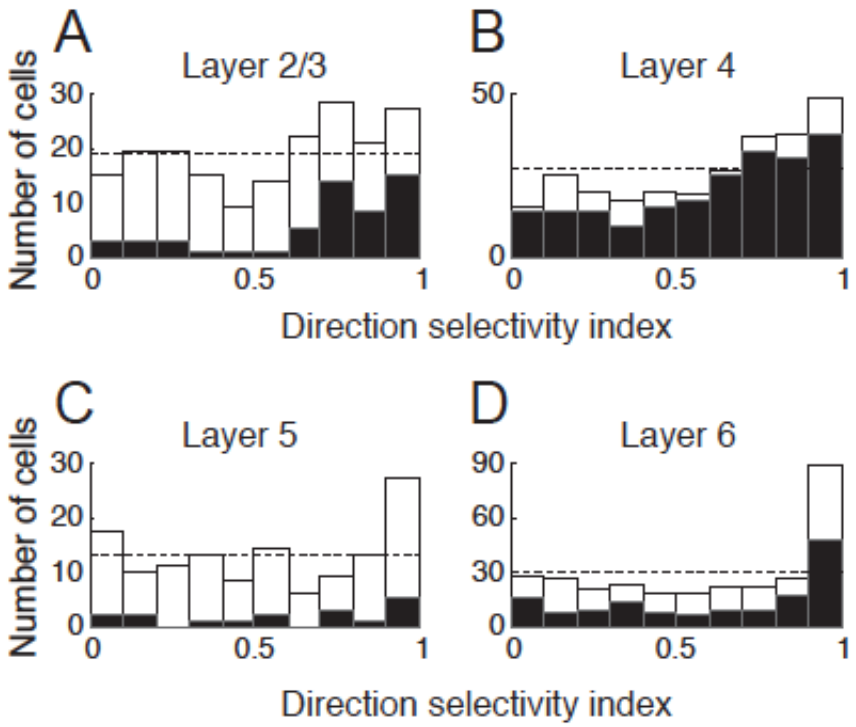

Figure 3.2. Direction selectivity index (DSI) distributions in 3 layer groups. DSI is calculated by $1-\frac{np}{p}$, where p and np indicate neural response for preferred and non-preferred (180deg away from the optimal value) direction, respectively. **A.** DSI distribution in layer 2/3. Filled bars represent simple cells (F1/F0 ratio greater than 1). The horizontal dotted line indicates a uniform DSI

distribution. **B.** DSI distribution in layer 4. The same format is used as in A. **C.** DSI distribution in layer 5. **D.** DSI distribution in layer 6.

In layer 2/3, dominance between simple and complex cells was reversed compared to the layer 4 (Figure 3.2A). DSI distribution of complex cells was almost uniform across the entire range of DSI values (0 to 1). Simple cells accounted for less than 30% of total population in layer 2/3, but their DSI distribution showed very unique characteristic. As for layer 4, simple cells tended to be more direction selective compared with complex cells in layer 2/3. However, this tendency was more prominent in layer 2/3 with 78.18% of simple cells (43 out of 55) having DSI values higher than 0.5 (Note that 50.74% in complex cells had DSI >0.5).

In infra-granular layers (layer 5 & 6), DSI histogram has a clear peak at the highest DSI value (DSI > 0.9) for both simple and complex cells. This feature was more salient in layer 6 compared to layer 5.

3.3.3. Non-linear component of direction selectivity

We measured space-time RFs for 158 simple cells. The numbers of simple cells from the supra-granular (layer 2/3), granular (layer 4) and infra-granular layers (layer 5 & 6) are 29, 61 and 68, respectively.

Figure 3.3A shows the neural activity of a direction selective simple cell recorded in the granular layer. Black and red curves indicate peri-stimulus time histogram calculated for preferred and non-preferred (opposite to preferred) directions, respectively. A grating stimulus drifting in the non-preferred direction caused significant non-zero spike activity, but it was much weaker than neural response for the preferred direction. DSI calculated for this cell's spike activity was 0.82.

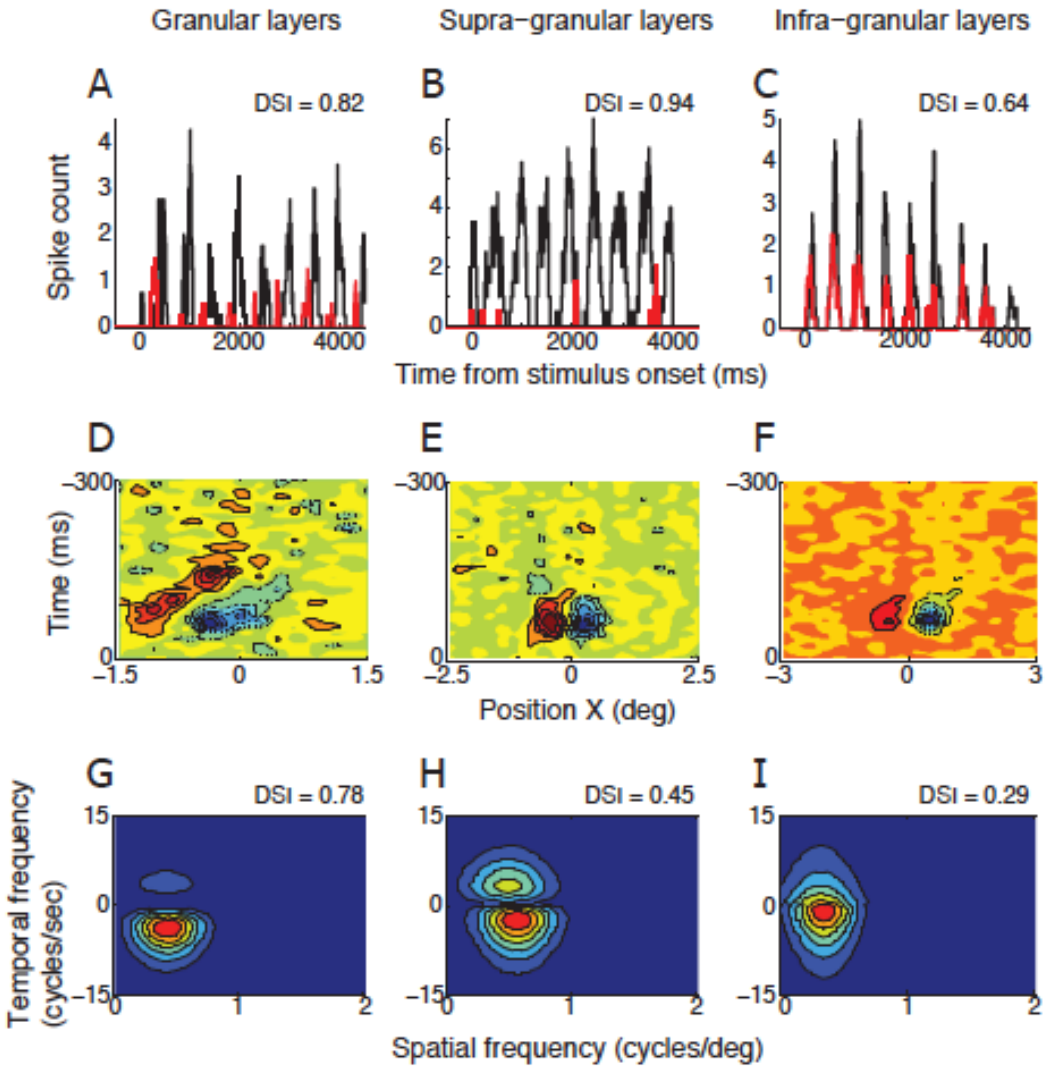

Figure 3.3. Linear estimation of DSIs made for three example simple cells. A. Peri-stimulus time histograms (PSTHs) for preferred (black) and non-preferred (red) direction of motion were calculated for a simple cell in the granular layer. The number of spikes was counted in a 50ms window sliding with 1ms step. DSI measured with moving grating stimuli in this cell was 0.82. **D.** X-T profile of spatiotemporal linear RF of the simple cell described in A. Red color with solid contour lines represents bright-excitatory (or ON) subregion of RF. Blue color with dashed contour lines represents dark-excitatory (or OFF) subregion of RF. **G.** A 2-dimensional Fourier transform was applied to X-T plot in D. The amplitude spectrum for positive temporal frequency reflects neural response for rightward direction of motion. Contour map shows the best fit of equation (2). DSI estimated from this amplitude spectrum was 0.78. **B, E, H.** Linear estimation of DSI was made for a simple cell in the supra-granular layer. The same conventions were used as in A, D, G. **C, F, I.** Linear estimation of DSI was made for a simple cell in the infra-granular layer. The same conventions were used as in A, D, G.

We compared DSI measured with grating stimuli to that estimated from the linear model. First, we created linear spatiotemporal RFs using a reverse correlation procedure. For most cells, the spatiotemporal linear RF was two-dimensional

(spatially one-dimensional), because the recordings included only a long bar stimulus with the preferred orientation that varied in its position along the X-axis. However, more time-consuming three-dimensional spatiotemporal RF was also measured in a smaller number of cells. In such cases, we integrated this three-dimensional dataset along the Y-axis to reduce it to a two-dimensional RF (i.e., X-T plot).

The X-T plot of this example cell has clearly defined subregions (Figure 3.3D). These subregions are slanted to the right, indicating that this cell would be direction selective. Fourier analysis of the X-T plot yielded a spatiotemporal amplitude spectrum (Figure 3.3G). Two quadrants of negative spatial frequencies were omitted because they have the same information as those of positive spatial frequencies. From the spatiotemporal amplitude spectrum, we could estimate direction selectivity of a neuron. The positive and negative temporal frequency quadrants provide relative neural response estimates for motion in the preferred and non-preferred direction, respectively. In this cell, estimated DSI was 0.78, which was quite similar to the DSI measured with grating stimuli (0.82).

The other two columns in Figure 3.3 illustrate two other example cells for which the same analysis was conducted. One was collected from supra-granular layers, and the other one was from infra-granular layers. Both cells showed clear directional selectivity in spike response for grating stimuli (Figure 3.3B & C). However, unlike the previous example cell from the granular layer, subregions of their spatiotemporal linear RFs of these cells were not substantially tilted to the left or to the right (Figure 3.3E & F). Consequently, the spatiotemporal amplitude spectrum showed comparable power in the positive and negative temporal quadrants, and estimated DSIs were much smaller compared with DSIs measured with grating stimuli (Figure 3.3H & I).

We assumed that any difference between measured DSI and linearly estimated DSI reflects a non-linear component of direction selectivity. From population data, we identified how this non-linear component of direction selectivity differs in size depending on cortical layers. In the granular layer (Figure 3.4A), measured and linearly estimated DSI values showed a strong positive correlation ($r = 0.7$, $p<10^{-9}$). A positive correlation was also observable for simple cells in the infra-granular layer (Figure 3.4C), but its magnitude ($r = 0.65$, $p<10^{-8}$) was slightly weaker than that of the granular layer.

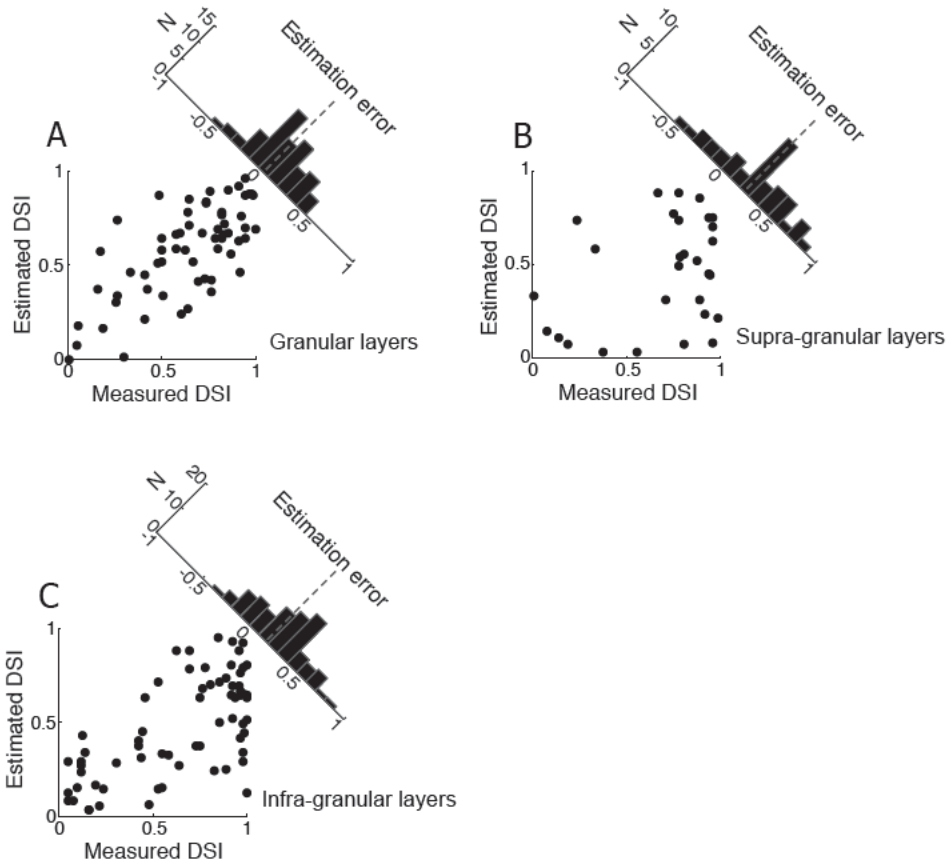

Figure 3.4. Comparison of measured and estimated DSIs. A. Simple cells in the granular layer. The values plotted in the X- and Y-axes indicate DSI measured with grating stimuli and that estimated from the spatiotemporal amplitude spectrum, respectively. The histogram in the upper-right corner shows the distribution of estimation errors (Measured DSI – Estimated DSI). Dashed line indicates the mean value of the distribution. **B.** Simple cells in supra-granular layers. The same format is used as in A. **C.** Simple cells in infra-granular layers. The same format is used as in A.

As described in Figure 3.2A, almost all simple cells in supra-granular layers are direction selective in our data population. However, spatiotemporal linear RF doesn't provide a reasonable prediction for measured DSIs ($r = 0.34$, $p = 0.07$), indicating a very high degree of non-linear component of direction selectivity.

The histogram in each panel in Figure 3.4 shows distribution of non-linear component of direction selectivity (the difference between measured DSI and estimated DSI). In the granular layer, the distribution of this non-linear component was centered at zero (Figure 3.4A), and there was no significant difference between measured DSIs and estimated DSIs (Wilcoxon signed rank test, $p = 0.12$). However, in supra-granular layers (Figure 3.4B), the mean of the distribution of non-linear component of direction selectivity is positive, indicating that linearly estimated DSIs are significantly smaller than DSIs measured with grating stimuli (Wilcoxon signed rank test, $p<10^{-3}$). The distribution of non-linear component values in the infra-

granular layers similar to that of the supra-granular layers (Wilcoxon signed rank test, $p<10^{-3}$).

3.4 Discussion

Previous studies reported that that linear estimation of direction selectivity of simple cells is often smaller than that measured with drifting sinusoidal grating stimuli (DeAngelis et al., 1993b; Peterson et al., 2004). We assumed that difference between measured and linearly estimated DSIs (non-linearity of DSI) is largely derived from intra-cortical connections. And based on this assumption, we hypothesized that the non-linearity of DSI would be differently distributed depending on cortical layers.

We assigned 899 cells to one out of four cortical layer groups. Low spontaneous activity and dominance of simple cell in the granular (major LGN input) layer verified that out assignment criterion was appropriate. Consistent with our hypothesis, non-linearity of DSI was the biggest in the supra-granular layer which is reported to contain well-developed horizontal connections and the smallest in the granular layer.

3.4.1. Difference between supra-granular and infra-granular layers

We have shown that neurons in supra- and infra-granular layers share several properties differentiating themselves from those in granular layer. They have a stronger spontaneous activity on average. Complex type of neurons dominates over simple type. Considerable amount of non-linearity was involved in direction selectivity of neurons in these layers.

From numerous anatomical and physiological evidences, we know that neurons in supra-granular layer (layer 2/3) receive their principal input from granular layer (layer 4). In a simplified projection pattern, thalamocortical input arriving in layer 4 is relayed from layer 4 to 3 (and 2), from layer 3 to layer 5, and from layer 5 to 6 (Thomson & Bannister, 2003). Information processed in the visual cortex is transmitted to other cortical areas through layer 3 and 6. Neurons in layer 6 are more interesting in that they receive direct LGN input and also provide feedback projections to LGN.

Consistent with these findings, our results show that the proportion of complex cells relative to simple cells increases gradually along the visual information flow from layer 4 to 3 and from layer 3 to 5 (20.71% in layer 4 → 71.2% in layer 2/3 → 86.72% in layer 5). In layer 6, simple and complex types of cells occupy comparable proportion of the total population. This is thought to be due to direct input from LGN cells.

One interesting characteristic shown in DSI distribution of infra-granular layer is that the distribution has a clear peak at the highest DSI value (DSI>0.9). It was most prominent in layer 6 but also observable in layer 5 regardless of cell types, although the number of simple cells in layer 5 might be too small to be characterized. This agrees with the result reported previously (Hawken, Parker, & Lund, 1988; Schiller, Finlay, & Volman, 1976). Hawken and colleagues reported that in monkey V1, the majority of cells, which are highly direction selective, are confined to the upper sublayers of 4 and layer 6. Especially, cells with their directional index > 10 (similar to our DSI > 0.9) are mainly found in layer 6. In the cat's visual cortex, reasonably uniform distribution of directionally selective cells throughout all cortical layers had been reported (Gilbert, 1977), but there has been not enough follow-up studies which can be compared with (Hawken et al., 1988).

3.4.2. Intra-cortical connection and direction selectivity

In the supra-granular layers (layer 2/3), simple cells accounted for less than 30% of total population, but their DSI distribution was strongly biased to high DSI values. Simple cells in layer 4 also showed similar characteristic, but the degree of high DSI bias was weaker compared with that in the supra-granular layers.

We previously reported that direction selective (DS) simple cells could be formed from excitatory non-DS simple cell inputs with variable temporal phase differences. Direct input from lagged LGN cells is not necessarily required (Peterson et al., 2004). This may be able to explain the results described above that how simple cells in layer 2/3 are more direction selective than their main input providers (simple cells in layer 4).

Role of intra-cortical inhibition on direction selectivity had been tested by injection of bicuculline methiodide (BMI), a selective antagonist for $GABA_A$ receptor (Sato, Katsuyama, Tamura, Hata, & Tsumoto, 1995). Blocking intra-cortical inhibition caused clear reduction (but not entire disappearance) of direction selectivity in most of cells in layer 2/3 and layer 4b. It suggests that excitatory inputs to layer 2/3 are bi-directional but slightly biased to one direction and that extra non-selective inhibitory inputs determine the degree of directionality by raising firing threshold to various levels.

However, the direction selectivity of cells in layer 6 was rarely affected by BMI (Sato et al., 1995). The authors explained it that the direction selectivity of layer 6 cells is largely dependent on already directionally tuned excitatory inputs rather than inhibitory mechanisms. Possible input sources of cells in layer 6 may include non-DS LGN cells as well as DS & non-DS cells in the supra-granular layers.

Chapter 4

Issues related to response variability

Preface: This chapter is the dissertation author's original unpublished work.

4.1 Introduction

In order to describe classical receptive fields (CRFs) of neurons in primary visual cortex, the most frequently used stimulus is a Gabor patch (a sine wave grating in a Gaussian window). This type of stimulus is generated with a few basic parameters which can be set independently – contrast, orientation, spatial frequency, temporal frequency, spatial phase, & size. Numerous studies have shown that spiking response of individual cell in primary visual cortex is differently tuned to each of these parameters. Therefore, each single neuron should be able to contribute to discrimination among various visual stimuli in terms of these parameters, based on magnitude of its spiking response. For example, in orientation discrimination task where a subject is required to discriminate 90deg from 80deg through 2 alternative force choice method, a V1 single neuron tuned for 90deg orientation can contribute to the task in the way that it evokes stronger spiking activity for 90deg orientation visual stimulus than for 80deg orientation visual stimulus.

However, spiking response of a V1 single neuron to repeated presentations of the same visual stimulus is too variable to explain excellent behavioral performance in discrimination task. From the viewpoint of experimenter who controls the parameters of visual stimuli systematically, this trial-to-trial variability can be regarded as unpredictable noise which may reduce potential performance of neural computation. The source and advantage of trial-to-trial variability is not yet understood. In the following sections, I will introduce several response variability related issues that we already know and need to know.

4.2 Response variability is proportional to response mean

Spontaneous variations in cortical state due to arousal or attention level have been suggested as a source of trial-to-trial variability (Arieli, Sterkin, Grinvald, & Aertsen, 1996; M. D. Fox, Snyder, Zacks, & Raichle, 2006). If the trial-to-trial variability is accounted by simple linear addition of spontaneous variation and visually evoked response, the trial-to-trial variability should be maintained at a stable level regardless of response mean. However, this is not true. Response variability is proportional to response mean (Tolhurst, Movshon, & Thompson, 1981).

These findings suggest that response variability should arise from at least two different sources – One is spontaneous variation and the other is stimulus dependent variation. Results from recent studies which investigated stimulus dependent response variability will be discussed in the following sections of this chapter.

4.3 Magnitude of response variability: sub-cortical structure vs. visual cortex

According to previous studies, response variability in subcortical structures, such as retinal ganglion cells and LGN cells, is substantially lower than that measured in primary visual cortex (Croner, Purpura, & Kaplan, 1993; Edwards, Purpura, & Kaplan, 1995). And these results lead us to think that the primary visual cortex is the area where high response variability arise from. Gur et al. (1997) reported that in awake monkey V1, large proportion of response variability is caused by fixational eye movements of the animal and that minimizing effects of fixational eye movements dramatically reduces the response variability in V1 cells to a level similar to that measured in LGN cells (Gur, Beylin, & Snodderly, 1997).

However Gur et al.'s study may have several limitations to be generalized. First, they didn't compare response variability in V1 with that in in LGN under the condition that they didn't minimize effects of fixational eye movements. If response variability in V1 is larger than that in LGN under this condition, it should mean that fixational eye movements affect spiking activity of V1 cells stronger than that of LGN cells. Second, fixational eye movements don't occur during experiments in which anesthetized and paralyzed animals are used. Instead, slow changes in responsiveness have been reported in anesthetized and paralyzed animals (M. S. Livingstone & Hubel, 1981). In order for response variability in V1 to be larger than that in LGN under anesthesia, effects of sleep and arousal should be stronger in V1 than LGN. If it is true, we may be able to observe stronger spontaneous variations in V1 cells than LGN cells under the condition where there is no visual stimulus.

4.4 Response variability is correlated among nearby cortical neurons

As described in the Introduction section, trial-to-trial variability (or noise) of individual neuron's spiking activity doesn't seem desirable for elaborate neural computation. If so, how can our visual system resolve this problem and yield precise behavioral performance.

If the noise is uncorrelated among nearby cortical neurons, the solution will be very simple. By taking population activities for neural computation, our visual system can make the noise canceled out one another. Consequently, the sum of population activities will be constant in repeated trials (trial-to-trial variability equals zero).

However, unfortunately, the noise among cortical neurons is correlated. Smith and Kohn (2008) investigated the spatial extent of correlated spontaneous and evoked activity while they recorded single unit activity with microelectrode arrays, and

showed that there are two mechanisms which generate correlated variability among neurons with similar orientation preferences on different spatial scales (Smith & Kohn, 2008). One has high temporal precision within a limited spatial extent (<3mm) so that it is revealed as significant cross-correlation. The other one causes correlation which extends 10mm or longer, but it is on a slow time scale so that it is revealed as significant spike count correlation. Spatial extent of correlation in spontaneous activity is similar to that of the second mechanism (>10mm), but it was about twice stronger. That is, visual stimuli caused a remarkable decrease in correlation.

It is well known from anatomical and physiological studies that horizontal connections in V1 are preferentially linking neurons with similar orientation preferences (Bosking et al., 1997; Gilbert & Wiesel, 1989). Therefore, it may not be surprising that the noise is correlated among similarly tuned neurons in V1. However, if the noise is correlated, activity of neural population with similar tuning should be also as noisy as single cell activity. Then, how can we overcome this problem?

In the first page, in order to explain neural computation, I exemplified how a V1 single neuron tuned for 90deg orientation contributes to discrimination between 90deg and 80deg orientation stimuli. But, in actual neural computation, the greatest contribution to the discrimination may come from a V1 single neuron tuned for 60deg or 110deg. Figure 4.1A~C depict schematic orientation tuning functions (black curves) of neurons tuned for 90deg, 60deg, and 110deg orientation respectively. It is assumed that these three orientation tuning curves have the same width (standard deviation = 20deg). And red and blue lines were added to indicate neural response of each neuron to 90deg and 80deg orientation stimulus. In case of a neuron tuned for 90deg (Figure 4.1A), difference between neural response to 90deg and that to 80deg is relatively small, because the slope of orientation tuning curve is not steep near the peak. So this small difference may easily disappear or be reversed by trial-to-trial variability.

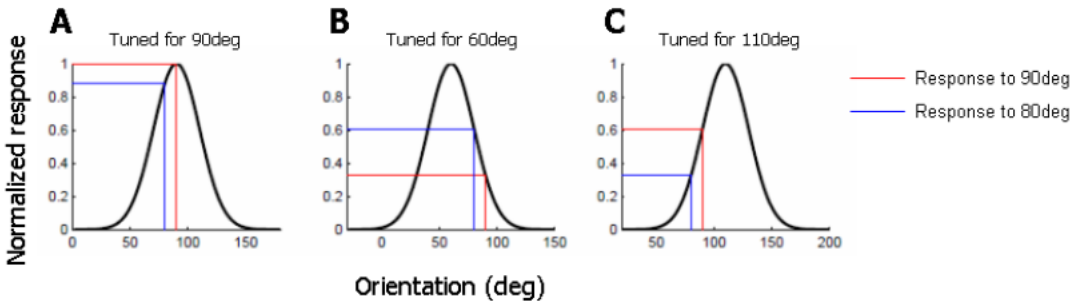

Figure 4.1. Orientation tuning functions of three cells tuned for 90deg, 60deg, and 110deg respectively. Tuning widths of these three functions were set as the same (standard deviation = 20deg). Red and blue lines indicate neural responses to two different orientations (90deg and 80deg) which should be discriminated in the task (see more detail in Introduction seciton). Therefore, each neuron's contribution to the orientation discrimination task is reflected in height difference between

red and blue lines in each panel.

In contrast, if a neuron tuned for 60deg or 110deg (Figure 4.1B,C), difference between neural response to 90deg and that to 80deg is relatively big, because 80~90deg orientations are in the section where the slope of orientation tuning curve is the steepest. Therefore, these cells can provide more reliable information which is not vulnerable to trial-to-trial variability. Furthermore, if differently tuned groups (e.g., Group1 tuned for 60deg & Group2 tuned for 110deg) are recruited together for neural computation, it may produce more precise result of neural computation. Response variabilities in Group1 & 2 are believed to be rarely correlated to each other owing to different tuning properties. However, even if they are significantly correlated to each other, this correlation will not worsen the neural computation. For example, we can imagine a situation that in a certain trial, neural response to 90deg stimulus was much stronger than mean neural response to the same stimulus. The increased response to 90deg stimulus will make information from Group1 (Figure 4.1B) neural computation less reliable, since it reduces the difference between neural response to 80deg and that to 90deg orientation stimuli. But if the same noise is applied to Group2 (Figure 4.1C), it can increase the neural response difference between two orientation stimuli so that make information from Group2 (Figure 4.1C) neural computation more reliable.

4.5 Future studies

According to Smith and Kohn (2008)'s study, response variability is significantly correlated among neurons with similar orientation tuning and it is thought to be mediated by intracortical connections such as horizontal and feedback connections (Smith & Kohn, 2008). The functions of intracortical connections are not yet fully understood. But we know that they are at least involved in two functions by integrating information from larger area outside the classical receptive field - sharpening of tuning properties and modulating response gain. Therefore, "relationship between tuning and response variability" also deserves to get researcher's attention.

The questions listed below are some of the unsolved problems in the issue about neuronal response variability.

- Are finely tuned cells less variable?
- Response variability for the optimal stimulus is smaller than that for the non-optimal stimulus?
- Does response variability in simple cell show different pattern compared with that in complex cell?
- How is the response variability affected by surround suppression or surround facilitation?

- If the response variability is affected by an additional surround stimulus or a change in stimulus parameter (e.g., orientation, spatial frequency, etc.), what is the time course of response variability change?

Bibliography

Adelson, E. H., & Bergen, J. R. (1985). Spatiotemporal energy models for the perception of motion. *Journal of the Optical Society of America. A, Optics and Image Science*, *2*, 284–299. doi:10.1364/JOSAA.2.000284

Albrecht, D., & Hamilton, D. (1982). Striate cortex of monkey and cat: contrast response function. *J Neurophysiol*, *48*, 217–237. Retrieved from http://jn.physiology.org/content/jn/48/1/217.full.pdf

Albus, K. (1975). A quantitative study of the projection area of the central and the paracentral visual field in area 17 of the cat. I. The precision of the topography. *Experimental Brain Research. Experimentelle Hirnforschung. Experimentation Cerebrale*, *24*, 159–179.

Allen, E. A., & Freeman, R. D. (2006). Dynamic spatial processing originates in early visual pathways. *The Journal of Neuroscience : The Official Journal of the Society for Neuroscience*, *26*, 11763–11774. doi:10.1523/JNEUROSCI.3297-06.2006

Allen, E. A., Pasley, B. N., Duong, T., & Freeman, R. D. (2007). Transcranial magnetic stimulation elicits coupled neural and hemodynamic consequences. *Science (New York, N.Y.)*, *317*, 1918–1921. doi:10.1126/science.1146426

Alonso, J. M. (2002). Neural connections and receptive field properties in the primary visual cortex. *Neuroscientist*, *8*, 443–456. doi:10.1177/107385802236967

Alonso, J. M., & Martinez, L. M. (1998). Functional connectivity between simple cells and complex cells in cat striate cortex. *Nature Neuroscience*, *1*, 395–403. doi:10.1038/1609

Alonso, J. M., Usrey, W. M., & Reid, R. C. (2001). Rules of connectivity between geniculate cells and simple cells in cat primary visual cortex. *The Journal of Neuroscience : The Official Journal of the Society for Neuroscience*, *21*, 4002–4015.

Angelucci, A., & Bressloff, P. C. (2006). Contribution of feedforward, lateral and feedback connections to the classical receptive field center and extra-classical receptive field surround of primate V1 neurons. *Progress in Brain Research*, *154*, 93–120. doi:10.1016/S0079-6123(06)54005-1

Angelucci, A., & Bullier, J. (2003). Reaching beyond the classical receptive field of V1 neurons: Horizontal or feedback axons? *Journal of Physiology Paris*. doi:10.1016/j.jphysparis.2003.09.001

Angelucci, A., Levitt, J. B., Walton, E. J. S., Hupe, J.-M., Bullier, J., & Lund, J. S. (2002). Circuits for local and global signal integration in primary visual cortex. *The Journal of Neuroscience : The Official Journal of the Society for Neuroscience*, *22*, 8633–8646.

Arieli, A., Sterkin, A., Grinvald, A., & Aertsen, A. (1996). Dynamics of ongoing activity: explanation of the large variability in evoked cortical responses. *Science (New York, N.Y.)*, *273*, 1868–1871. doi:10.1126/science.273.5283.1868

Aydin-Abidin, S., Moliadze, V., Eysel, U. T., & Funke, K. (2006). Effects of repetitive TMS on visually evoked potentials and EEG in the anaesthetized cat: dependence on stimulus frequency and train duration. *The Journal of Physiology*, *574*, 443–455. doi:10.1113/jphysiol.2006.108464

Bair, W., Cavanaugh, J. R., & Movshon, J. A. (2003). Time course and time-distance relationships for surround suppression in macaque V1 neurons. *The Journal of Neuroscience : The Official Journal of the Society for Neuroscience*, *23*, 7690–7701. doi:23/20/7690 [pii]

Barker, A., Jalinous, R., & Freeston, I. (1985). Non-invasive magnetic stimulation of human motor cortex. *The Lancet*, *1*, 1106–1107. doi:10.1016/S0140-6736(85)92413-4

Bauman, L. A., & Bonds, A. B. (1991). Inhibitory refinement of spatial frequency selectivity in single cells of the cat striate cortex. *Vision Research*, *31*, 933–944. doi:10.1016/0042-6989(91)90201-F

Belitski, A., Gretton, A., Magri, C., Murayama, Y., Montemurro, M. A., Logothetis, N. K., & Panzeri, S. (2008). Low-frequency local field potentials and spikes in primary visual cortex convey independent visual information. *The Journal of Neuroscience : The Official Journal of the Society for Neuroscience*, *28*, 5696–5709. doi:10.1523/JNEUROSCI.0009-08.2008

Berens, P., Keliris, G. A., Ecker, A. S., Logothetis, N. K., & Tolias, A. S. (2008a). Comparing the feature selectivity of the gamma-band of the local field potential and the underlying spiking activity in primate visual cortex. *Frontiers in Systems Neuroscience*, *2*, 2. doi:10.3389/neuro.06.002.2008

Berens, P., Keliris, G. A., Ecker, A. S., Logothetis, N. K., & Tolias, A. S. (2008b). Feature selectivity of the gamma-band of the local field potential in primate primary visual cortex. *Frontiers in Neuroscience*, *2*, 199–207. doi:10.3389/neuro.01.037.2008

Blakemore, C., & Tobin, E. A. (1972). Lateral inhibition between orientation detectors in the cat's visual cortex. *Experimental Brain Research. Experimentelle Hirnforschung. Experimentation Cerebrale*, *15*, 439–440. doi:10.1007/BF00234129

Bonds, A. (1991). Temporal dynamics of contrast gain in single cells of the cat striate cortex. *Visual Neuroscience*, *6*, 239–255. Retrieved from http://journals.cambridge.org/abstract_S0952523800006258

Bosking, W. H., Zhang, Y., Schofield, B., & Fitzpatrick, D. (1997). Orientation selectivity and the arrangement of horizontal connections in tree shrew striate cortex. *The Journal of Neuroscience : The Official Journal of the Society for Neuroscience*, *17*, 2112–2127.

Bredfeldt, C., & Ringach, D. (2002). Dynamics of spatial frequency tuning in macaque V1. *The Journal of Neuroscience*, *22*, 1976–1984. Retrieved from http://www.jneurosci.org/content/22/5/1976.short

Bringuier, V., Chavane, F., Glaeser, L., & Frégnac, Y. (1999). Horizontal propagation of visual activity in the synaptic integration field of area 17 neurons. *Science (New York, N.Y.)*, *283*, 695–699. doi:10.1126/science.283.5402.695

Budd, J. M. (1998). Extrastriate feedback to primary visual cortex in primates: a quantitative analysis of connectivity. *Proceedings. Biological Sciences / The Royal Society*, *265*, 1037–1044. doi:10.1098/rspb.1998.0396

Bullier, J., Hupé, J. M., James, A. C., & Girard, P. (2001). The role of feedback connections in shaping the responses of visual cortical neurons. In *Progress in Brain Research* (Vol. 134, pp. 193–204). doi:10.1016/S0079-6123(01)34014-1

Carandini, M. (2000). Visual cortex: Fatigue and adaptation. *Current Biology*, *10*. doi:10.1016/S0960-9822(00)00637-0

Carandini, M., & Ferster, D. (1997). A tonic hyperpolarization underlying contrast adaptation in cat visual cortex. *Science*, *276*, 949–952. doi:10.1126/science.276.5314.949

Cattaneo, Z., Rota, F., Walsh, V., Vecchi, T., & Silvanto, J. (2009). TMS-adaptation reveals abstract letter selectivity in the left posterior parietal cortex. *Cerebral Cortex*, *19*, 2321–2325. doi:10.1093/cercor/bhn249

Cavanaugh, J. R., Bair, W., & Movshon, J. A. (2002a). Nature and interaction of signals from the receptive field center and surround in macaque V1 neurons. *Journal of Neurophysiology*, *88*, 2530–2546. doi:10.1152/jn.00692.2001

Cavanaugh, J. R., Bair, W., & Movshon, J. A. (2002b). Selectivity and spatial distribution of signals from the receptive field surround in macaque V1 neurons. *Journal of Neurophysiology*, *88*, 2547–2556. doi:10.1152/jn.00693.2001

Chen, G., Dan, Y., & Li, C. (2005). Stimulation of non-classical receptive field enhances orientation selectivity in the cat. *The Journal of Physiology*, *564*, 233–243. doi:10.1113/jphysiol.2004.080051

Chen, R., Classen, J., & Gerloff, C. (1997). Depression of motor cortex excitability by low-frequency transcranial magnetic stimulation. *Neurology*, *48*, 1398–1403. doi:10.1212/WNL.48.5.1398

Chisum, H. J., Mooser, F., & Fitzpatrick, D. (2003). Emergent properties of layer 2/3 neurons reflect the collinear arrangement of horizontal connections in tree shrew visual cortex. *The Journal of Neuroscience : The Official Journal of the Society for Neuroscience*, *23*, 2947–2960. doi:23/7/2947 [pii]

Croner, L. J., Purpura, K., & Kaplan, E. (1993). Response variability in retinal ganglion cells of primates. *Proc Natl Acad Sci U S A*, *90*, 8128–8130.

De Valois, K. K., & Tootell, R. B. (1983). Spatial-frequency-specific inhibition in cat striate cortex cells. *The Journal of Physiology*, *336*, 359–376.

De Valois, R. L., Cottaris, N. P., Mahon, L. E., Elfar, S. D., & Wilson, J. A. (2000). Spatial and temporal receptive fields of geniculate and cortical cells and directional selectivity. *Vision Research*, *40*, 3685–3702. doi:10.1016/S0042-6989(00)00210-8

DeAngelis, G. C., Freeman, R. D., & Ohzawa, I. (1994). Length and width tuning of neurons in the cat's primary visual cortex. *Journal of Neurophysiology*, *71*, 347–374. doi:8158236

DeAngelis, G. C., Ohzawa, I., & Freeman, R. D. (1993a). Spatiotemporal organization of simple-cell receptive fields in the cat's striate cortex. I. General characteristics and postnatal development. *Journal of Neurophysiology*, *69*, 1091–1117.

DeAngelis, G. C., Ohzawa, I., & Freeman, R. D. (1993b). Spatiotemporal organization of simple-cell receptive fields in the cat's striate cortex. II. Linearity of temporal and spatial summation. *Journal of Neurophysiology*, *69*, 1118–1135.

Dragoi, V., Sharma, J., & Sur, M. (2000). Adaptation-induced plasticity of orientation tuning in adult visual cortex. *Neuron*, *28*, 287–298. doi:10.1016/S0896-6273(00)00103-3

Edwards, D. P., Purpura, K. P., & Kaplan, E. (1995). Contrast sensitivity and spatial frequency response of primate cortical neurons in and around the cytochrome oxidase blobs. *Vision Research*, *35*, 1501–1523. doi:10.1016/0042-6989(94)00253-I

Eldaief, M. C., Halko, M. A., Buckner, R. L., & Pascual-Leone, A. (2011). Transcranial magnetic stimulation modulates the brain's intrinsic activity in a frequency-dependent manner. *Proceedings of the National Academy of Sciences*. doi:10.1073/pnas.1113103109

Emerson, R. C., Bergen, J. R., & Adelson, E. H. (1992). Directionally selective complex cells and the computation of motion energy in cat visual cortex. *Vision Research*, *32*, 203–218. doi:10.1016/0042-6989(92)90130-B

Fierro, B., Brighina, F., Vitello, G., Piazza, A., Scalia, S., Giglia, G., … Pascual-Leone, A. (2005). Modulatory effects of low- and high-frequency repetitive transcranial magnetic stimulation on visual cortex of healthy subjects undergoing light deprivation. *The Journal of Physiology*, *565*, 659–665. doi:10.1113/jphysiol.2004.080184

Fox, C. H., Johnson, F. B., Whiting, J., & Roller, P. P. (1985). Formaldehyde fixation. *The Journal of Histochemistry and Cytochemistry : Official Journal of the Histochemistry Society*, *33*, 845–853. doi:10.1152/ajpgi.00048.2011

Fox, M. D., Snyder, A. Z., Zacks, J. M., & Raichle, M. E. (2006). *Coherent spontaneous activity accounts for trial-to-trial variability in human evoked brain responses. Nature neuroscience* (Vol. 9, pp. 23–25). doi:10.1038/nn1616

Frazor, R. A., Albrecht, D. G., Geisler, W. S., & Crane, A. M. (2004). Visual cortex neurons of monkeys and cats: temporal dynamics of the spatial frequency response function. *Journal of Neurophysiology*, *91*, 2607–2627. doi:10.1152/jn.00858.2003

Freund, T. F., Martin, K. A., Soltesz, I., Somogyi, P., & Whitteridge, D. (1989). Arborisation pattern and postsynaptic targets of physiologically identified thalamocortical afferents in striate cortex of the macaque monkey. *The Journal of Comparative Neurology*, *289*, 315–336. doi:10.1002/cne.902890211

Funke, K., & Benali, A. (2011). Modulation of cortical inhibition by rTMS–findings obtained from animal models. *The Journal of Physiology*, *589*, 4423–4435. doi:10.1113/jphysiol.2011.206573

Galuske, R. A. W., Schmidt, K. E., Goebel, R., Lomber, S. G., & Payne, B. R. (2002). The role of feedback in shaping neural representations in cat visual cortex. *Proceedings of the National Academy of Sciences of the United States of America*, *99*, 17083–17088. doi:10.1073/pnas.242399199

Gardner, J. L., Sun, P., Waggoner, R. A., Ueno, K., Tanaka, K., & Cheng, K. (2005). Contrast adaptation and representation in human early visual cortex. *Neuron*, *47*, 607–620. doi:10.1016/j.neuron.2005.07.016

Garry, M. I., & Thomson, R. H. S. (2009). The effect of test TMS intensity on short-interval intracortical inhibition in different excitability states. *Experimental Brain Research*, *193*, 267–274. doi:10.1007/s00221-008-1620-5

George, M. S., Lisanby, S. H., & Sackeim, H. A. (1999). Transcranial magnetic stimulation: applications in neuropsychiatry. *Archives of General Psychiatry*, *56*, 300–311. doi:10.1001/archpsyc.56.4.300

Ghisovan, N., Nemri, A., Shumikhina, S., & Molotchnikoff, S. (2009). Long adaptation reveals mostly attractive shifts of orientation tuning in cat primary visual cortex. *Neuroscience*, *164*, 1274–1283. doi:10.1016/j.neuroscience.2009.09.003

Gieselmann, M. A., & Thiele, A. (2008). Comparison of spatial integration and surround suppression characteristics in spiking activity and the local field potential in macaque V1. *The European Journal of Neuroscience*, *28*, 447–459. doi:10.1111/j.1460-9568.2008.06358.x

Gilbert, C. D. (1977). Laminar differences in receptive field properties of cells in cat primary visual cortex. *J Physiol*, *268*, 391–421. Retrieved from http://www.ncbi.nlm.nih.gov/entrez/query.fcgi?cmd=Retrieve&db=PubMed&dopt=Citation&list_uids=874916

Gilbert, C. D., & Wiesel, T. N. (1989). Columnar specificity of intrinsic horizontal and corticocortical connections in cat visual cortex. *The Journal of Neuroscience : The Official Journal of the Society for Neuroscience*, *9*, 2432–2442.

Girard, P., Hupé, J. M., & Bullier, J. (2001). Feedforward and feedback connections between areas V1 and V2 of the monkey have similar rapid conduction velocities. *Journal of Neurophysiology*, *85*, 1328–1331.

Goddard, G., McIntyre, D., & Leech, C. (1969). A permanent change in brain function resulting from daily electrical stimulation. *Experimental Neurology*, *25*, 295–330. doi:10.1016/0014-4886(69)90128-9

Grinvald, A., Lieke, E. E., Frostig, R. D., & Hildesheim, R. (1994). Cortical point-spread function and long-range lateral interactions revealed by real-time optical imaging of macaque monkey primary visual cortex. *The Journal of Neuroscience : The Official Journal of the Society for Neuroscience*, *14*, 2545–2568.

Gur, M., Beylin, A., & Snodderly, D. M. (1997). Response variability of neurons in primary visual cortex (V1) of alert monkeys. *The Journal of Neuroscience : The Official Journal of the Society for Neuroscience*, *17*, 2914–2920.

Hallett, M. (2000). Transcranial magnetic stimulation and the human brain. *Nature*, *406*, 147–150. doi:10.1038/35018000

Hallett, M. (2007). Transcranial magnetic stimulation: a primer. *Neuron*, *55*, 187–199. doi:10.1016/j.neuron.2007.06.026

Hashemi-Nezhad, M., & Lyon, D. C. (2012). Orientation tuning of the suppressive extraclassical surround depends on intrinsic organization of V1. *Cerebral Cortex (New York, N.Y. : 1991)*, *22*, 308–26. doi:10.1093/cercor/bhr105

Hawken, M. J., Parker, A. J., & Lund, J. S. (1988). Laminar organization and contrast sensitivity of direction-selective cells in the striate cortex of the Old World monkey. *The Journal of Neuroscience : The Official Journal of the Society for Neuroscience*, *8*, 3541–3548.

Henrie, J. A., & Shapley, R. (2005). LFP power spectra in V1 cortex: the graded effect of stimulus contrast. *Journal of Neurophysiology*, *94*, 479–490. doi:10.1152/jn.00919.2004

Henry, C. A., Joshi, S., Xing, D., Shapley, R. M., & Hawken, M. J. (2013). Functional characterization of the extraclassical receptive field in macaque V1: contrast, orientation, and temporal dynamics. *The Journal of Neuroscience : The Official Journal of the Society for Neuroscience*, *33*, 6230–42. doi:10.1523/JNEUROSCI.4155-12.2013

Henry, G. H., Salin, P. a., & Bullier, J. (1991). Projections from Areas 18 and 19 to Cat Striate Cortex: Divergence and Laminar Specificity. *The European Journal of Neuroscience*, *3*, 186–200. doi:ejn_03020186 [pii]

Hirsch, J. A., & Gilbert, C. D. (1991). Synaptic physiology of horizontal connections in the cat's visual cortex. *The Journal of Neuroscience : The Official Journal of the Society for Neuroscience*, *11*, 1800–1809.

Hotson, J., Braun, D., Herzberg, W., & Boman, D. (1994). Transcranial magnetic stimulation of extrastriate cortex degrades human motion direction discrimination. *Vision Research*, *34*, 2115–2123.

Huang, Y.-Z., Edwards, M. J., Rounis, E., Bhatia, K. P., & Rothwell, J. C. (2005). *Theta burst stimulation of the human motor cortex. Neuron* (Vol. 45, pp. 201–206). doi:10.1016/j.neuron.2004.12.033

Hubel, D. H., & Wiesel, T. N. (1962). Receptive fields, binocular interaction and functional architecture in the cat's visual cortex. *The Journal of Physiology* , *160* (1), 106–154. Retrieved from http://jp.physoc.org/content/160/1/106.short

Hupé, J. M., James, A. C., Girard, P., Lomber, S. G., Payne, B. R., & Bullier, J. (2001). Feedback connections act on the early part of the responses in monkey visual cortex. *Journal of Neurophysiology*, *85*, 134–145. doi:11152714

Hupé, J. M., James, A. C., Payne, B. R., Lomber, S. G., Girard, P., & Bullier, J. (1998). Cortical feedback improves discrimination between figure and background by V1, V2 and V3 neurons. *Nature*, *394*, 784–787. doi:10.1038/29537

Ichida, J. M., Schwabe, L., Bressloff, P. C., & Angelucci, A. (2007). Response facilitation from the "suppressive" receptive field surround of macaque V1 neurons. *Journal of Neurophysiology*, *98*, 2168–2181. doi:10.1152/jn.00298.2007

Jagadeesh, B., Wheat, H. S., & Ferster, D. (1993). Linearity of summation of synaptic potentials underlying direction selectivity in simple cells of the cat visual cortex. *Science (New York, N.Y.)*, *262*, 1901–1904.

Jagadeesh, B., Wheat, H. S., Kontsevich, L. L., Tyler, C. W., & Ferster, D. (1997). Direction selectivity of synaptic potentials in simple cells of the cat visual cortex. *Journal of Neurophysiology*, *78*, 2772–2789.

Jia, X., Smith, M. A., & Kohn, A. (2011). Stimulus selectivity and spatial coherence of gamma components of the local field potential. *The Journal of Neuroscience : The Official Journal of the Society for Neuroscience*, *31*, 9390–9403. doi:10.1523/JNEUROSCI.0645-11.2011

Jones, J. P., & Palmer, L. A. (1987). The two-dimensional spatial structure of simple receptive fields in cat striate cortex. *Journal of Neurophysiology*, *58*, 1187–1211.

Kammer, T., Puls, K., Erb, M., & Grodd, W. (2005). Transcranial magnetic stimulation in the visual system. II. Characterization of induced phosphenes and scotomas. *Experimental Brain Research*, *160*, 129–140. doi:10.1007/s00221-004-1992-0

Kapadia, M. K., Ito, M., Gilbert, C. D., & Westheimer, G. (1995). Improvement in visual sensitivity by changes in local context: parallel studies in human observers and in V1 of alert monkeys. *Neuron*, *15*, 843–856. doi:10.1016/0896-6273(95)90175-2

Kapadia, M. K., Westheimer, G., & Gilbert, C. D. (2000). Spatial distribution of contextual interactions in primary visual cortex and in visual perception. *Journal of Neurophysiology*, *84*, 2048–2062.

Katzner, S., Busse, L., & Carandini, M. (2011). GABAA inhibition controls response gain in visual cortex. *The Journal of Neuroscience*, *31*, 5931–5941. doi:10.1523/JNEUROSCI.5753-10.2011

Kharazia, V., & Weinberg, R. (1994). Glutamate in thalamic fibers terminating in layer IV of primary sensory cortex. *The Journal of Neuroscience*, *14*, 6021–6032. Retrieved from http://www.jneurosci.org/content/14/10/6021.short

Kim, T., Kim, H. R., Kim, K., & Lee, C. (2012). Modulation of V1 Spike Response by Temporal Interval of Spatiotemporal Stimulus Sequence. *PLoS ONE*, *7*. doi:10.1371/journal.pone.0047543

Kisvárday, Z. F., Tóth, E., Rausch, M., & Eysel, U. T. (1997). Orientation-specific relationship between populations of excitatory and inhibitory lateral connections in the visual cortex of the cat. *Cerebral Cortex* , *7* (7), 605–618. doi:10.1093/cercor/7.7.605

Kreiman, G., Hung, C. P., Kraskov, A., Quiroga, R. Q., Poggio, T., & DiCarlo, J. J. (2006). Object selectivity of local field potentials and spikes in the macaque inferior temporal cortex. *Neuron*, *49*, 433–445. doi:10.1016/j.neuron.2005.12.019

LeVay, S., & Gilbert, C. D. (1976). Laminar patterns of geniculocortical projection in the cat. *Brain Research*, *113*, 1–19. doi:10.1016/0006-8993(76)90002-0

Levitt, J. B., & Lund, J. S. (1997). Contrast dependence of contextual effects in primate visual cortex. *Nature*, *387*, 73–76. doi:10.1038/387073a0

Liu, Y. J., Hashemi-Nezhad, M., & Lyon, D. C. (2013). Sharper orientation tuning of the extraclassical suppressive-surround due to a neuron's location in the V1 orientation map emerges late in time. *Neuroscience*, *229*, 100–117. doi:10.1016/j.neuroscience.2012.10.071

Livingstone, M., & Hubel, D. (1988). Segregation of form, color, movement, and depth: anatomy, physiology, and perception. *Science (New York, N.Y.)*, *240*, 740–749. doi:10.1126/science.3283936

Livingstone, M. S., & Hubel, D. H. (1981). Effects of sleep and arousal on the processing of visual information in the cat. *Nature*, *291*, 554–561. doi:10.1038/291554a0

Logothetis, N. K. (2003). The underpinnings of the BOLD functional magnetic resonance imaging signal. *The Journal of Neuroscience : The Official Journal of the Society for Neuroscience*, *23*, 3963–3971. doi:23/10/3963 [pii]

Maeda, F., Keenan, J. P., Tormos, J. M., Topka, H., & Pascual-Leone, A. (2000). Interindividual variability of the modulatory effects of repetitive transcranial magnetic stimulation on cortical excitability. *Experimental Brain Research*, *133*, 425–430. doi:10.1007/s002210000432

Maffei, L., & Fiorentini, A. (1973). The visual cortex as a spatial frequency analyser. *Vision Research*, *13*, 1255–1267. doi:10.1016/0042-6989(73)90201-0

Malach, R., Amir, Y., Harel, M., & Grinvald, A. (1993). Relationship between intrinsic connections and functional architecture revealed by optical imaging and in vivo targeted biocytin injections in primate striate cortex. *Proceedings of the National Academy of Sciences of the United States of America*, *90*, 10469–10473. doi:10.1073/pnas.90.22.10469

Malone, B. J., Kumar, V. R., & Ringach, D. L. (2007). Dynamics of receptive field size in primary visual cortex. *Journal of Neurophysiology*, *97*, 407–414. doi:10.1152/jn.00830.2006

Martinez, L. M., Wang, Q., Reid, R. C., Pillai, C., Alonso, J.-M., Sommer, F. T., & Hirsch, J. A. (2005). Receptive field structure varies with layer in the primary visual cortex. *Nature Neuroscience*, *8*, 372–379. doi:10.1038/nn1404

Mazer, J. A., Vinje, W. E., McDermott, J., Schiller, P. H., & Gallant, J. L. (2002). Spatial frequency and orientation tuning dynamics in area V1. *Proceedings of the National Academy of Sciences of the United States of America*, *99*, 1645–1650. doi:10.1073/pnas.022638499

McGuire, B. A., Gilbert, C. D., Rivlin, P. K., & Wiesel, T. N. (1991). Targets of horizontal connections in macaque primary visual cortex. *The Journal of Comparative Neurology*, *305*, 370–392. doi:10.1002/cne.903050303

McGuire, B. A., Hornung, J. P., Gilbert, C. D., & Wiesel, T. N. (1984). Patterns of synaptic input to layer 4 of cat striate cortex. *The Journal of Neuroscience*, *4*, 3021–33. Retrieved from http://www.ncbi.nlm.nih.gov/pubmed/6502220

McIntyre, C. C., & Grill, W. M. (1999). Excitation of central nervous system neurons by nonuniform electric fields. *Biophysical Journal*, *76*, 878–888. doi:10.1016/S0006-3495(99)77251-6

Menz, M. D., & Freeman, R. D. (2003). Stereoscopic depth processing in the visual cortex: a coarse-to-fine mechanism. *Nature Neuroscience*, *6*, 59–65. doi:10.1038/nn986

Merton, P., & Morton, H. (1980). Stimulation of the cerebral cortex in the intact human subject. *Nature*, *285*, 227. doi:10.1038/285227a0

Mitzdorf, U. (1985). Current source-density method and application in cat cerebral cortex: investigation of evoked potentials and EEG phenomena. *Physiological Reviews*, *65*, 37–100.

Mitzdorf, U. (1987). Properties of the evoked potential generators: current source-density analysis of visually evoked potentials in the cat cortex. *International Journal of Neuroscience*, *33*, 33–59. doi:10.3109/00207458708985928

Mizobe, K., & Polat, U. (2001). Facilitation and suppression of single striate-cell activity by spatially discrete pattern stimuli presented beyond the receptive field. *Visual …*, *18*(3), 377–91. Retrieved from http://journals.cambridge.org/abstract_S0952523801183045

Moliadze, V., Zhao, Y., Eysel, U., & Funke, K. (2003). Effect of transcranial magnetic stimulation on single-unit activity in the cat primary visual cortex. *The Journal of Physiology*, *553*, 665–679. doi:10.1113/jphysiol.2003.050153

Nakamura, H., Kitagawa, H., Kawaguchi, Y., & Tsuji, H. (1997). *Intracortical facilitation and inhibition after transcranial magnetic stimulation in conscious humans. The Journal of physiology* (Vol. 498 (Pt 3, pp. 817–823).

Nassi, J. J., & Callaway, E. M. (2009). Parallel processing strategies of the primate visual system. *Nature Reviews. Neuroscience*, *10*, 360–372. doi:10.1038/nrn2619

Nelson, J. I., & Frost, B. J. (1985). Intracortical facilitation among co-oriented, co-axially aligned simple cells in cat striate cortex. *Experimental Brain Research. Experimentelle Hirnforschung. Experimentation Cerebrale*, *61*, 54–61. doi:10.1007/BF00235620

Nowak, L. G., & Bullier, J. (1998). Axons, but not cell bodies, are activated by electrical stimulation in cortical gray matter. I. Evidence from chronaxie measurements. *Experimental Brain Research*, *118*, 477–488. doi:10.1007/s002210050304

Oberman, L., Edwards, D., Eldaief, M., & Pascual-Leone, A. (2011). Safety of theta burst transcranial magnetic stimulation: a systematic review of the literature. *Journal of Clinical Neurophysiology : Official Publication of the American Electroencephalographic Society*, *28*, 67–74. doi:10.1097/WNP.0b013e318205135f

Ohzawa, I., Sclar, G., & Freeman, R. (1982). Contrast gain control in the cat visual cortex. *Nature*, *298*, 266–268. doi:10.1038/298266a0

Ohzawa, I., Sclar, G., & Freeman, R. (1985). Contrast gain control in the cat's visual system. *J Neurophysiol*, *54*, 651–667. Retrieved from http://jn.physiology.org/content/jn/54/3/651.full.pdf

Okamoto, M., Naito, T., Sadakane, O., Osaki, H., & Sato, H. (2009). Surround suppression sharpens orientation tuning in the cat primary visual cortex. *The*

European Journal of Neuroscience, *29*, 1035–1046. doi:10.1111/j.1460-9568.2009.06645.x

Ozeki, H., Sadakane, O., Akasaki, T., Naito, T., Shimegi, S., & Sato, H. (2004). Relationship between excitation and inhibition underlying size tuning and contextual response modulation in the cat primary visual cortex. *The Journal of Neuroscience : The Official Journal of the Society for Neuroscience*, *24*, 1428–1438. doi:10.1523/JNEUROSCI.3852-03.2004

Pascual-Leone, A., Nguyet, D., Cohen, L. G., Brasil-Neto, J. P., Cammarota, A., & Hallett, M. (1995). Modulation of muscle responses evoked by transcranial magnetic stimulation during the acquisition of new fine motor skills. *Journal of Neurophysiology*, *74*, 1037–1045.

Pascual-Leone, A., Tormos, J. M., Keenan, J., Tarazona, F., Canete, C., & Catala, M. D. (1998). Study and modulation of human cortical excitability with transcranial magnetic stimulation. *Journal of Clinical Neurophysiology*, *15*, 333–343. Retrieved from http://www.ncbi.nlm.nih.gov/pubmed/9736467

Pascual-Leone, A., Valls-Solé, J., Wassermann, E. M., & Hallett, M. (1994). Responses to rapid-rate transcranial magnetic stimulation of the human motor cortex. *Brain : A Journal of Neurology*, *117 (Pt 4*, 847–858.

Pashut, T., Wolfus, S., Friedman, A., Lavidor, M., Bar-Gad, I., Yeshurun, Y., & Korngreen, A. (2011). Mechanisms of magnetic stimulation of central nervous system neurons. *PLoS Computational Biology*, *7*, e1002022. doi:10.1371/journal.pcbi.1002022

Pasley, B., Allen, E., & Freeman, R. (2009). State-dependent variability of neuronal responses to transcranial magnetic stimulation of the visual cortex. *Neuron*, *62*, 291–303. doi:10.1016/j.neuron.2009.03.012

Peinemann, A., Reimer, B., L??er, C., Quartarone, A., M??nchau, A., Conrad, B., & Siebner, H. R. (2004). Long-lasting increase in corticospinal excitability after 1800 pulses of subthreshold 5 Hz repetitive TMS to the primary motor cortex. *Clinical Neurophysiology*, *115*, 1519–1526. doi:10.1016/j.clinph.2004.02.005

Peters, A., Payne, B., & Budd, J. (1994). A numerical analysis of the geniculocortical input to striate cortex in the monkey. *Cerebral Cortex*, *4*(3), 215–29. Retrieved from http://cercor.oxfordjournals.org/content/4/3/215.short

Peterson, M. R., Li, B., & Freeman, R. D. (2004). The derivation of direction selectivity in the striate cortex. *The Journal of Neuroscience : The Official Journal of the Society for Neuroscience*, *24*, 3583–3591. doi:10.1523/JNEUROSCI.5398-03.2004

Platz, T., & Rothwell, J. C. (2010). Brain stimulation and brain repair--rTMS: from animal experiment to clinical trials--what do we know? *Restorative Neurology and Neuroscience*, *28*, 387–398. doi:10.3233/RNN-2010-0570

Polat, U., Mizobe, K., Pettet, M. W., Kasamatsu, T., & Norcia, A. M. (1998). Collinear stimuli regulate visual responses depending on cell's contrast threshold. *Nature*, *391*, 580–584. doi:10.1038/35372

Racine, R. (1972). Modification of seizure activity by electrical stimulation: II. Motor seizure. *Electroencephalography and Clinical Neurophysiology*, *32*, 281–294. doi:10.1016/0013-4694(72)90177-0

Rattay, F. (1999). The basic mechanism for the electrical stimulation of the nervous system. *Neuroscience*, *89*, 335–346. doi:10.1016/S0306-4522(98)00330-3

Ray, S., & Maunsell, J. (2011). Different origins of gamma rhythm and high-gamma activity in macaque visual cortex. *PLoS Biology*, *9*. doi:10.1371/journal.pbio.1000610

Reynolds, J., Pasternak, T., & Desimone, R. (2000). Attention increases sensitivity of V4 neurons. *Neuron*, *26*, 703–714. doi:10.1016/S0896-6273(00)81206-4

Ringach, D., Hawken, M., & Shapley, R. (1997). Dynamics of orientation tuning in macaque primary visual cortex. *Nature*, *387*, 281–284. doi:10.1038/387281a0

Ringach, D. L., Shapley, R. M., & Hawken, M. J. (2002). Orientation selectivity in macaque V1: diversity and laminar dependence. *The Journal of Neuroscience : The Official Journal of the Society for Neuroscience*, *22*, 5639–5651. doi:20026567

Rockland, K. S., & Lund, J. S. (1983). Intrinsic laminar lattice connections in primate visual cortex. *The Journal of Comparative Neurology*, *216*, 303–318. doi:10.1002/cne.902160307

Rossi, S., Hallett, M., Rossini, P. M., & Pascual-Leone, A. (2009). Safety, ethical considerations, and application guidelines for the use of transcranial magnetic stimulation in clinical practice and research. In *Clinical neurophysiology : official journal of the International Federation of Clinical Neurophysiology* (Vol. 120, pp. 2008–2039). doi:10.1016/j.clinph.2009.08.016

Salami, M., Itami, C., Tsumoto, T., & Kimura, F. (2003). Change of conduction velocity by regional myelination yields constant latency irrespective of distance between thalamus and cortex. *Proceedings of the National Academy of Sciences of the United States of America*, *100*, 6174–6179. doi:10.1073/pnas.0937380100

Salin, P. A., Bullier, J., & Kennedy, H. (1989). Convergence and divergence in the afferent projections to cat area 17. *The Journal of Comparative Neurology*, *283*, 486–512. doi:10.1002/cne.902830405

Salin, P. A., Girard, P., Kennedy, H., & Bullier, J. (1992). Visuotopic organization of corticocortical connections in the visual system of the cat. *The Journal of Comparative Neurology*, *320*, 415–434. doi:10.1002/cne.903200402

Salinas, F. S., Lancaster, J. L., & Fox, P. T. (2007). Detailed 3D models of the induced electric field of transcranial magnetic stimulation coils. *Physics in Medicine and Biology*, *52*, 2879–2892. doi:10.1088/0031-9155/52/10/016

Sato, H., Katsuyama, N., Tamura, H., Hata, Y., & Tsumoto, T. (1995). Mechanisms underlying direction selectivity of neurons in the primary visual cortex of the macaque. *Journal of Neurophysiology*, *74*, 1382–1394.

Sceniak, M. P., Hawken, M. J., & Shapley, R. (2002). Contrast-dependent changes in spatial frequency tuning of macaque V1 neurons: effects of a changing receptive field size. *Journal of Neurophysiology*, *88*, 1363–1373. doi:10.1152/jn.00967.2001

Sceniak, M. P., Ringach, D. L., Hawken, M. J., & Shapley, R. (1999). Contrast's effect on spatial summation by macaque V1 neurons. *Nature Neuroscience*, *2*, 733–739. doi:10.1038/11197

Schiller, P. H., Finlay, B. L., & Volman, S. F. (1976). Quantitative studies of single-cell properties in monkey striate cortex. I. Spatiotemporal organization of receptive fields. *Journal of Neurophysiology*, *39*, 1288–1319.

Schwabe, L., Obermayer, K., Angelucci, A., & Bressloff, P. C. (2006). The role of feedback in shaping the extra-classical receptive field of cortical neurons: a recurrent network model. *The Journal of Neuroscience : The Official Journal of the Society for Neuroscience*, *26*, 9117–9129. doi:10.1523/JNEUROSCI.1253-06.2006

Schwarzkopf, D. S., Silvanto, J., & Rees, G. (2011). Stochastic resonance effects reveal the neural mechanisms of transcranial magnetic stimulation. *The Journal of Neuroscience : The Official Journal of the Society for Neuroscience*, *31*, 3143–3147. doi:10.1523/JNEUROSCI.4863-10.2011

Sclar, G., & Freeman, R. (1982). Orientation selectivity in the cat's striate cortex is invariant with stimulus contrast. *Experimental Brain Research*, *46*, 457–461. doi:10.1007/BF00238641

Sengpiel, F., Baddeley, R. J., Freeman, T. C. B., Harrad, R., & Blakemore, C. (1998). Different mechanisms underlie three inhibitory phenomena in cat area 17. *Vision Research*, *38*, 2067–2080. doi:10.1016/S0042-6989(97)00413-6

Seriès, P., Lorenceau, J., & Frégnac, Y. (2003). The "silent" surround of V1 receptive fields: Theory and experiments. In *Journal of Physiology Paris* (Vol. 97, pp. 453–474). doi:10.1016/j.jphysparis.2004.01.023

Shapley, R., Hawken, M., & Xing, D. (2007). The dynamics of visual responses in the primary visual cortex. *Progress in Brain Research*, *165*, 21–32. doi:10.1016/S0079-6123(06)65003-6

Sherman, S. M., & Guillery, R. W. (1996). Functional organization of thalamocortical relays. *Journal of Neurophysiology*, *76*, 1367–1395. doi:0022-3077/96

Shushruth, S., Nurminen, L., Bijanzadeh, M., Ichida, J. M., Vanni, S., & Angelucci, A. (2013). Different orientation tuning of near- and far-surround suppression in macaque primary visual cortex mirrors their tuning in human perception. *The Journal of Neuroscience : The Official Journal of the Society for Neuroscience*, *33*, 106–19. doi:10.1523/JNEUROSCI.2518-12.2013

Siebner, H. R., Lang, N., Rizzo, V., Nitsche, M. A., Paulus, W., Lemon, R. N., & Rothwell, J. C. (2004). Preconditioning of low-frequency repetitive transcranial magnetic stimulation with transcranial direct current stimulation: evidence for homeostatic plasticity in the human motor cortex. *The Journal of Neuroscience : The Official Journal of the Society for Neuroscience*, *24*, 3379–3385. doi:10.1523/JNEUROSCI.5316-03.2004

Sillito, A. (1975). The contribution of inhibitory mechanisms to the receptive field properties of neurones in the striate cortex of the cat. *The Journal of Physiology*, *250*, 305–329. Retrieved from http://jp.physoc.org/content/250/2/305.short

Silvanto, J., Muggleton, N. G., Cowey, A., & Walsh, V. (2007). Neural adaptation reveals state-dependent effects of transcranial magnetic stimulation. *European Journal of Neuroscience*, *25*, 1874–1881. doi:10.1111/j.1460-9568.2007.05440.x

Silvanto, J., Muggleton, N., & Walsh, V. (2008). State-dependency in brain stimulation studies of perception and cognition. *Trends in Cognitive Sciences*, *12*, 447–454. doi:10.1016/j.tics.2008.09.004

Skottun, B. C., De Valois, R. L., Grosof, D. H., Movshon, J. A., Albrecht, D. G., & Bonds, A. B. (1991). Classifying simple and complex cells on the basis of response modulation. *Vision Research*, *31*, 1079–1086. doi:10.1016/0042-6989(91)90033-2

Smith, M. A., & Kohn, A. (2008). Spatial and Temporal Scales of Neuronal Correlation in Primary Visual Cortex. *Journal of Neuroscience*. doi:10.1523/JNEUROSCI.2929-08.2008

Somers, D., Todorov, E., & Siapas, A. (1998). A local circuit approach to understanding integration of long-range inputs in primary visual cortex. *Cerebral …*, *8*(3), 204–17. Retrieved from http://cercor.oxfordjournals.org/content/8/3/204.short

Thompson, K. G., Hanes, D. P., Bichot, N. P., & Schall, J. D. (1996). Perceptual and motor processing stages identified in the activity of macaque frontal eye field neurons during visual search. *Journal of Neurophysiology*, *76*, 4040–4055.

Thomson, A. M., & Bannister, A. P. (2003). Interlaminar connections in the neocortex. *Cerebral Cortex (New York, N.Y. : 1991)*, *13*, 5–14. doi:10.1093/cercor/13.1.5

Tolhurst, D. J., Movshon, J. A., & Thompson, I. D. (1981). The dependence of response amplitude and variance of cat visual cortical neurones on stimulus contrast. *Experimental Brain Research*, *41*, 414–419. doi:10.1007/BF00238900

Toth, L. J., Rao, S. C., Kim, D. S., Somers, D., & Sur, M. (1996). Subthreshold facilitation and suppression in primary visual cortex revealed by intrinsic signal imaging. *Proceedings of the National Academy of Sciences of the United States of America*, *93*, 9869–9874. doi:10.1073/pnas.93.18.9869

Troyer, T. W., Krukowski, A. E., Priebe, N. J., & Miller, K. D. (1998). Contrast-invariant orientation tuning in cat visual cortex: thalamocortical input tuning and correlation-based intracortical connectivity. *The Journal of Neuroscience : The Official Journal of the Society for Neuroscience*, *18*, 5908–5927.

Valero-Cabre, A., Payne, B. R., & Pascual-Leone, A. (2007). Opposite impact on (14)C-2-deoxyglucose brain metabolism following patterns of high and low frequency repetitive transcranial magnetic stimulation in the posterior parietal cortex. *Exp Brain Res*, *176*, 603–615. Retrieved from http://www.ncbi.nlm.nih.gov/entrez/query.fcgi?cmd=Retrieve&db=PubMed&dopt=Citation&list_uids=16972076

Valls-Sole, J., Pascual-Leone, A., Brasil-Neto, J. P., Cammarota, A., McShane, L., & Hallett, M. (1994). Abnormal facilitation of the response to transcranial magnetic stimulation in patients with Parkinson's disease. *Neurology*. doi:10.1212/WNL.44.4.735

Vaney, D. I., & Taylor, W. R. (2002). Direction selectivity in the retina. *Current Opinion in Neurobiology*. doi:10.1016/S0959-4388(02)00337-9

Walker, G. A., Ohzawa, I., & Freeman, R. D. (1999). Asymmetric suppression outside the classical receptive field of the visual cortex. *The Journal of Neuroscience : The Official Journal of the Society for Neuroscience*, *19*, 10536–10553. doi:10.1109/LPT.2009.2020494

Wassermann, E., & Lisanby, S. (2001). Therapeutic application of repetitive transcranial magnetic stimulation: a review. *Clinical Neurophysiology*, *112*, 1367–1377. doi:10.1016/S1388-2457(01)00585-5

Webb, B. S., Dhruv, N. T., Solomon, S. G., Tailby, C., & Lennie, P. (2005). Early and late mechanisms of surround suppression in striate cortex of macaque. *The Journal of Neuroscience : The Official Journal of the Society for Neuroscience*, *25*, 11666–11675. doi:10.1523/JNEUROSCI.3414-05.2005

Xing, D., Shapley, R. M., Hawken, M. J., & Ringach, D. L. (2005). Effect of stimulus size on the dynamics of orientation selectivity in Macaque V1. *Journal of Neurophysiology*, *94*, 799–812. doi:10.1152/jn.01139.2004

Yao, H., & Li, C. Y. (2002). Clustered organization of neurons with similar extra-receptive field properties in the primary visual cortex. *Neuron*, *35*, 547–553. doi:10.1016/S0896-6273(02)00782-1

Ziemann, U., Paulus, W., Nitsche, M. A., Pascual-Leone, A., Byblow, W. D., Berardelli, A., … Rothwell, J. C. (2008). Consensus: Motor cortex plasticity protocols. *Brain Stimulation*. doi:10.1016/j.brs.2008.06.006